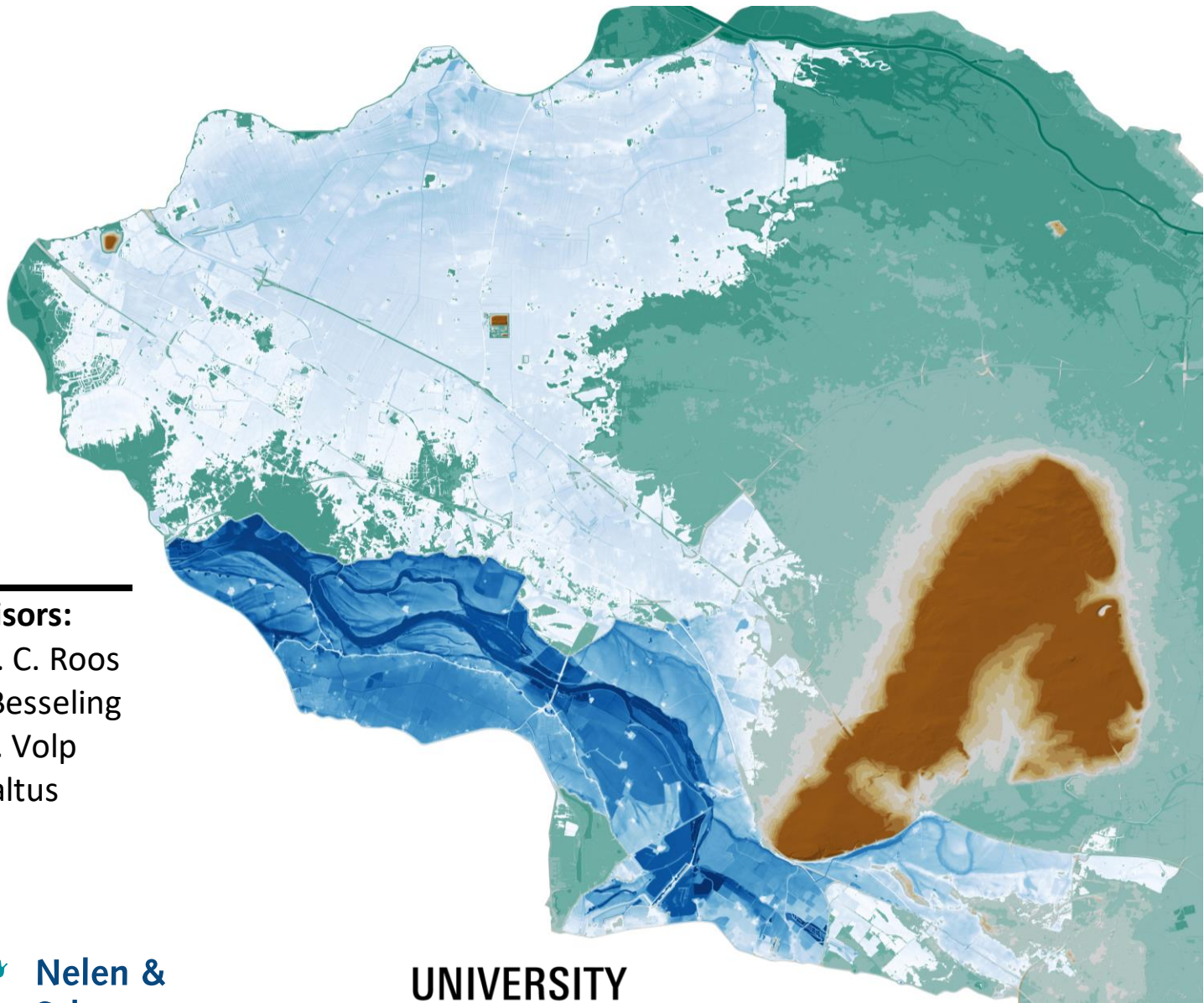


# The sensitivity of spatiotemporal inundation patterns to the dike breach location

*Tjerk-Jan van Leerdam*

*MSc thesis*

*26<sup>th</sup> of August 2023*



---

## **Supervisors:**

dr. ir. P. C. Roos

ir. L.S. Besseling

dr. N.D. Volp

ir. O. Baltus



**Nelen &  
Schuurmans**

**UNIVERSITY  
OF TWENTE.**

# PREFACE

---

In front of you lies my thesis “The sensitivity of spatiotemporal inundation patterns to dike breach location”, which I wrote as the final part of my master Civil Engineering and Management at the University of Twente.

This thesis was written during an internship at Nelen & Schuurmans from February till August 2023. I want to thank my supervisor at Nelen & Schuurmans, Nicolette Volp, for her constructive and valuable feedback and your guidance, without which the result of this project would have been much different. Furthermore, I would like to thank my other supervisor at Nelen & Schuurmans, Olof Baltus, for his extensive help in setting up the model. Without his help and guidance, I would not have been able to set up a model of this quality. Next to my supervisors, I would like to thank all other colleagues at Nelen & Schuurmans who were available for questions during my internship. Furthermore, I want to thank my daily University supervisor, Leon Besseling, for his flexibility and all the interest he showed during our regular meetings. I really appreciated his practical suggestions and constructive feedback. Lastly, I also want to thank Pieter Roos for his guidance during the process.

I hope you have an interesting read,

Tjerk-Jan van Leerdam  
Ede, August 25<sup>th</sup>, 2023

# ABSTRACT

---

Hydrodynamic models are often used to simulate inundation patterns. Based on these simulations, a well-informed decision on evacuation planning in case of a dike breach can be made. Yet, hydrodynamic models are affected by uncertainties in, among others, the dike breach location. Sensitivity analyses are often used to assess the effect of the variability in uncertain input factors on the output of hydrodynamic models. However, a sensitivity analysis of the inundation pattern to the dike breach location in a systematic way with a larger dataset of breach locations is missing in literature. The aim of this study is therefore to assess the spatial and temporal sensitivity of inundation patterns to the location of a dike breach.

In order to simulate inundation patterns, an accurate and computationally efficient model was setup of the study area, dike ring 48, in the hydrodynamic modelling package 3Di. This modelling package uses a subgrid method which accounts for high resolution spatial data in a computationally efficient way. Part of the model set-up was a sensitivity analysis of the computational grid. In this analysis, the effect of computational grid size on the inundation pattern and the computational time (wall-clock time) was determined. The set-up model was used to simulate a dike breach at 15 potential dike breach locations. After the simulations, the maximum inundation extents of the different simulations were qualitatively compared. Based on the comparison, clusters of dike breaches which resulted in qualitatively similar inundation extents were made. For every cluster, the spatial sensitivity of the arrival times and the spatiotemporal sensitivity of the maximum water depths to the dike breach location in the cluster are analysed. As an indicator of the spatial sensitivity of the arrival times, the Mean Absolute Difference (MAD) of the arrival times of the different simulations in the cluster was computed for every inundated location in the hinterland. Furthermore, for every inundated location in the hinterland, the MAD of the maximum water depths at every day of the different simulations in the cluster was computed.

The sensitivity analysis of the computational grid mainly showed that the computational grid barely influences the accuracy of the simulated inundation pattern. However, an incorrect schematization of underpasses in the computational grid can have a large influence on this accuracy. Therefore, the computational grid was locally refined around the underpasses which increased the accuracy of the inundation pattern. The analysis of the maximum inundation extents showed that dike breaches south of the high regional dike along the Rijnstrangen area result in a qualitatively similar maximum inundation extent while dike breaches north of this dike also result in a qualitatively similar maximum inundation extent. Based on the analysis of the arrival times and maximum water depth in both clusters, it was found that the spatiotemporal sensitivity of the inundation pattern to the dike breach location are determined by the elevation, the presence of higher line elements and the distance to the dike breach locations. In lower-lying and centrally located areas, the inundation pattern is only slightly sensitive to the dike breach location and for a short period. In areas with similar elevation and at a less central location, the inundation pattern is slightly more sensitive to the dike breach location. In more elevated areas which are less centrally located, the inundation pattern is significantly sensitive to the dike breach location and for a longer period. Contrary to this, if these elevated areas are located at the edges of the lower areas and further away from all dike breach locations, the inundation pattern will be almost insensitive to the dike breach location. Moreover, the inundation pattern in small compartments which are completely enclosed by obstacles without large openings and underpasses is significantly sensitive to the dike breach location and for a long period. Furthermore, in general, it can be concluded that the sensitivity of inundation pattern mostly decreases over time.

# ABBREVIATIONS

---

BGT	Basisregistratie Grootchalige Topografie
DEM	Digital Elevation Model
MAD	Mean Absolute Difference
MAE	Mean Absolute Error
MLS	Multi-layered safety
VNK	National Flood Risk Analysis in the Netherlands (Veiligheid Nederland in Kaart)

# TABLE OF CONTENTS

---

<b>PREFACE</b> .....	<b>I</b>
<b>ABSTRACT</b> .....	<b>II</b>
<b>ABBREVIATIONS</b> .....	<b>III</b>
<b>1. INTRODUCTION</b> .....	<b>1</b>
1.1 FLOODS AND FLOOD MITIGATION MEASURES IN RIVERINE AREAS.....	1
1.2 PROBLEM DEFINITION.....	1
1.3 OBJECTIVE.....	2
1.4 RESEARCH QUESTIONS.....	3
1.5 OUTLINE.....	4
<b>2. THEORETICAL FRAMEWORK</b> .....	<b>5</b>
2.1 DUTCH FLOOD SAFETY APPROACH.....	5
2.2 MODELLING DIKE BREACHES AND THEIR RESULTING INUNDATIONS.....	8
2.2.1 <i>Selection of dike breach locations</i> .....	9
2.2.2 <i>Modelling dike breach evolution</i> .....	10
2.2.3 <i>Equations describing inundation flow</i> .....	11
2.3 2D HYDRODYNAMIC MODELLING SOFTWARE.....	12
<b>3. METHODOLOGY</b> .....	<b>15</b>
3.1 CHARACTERISTICS OF THE STUDY AREA.....	16
3.2 DATA.....	17
3.3 MODEL SET-UP.....	19
3.3.1 <i>Model rasters</i> .....	19
3.3.2 <i>Obstacles</i> .....	19
3.3.3 <i>Computational grid</i> .....	20
3.4 SCENARIO SET UP.....	21
3.4.1 <i>Selected dike breach locations</i> .....	21
3.4.2 <i>Schematisation breaches and inflow hydrograph</i> .....	22
3.4.3 <i>Initial and boundary conditions</i> .....	23
3.5 ANALYSIS OF THE SIMULATION RESULTS.....	24
3.5.1 <i>Analysis maximum inundation extent</i> .....	24
3.5.2 <i>Analysis arrival times</i> .....	24
3.5.3 <i>Analysis maximum water depths</i> .....	25
<b>4. RESULTS OF THE SENSITIVITY ANALYSIS OF THE COMPUTATIONAL GRID</b> .....	<b>27</b>
4.1 FIRST PHASE: DIKE BREACH AT LOO.....	28
4.2 SECOND PHASE: DIKE BREACHES AT DOESBURG AND SPIJK.....	29
<b>5. RESULTS</b> .....	<b>34</b>
5.1 MAXIMUM INUNDATION EXTENT.....	34
5.2 CLUSTER SOUTH.....	36
5.2.1 <i>Arrival times</i> .....	37
5.2.2 <i>Maximum water depths at day 1</i> .....	42
5.2.3 <i>Maximum water depths at day 2</i> .....	45

5.2.4	<i>Maximum water depths at day 3</i> .....	47
5.3	CLUSTER NORTH.....	48
5.3.1	<i>Arrival times</i> .....	49
5.3.2	<i>Maximum water depths at day 1</i> .....	53
5.3.3	<i>Maximum water depths at day 2</i> .....	55
5.3.4	<i>Maximum water depths at day 3</i> .....	56
<b>6.</b>	<b>DISCUSSION</b> .....	<b>59</b>
6.1	MAIN FINDINGS .....	59
6.1.1	<i>Sensitivity analysis of the computational grid</i> .....	59
6.1.2	<i>Analysis of the maximum inundation extent</i> .....	59
6.1.3	<i>Analysis of the arrival times</i> .....	60
6.1.4	<i>Analysis of the maximum water depth</i> .....	61
6.2	LIMITATIONS IN THE METHODOLOGY.....	63
6.2.1	<i>Model set up</i> .....	63
6.2.2	<i>Used hydrograph</i> .....	64
6.2.3	<i>Significance of the sensitivity of the maximum water depths to the dike breach location</i> .....	65
<b>7.</b>	<b>CONCLUSION AND RECOMMENDATIONS</b> .....	<b>66</b>
7.1	CONCLUSIONS .....	66
7.2	RECOMMENDATIONS FOR FUTURE RESEARCH.....	67
	<b>REFERENCES</b> .....	<b>68</b>
	<b>APPENDIX A: ROUGHNESS</b> .....	<b>74</b>
	<b>APPENDIX B: OBSTACLES</b> .....	<b>76</b>
	<b>APPENDIX C: GRID REFINEMENTS</b> .....	<b>77</b>
	<b>APPENDIX D: INITIAL WATER LEVELS OUDE IJSSEL</b> .....	<b>78</b>
	<b>APPENDIX E: RESULTS OF THE SENSITIVITY ANALYSIS OF THE COMPUTATIONAL GRID</b> .....	<b>79</b>
E.1	RESULTS PHASE 1: DIKE BREACH AT LOO .....	79
E.1.1	<i>Arrival times</i> .....	79
E.1.2	<i>Water depths after 12 hours</i> .....	81
E.1.3	<i>Water depths after 1 day</i> .....	82
E.2	RESULTS PHASE 2: DIKE BREACH AT DOESBURG.....	84
E.3	RESULTS PHASE 2: DIKE BREACH AT SPIJK .....	86
E.3.1	<i>Arrival times</i> .....	86
E.3.2	<i>Water depths after 12 hours</i> .....	88
E.3.3	<i>Water depths after 1 day</i> .....	91

# 1. INTRODUCTION

---

## 1.1 FLOODS AND FLOOD MITIGATION MEASURES IN RIVERINE AREAS

Floods are among the most devastating natural hazards worldwide (Verwey et al., 2017). Compared to other weather-related disasters, floods annually affect the most people (Jongman, 2021; Tellman et al., 2021). In the period 2011-2020, 82.7 million people worldwide were affected by floods (CRED, 2022). Generally, three different types of flooding are distinguished, namely coastal, pluvial (extreme rainfall) and fluvial (river) floods (Xu et al., 2023). For river floods specifically, it is expected that the affected global population will increase from 21 million in 2015 to 54 million in 2030. This is due to climate change and socio-economic development (Verwey et al., 2017). Furthermore, the exposure of people and assets to river flooding will also increase in the coming decades. It is expected that in 2050, the total exposed population will have increased to 1.05 billion. Moreover, in the same year, the value of exposed assets to river flooding will increase to 126 trillion USD which is an increase of 250% with respect to 2010 (Jongman et al., 2012). Causes for this increase in exposure to river flooding are climate change (Maranzoni et al., 2022; Verwey et al., 2017; Winsemius et al., 2016), economic development and population growth in flood-prone areas, and inadequate river management (di Baldassarre et al., 2009; Verwey et al., 2017; Winsemius et al., 2016).

Several structural and non-structural measures are widely adopted to mitigate flood risk in riverine areas and improve fluvial flood resilience. Structural measures include dike systems and retention basins. Due to the presence of dikes, the perception of risk decreases, which can encourage further economic development and population growth in the embanked area (di Baldassarre et al., 2009; Ferrari et al., 2020; Maranzoni et al., 2022). This will result in higher flood damages and deaths in the event of dike failure (Maranzoni et al., 2022). One of the increasingly applied non-structural measures is an early-warning system. These systems enable the prediction of inundation patterns. Based on these predictions, emergency actions can be taken such as evacuation and deployment of temporary flood barriers (Maranzoni et al., 2022). These systems are not only important in areas without structural measures. Despite all efforts adopted in dike design and maintenance, dikes can still breach (Ferrari et al., 2020). Timely warning and subsequent evacuation can reduce the mortality with several orders of magnitude (Jonkman & Vrijling, 2008). When people are not warned and evacuate based on directly perceiving the flood danger, casualties can be up to six times higher in riverine areas (Alonso Vicario et al., 2020). Both facts clearly stress the importance of early warning and subsequent evacuation.

## 1.2 PROBLEM DEFINITION

Hydrodynamic models may help to make a well-informed decision on evacuation planning in case of a dike breach. Simulations of these models can be used to identify crucial flood processes such as inundation extents and inundation water depths (D’Oria et al., 2019; Ferrari et al., 2020; Huthoff et al., 2015; Maranzoni et al., 2022). Yet, as all other numerical models, hydrodynamic models approximate physical processes and are affected by uncertainties in the input data (Alipour et al., 2022; Oubennaceur et al., 2019). One of these uncertain input parameters is the location of a dike breach (D’Oria et al., 2019; Maranzoni et al., 2022). The dike breach location is highly dependent on the geometrical and geotechnical characteristics of the dike as well as on the water level in the river (Maranzoni et al., 2022). These factors are uncertain as well (Beven et al., 2014).

The uncertainty in these factors is often captured by fragility functions in probabilistic analyses (e.g., Apel et al., 2009; Bomers et al., 2019; De Bruijn et al., 2014; D’Oria et al., 2019; Maranzoni et al., 2022; Vorogushyn et al., 2010). Fragility functions describe the probability of a breach as a function of the water level and are used to determine if a dike at a certain location will breach (De Bruijn et al., 2014). Although the uncertainties in dike breach location are accounted for in several studies by using fragility functions, the effects of the uncertainty in the dike breach location on the inundation pattern have not been systematically studied. When inundation patterns are mentioned in the rest of this report, flood arrival times and inundation water depths are considered unless otherwise stated.

Sensitivity analyses are often used to assess the effect of the variability in the input factors on the output of hydrodynamic models (D’Oria et al., 2019; Hall et al., 2019). The sensitivity of the modelled inundation patterns to some input factors is studied extensively such as the sensitivity to bottom roughness, ground elevation and the grid resolution (e.g., Alipour et al., 2022; Hesselink et al., 2003; Liu et al., 2019). However, the sensitivity of inundation patterns to different dike breach locations has not yet been studied in depth. Tadesse and Fröhle (2020) researched the sensitivity of inundation water depth to breach process parameters which included dike breach location. They concluded that the inundation water depth is very sensitive to dike breach location. However, this conclusion was based on the analysis of only two dike breach locations on the same river stretch. Furthermore, it was based on the modelled water depth at only one location in the floodplain. Ferrari et al. (2020) selected dike breach locations every 2 km for flooding scenarios. They observed that two close breaches often result in similar inundation patterns, but sometimes the inundation pattern may change dramatically even for relatively close breaches. In case the inundation pattern changes dramatically even for relatively close breaches, water authorities need to model many dike breaches which are close together. This is necessary to get an overview of potential inundation patterns. This in turn will help to accurately predict the inundations pattern during a dike breach. However, modelling many dike breaches results in a large computational time which is undesirable. A sensitivity analysis may reveal how sensitive the inundation pattern is to the dike breach location. Based on this information, it can be decided how accurately it should be determined where a dike will breach, and thereby how many dike breaches should be simulated, to accurately predict the inundation pattern in case of a dike breach. Still, a sensitivity analysis of the inundation pattern to dike breach location in a systematic way with a larger dataset of breach locations is missing in literature.

### 1.3 OBJECTIVE

The objective of this research is to assess the spatial and temporal sensitivity of inundation patterns to the location of a dike breach. Sensitivity refers to the difference in the arrival times and water depths due to a dike breach at another location. This sensitivity may vary both spatially and temporally. This spatial variance in the sensitivity means that the water depth or the arrival time at a location in the hinterland may be more sensitive to the dike breach location than the water depth or the arrival time at another location in the hinterland. Furthermore, at one moment in time, the water depth at a particular location in the dike ring may be more sensitive to the dike breach location than at a later instance during the inundation. This is the temporal variance in the sensitivity of the inundation pattern to the dike breach location.

A hydrodynamic model is set up of a study area. The inundation patterns caused by the dike breaches at different locations in the primary flood defences of this study area will be compared. Dike ring 48 in the Netherlands is selected to serve as a study area. A dike ring area is an administrative area which is protected against flooding by a system of primary flood defences (TAW, 1998). Dike ring 48 is situated in

the province of Gelderland and is part of the management area of waterboard Rijn en IJssel. This dike ring is protected by primary flood defences along the rivers Rhine, Pannerdensch Kanaal, IJssel and Oude IJssel. More information about the case study can be found in Section 3.1.

The scope of this research is limited to single dike breaches at pre-selected locations in the primary flood defences along the Rhine, Pannerdensch Kanaal and IJssel. Moreover, modelling the discharge through the rivers and the moment of dike failure will not be part of this study. This is done to ensure that the focus is on the sensitivity of the inundation pattern to the dike breach location.

## 1.4 RESEARCH QUESTIONS

The main research question of this study is as follows:

*To which extent is the evolution of the inundation pattern sensitive to the location of a dike breach in the primary flood defences of dike ring 48?*

To answer the main research question and to structure the research, four research sub-questions are formulated. The first sub-question deals with setting up the hydrodynamic model. To be able to analyse the sensitivity of the inundation patterns, these patterns should first be accurately simulated using a hydrodynamic model. Unfortunately, there are no field measurements of (historic) inundation water levels and arrival times in the study area. This means that the accuracy of the simulated inundation pattern cannot be determined with respect to field measurements. Therefore, accuracy in this study is defined as the extent to which the simulated inundation pattern is consistent with the simulated inundation pattern in a reference model. Furthermore, a balance should be found between accuracy and computational time. A very accurate model may result in large computational times. Due to the potential large number of simulated dike breaches, a large computational time is not preferable. The first sub-question is:

1. *How can an accurate and computationally efficient hydrodynamic model be set up to compute inundation patterns?*

After an accurate and computationally efficient hydrodynamic model is set up, inundation patterns can be derived from the results. These inundation patterns will be clustered based on the similarity of their maximum inundation extents. The second sub-question deals with finding dike breaches which result in qualitatively similar maximum inundation extents:

2. *Which dike breaches result in qualitatively similar maximum inundation extents?*

Although several dike breaches may result in qualitatively similar maximum inundation extents, the arrival times of the inundation caused by these dike breaches may differ. Yet, this difference may be larger at one location than another. In the third sub-question, this spatial sensitivity of the arrival times to dike breaches with qualitatively similar maximum inundation extents will be studied:

3. *What is the spatial sensitivity of the arrival times to dike breach location?*

Similar to the arrival times, the differences in the maximum water depths of dike breaches with qualitative similar maximum inundation extents may be larger at one location than another. Yet, these differences at a certain location may also change during the flood event. Therefore, the fourth sub-question is as follows:

4. *What is the spatial and temporal sensitivity of the maximum inundation water depths to dike breach location?*

## 1.5 OUTLINE

The outline of this thesis is as follows. Firstly, the Dutch flood safety approach, the way to model dike breach-induced inundations and the used hydrodynamic modelling package will be described in the theoretical framework (Chapter 2). Secondly, the methodology will be presented along with an introduction of the study area and used datasets (Chapter 3). Important steps in the methodology are the model and scenario set-up, the sensitivity analysis of the computational grid and the analysis of the simulation results. Afterwards, the results of the sensitivity analysis of the computational grid and the analysis of the simulation results are presented in detail in respectively Chapter 4 and 5. In Chapter 6, the main findings and limitations of this research are discussed. Finally, conclusions to the research questions are drawn and recommendations for future research will be given in Chapter 7.

## 2. THEORETICAL FRAMEWORK

---

### 2.1 DUTCH FLOOD SAFETY APPROACH

The Netherlands is at a constant threat of flooding by the sea or rivers. Figure 1 shows the water depths that would be experienced in the Netherlands in the absence of any primary flood defences. Primary flood defences protect against flooding from the sea, the major rivers and the large lakes. To prevent flooding, the Dutch national government drafted the Water Act which forms the basis of flood protection standards for the primary flood defences. In addition to primary defences, regional defences protect against flooding from smaller rivers, canals and man-made lakes. A breach in regional defences will generally have a smaller impact than a breach in the primary defences. The safety standards for these defences are set by the provincial authorities and not by the national government (Kok et al., 2017).

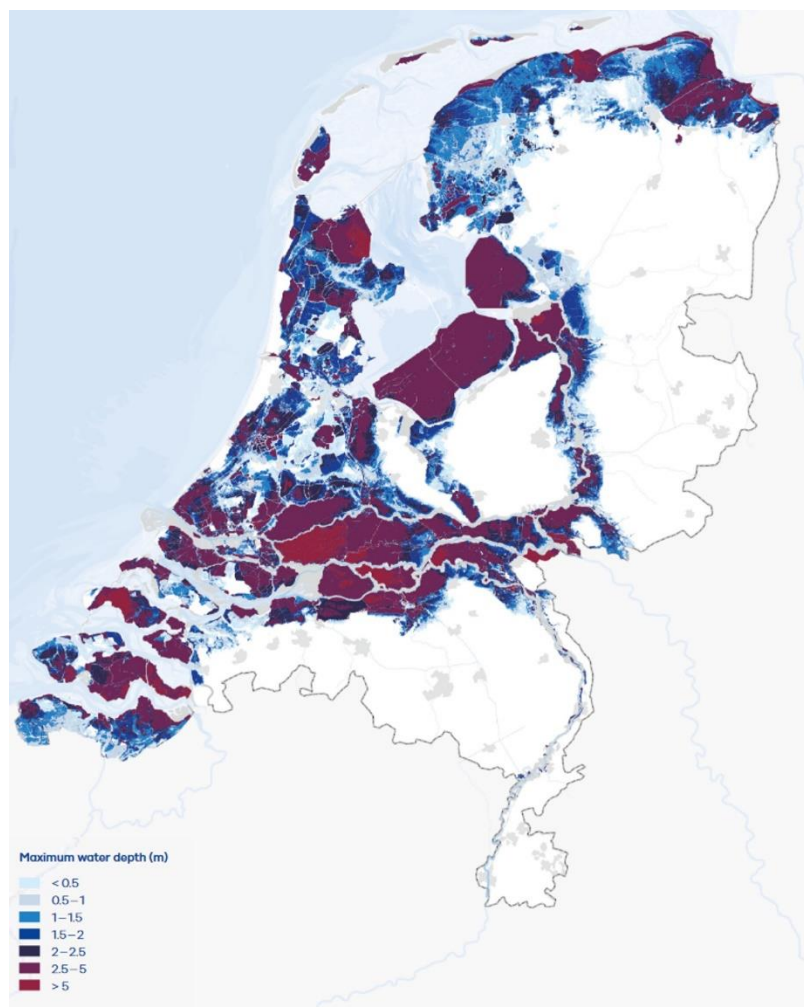


Figure 1 Water depths in the Netherlands in the case without primary flood defences (Kok et al., 2017)

In 2017, a new flood protection standard for the primary flood defences was defined which meant a shift in the Dutch flood safety approach. In the old standard, as described in *Fundamentals on Water Defences* (TAW, 1998), an optimum safety level was determined per dike ring which only considered the hydraulic load on the flood defences. This safety level was expressed as a water level with a certain exceedance

probability. The primary flood defences in a dike ring should be able to withstand this design water level. The dike rings and the corresponding standard exceedance probabilities are shown in Figure 2. In fact, due to the focus on withstanding design water levels, this standard mainly focused on the safety against overtopping and assumes that this is the main failure mechanism. However, this assumption is not entirely correct according to findings of the National Flood Risk Analysis in the Netherlands (VNK). In the report of this analysis, it was concluded that piping was the most important determinant of the probability of flooding for dikes along the rivers (VNK2 Project Office, 2012).

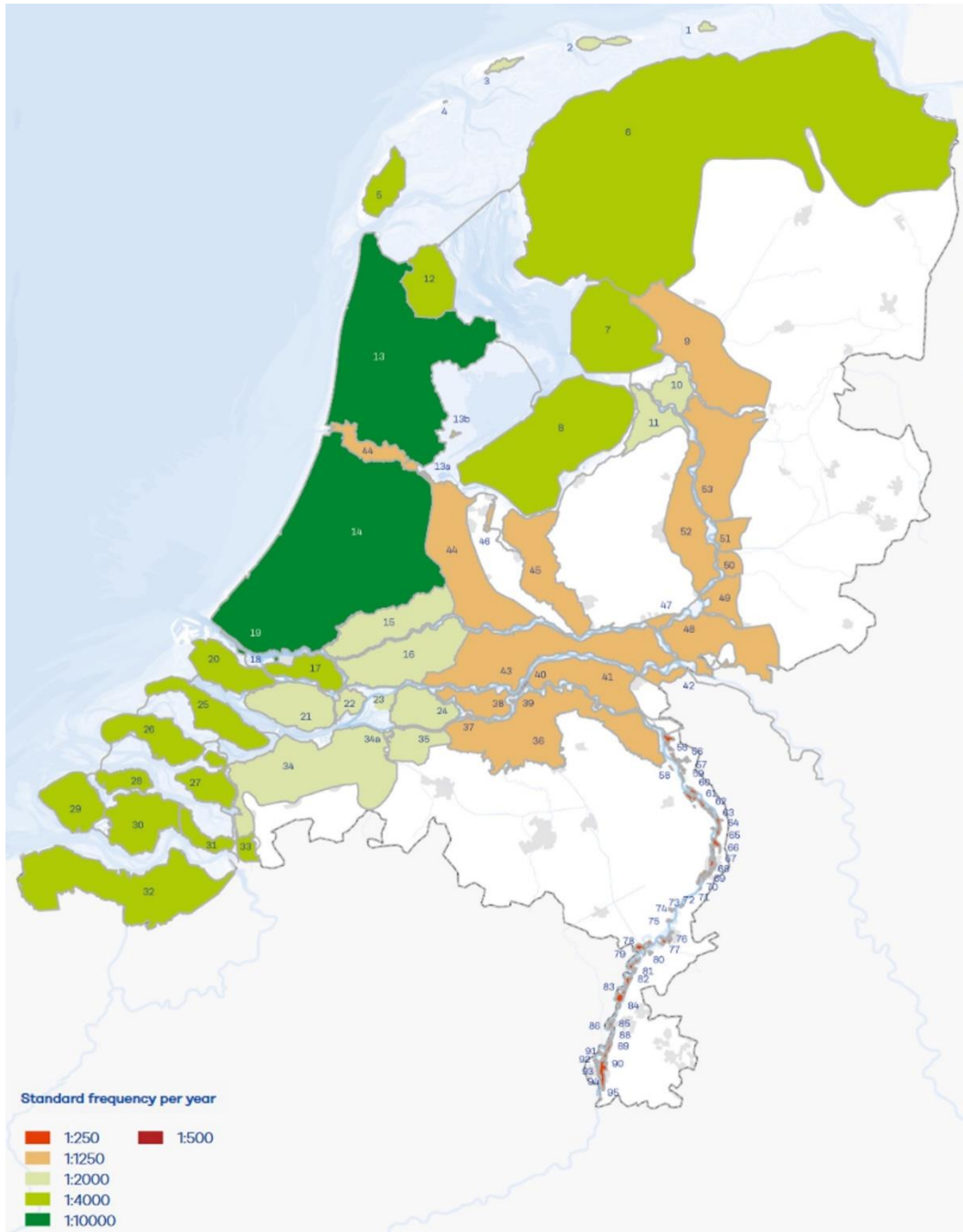


Figure 2 Dike ring areas and their exceedance probabilities (Kok et al., 2017)

Due to, among others, the described one-sided focus on hydraulic load and the failure mechanism overtopping in the old standard, a new flood safety standard was developed. This standard is extensively described in the document *Fundamentals of Flood Protection* by the Expert Network for Flood Protection (Expertisenetwerk Waterveiligheid: ENW) (Kok et al., 2017). In the new standard, the optimum safety level is based on the concept of flood risk. Flood risk refers to both the probability and the consequences of flooding. Based on the expected societal impact, economic damage and number of casualties, it is decided which probability of flooding is appropriate per dike segment. In general, if the expected consequences of a flood are higher, the allowed probability of flooding is lower. Using this approach, an almost equal risk is given to all parts of the Netherlands which are liable to flooding. Yet, due to the differences in consequences at every dike segment, the maximum probability of flooding is different from one dike segment to another. The probability of flooding for all primary dike segments in the Netherlands is shown in Figure 3. Note that the maximum probability of flooding is not the same as the exceedance probability which was prescribed in the old standard. The probability of flooding refers to both the exceedance frequency of a certain hydraulic load (as in the old standard) and the probability of a flood defence failure at this hydraulic load. So, in the new standard, both the hydraulic load and flood defence properties are considered while in the old standard, the hydraulic load was only considered.

The change in standard can also be seen in the study area, dike ring 48. In the old standard, the exceedance probability was 1/1250 year. In the new standard, the dikes around the dike ring were split into three dike segments which were assigned a maximum allowed probability of flooding of 1/10000, 1/3000 and 1/3000 year. The first segment extends from the Dutch-German border along the Rhine and the Pannerdensch Canal. The second and third segment run along respectively the IJssel and the Oude IJssel. The segments and their corresponding probability of flooding are shown in the close-up in Figure 3. The difference in the allowed probability of flooding between the segments is caused by the difference in the consequences. The southern part, directly behind the first segment is more densely populated and more companies are present which makes that the consequences will be larger in case of a flood.

In the old approach, flood safety measures were mainly aimed at the prevention of floods (e.g., higher dikes). However, in the case of a flood, the consequences would be devastating. Therefore, in the new risk approach, the multi-layered safety (MLS) was introduced which is described by Hoss et al. (2013). MLS assists in finding measures which also reduce the consequences of floods and thereby enhance flood safety. MLS consists of three layers. The first layer consists of physical measures such as flood defences which aim to prevent flooding. The second layer contains physical measures such as spatial planning and adaptation of buildings which aim to reduce the consequences of flooding. The third layer concentrates on organisational measures which can reduce the consequences of flooding. This layer is also referred to as crisis management and includes disaster plans, risk maps, early-warning systems, evacuation, temporary physical measures and medical help. So, in the new approach, more attention is paid to measures which reduce the consequences of floods.

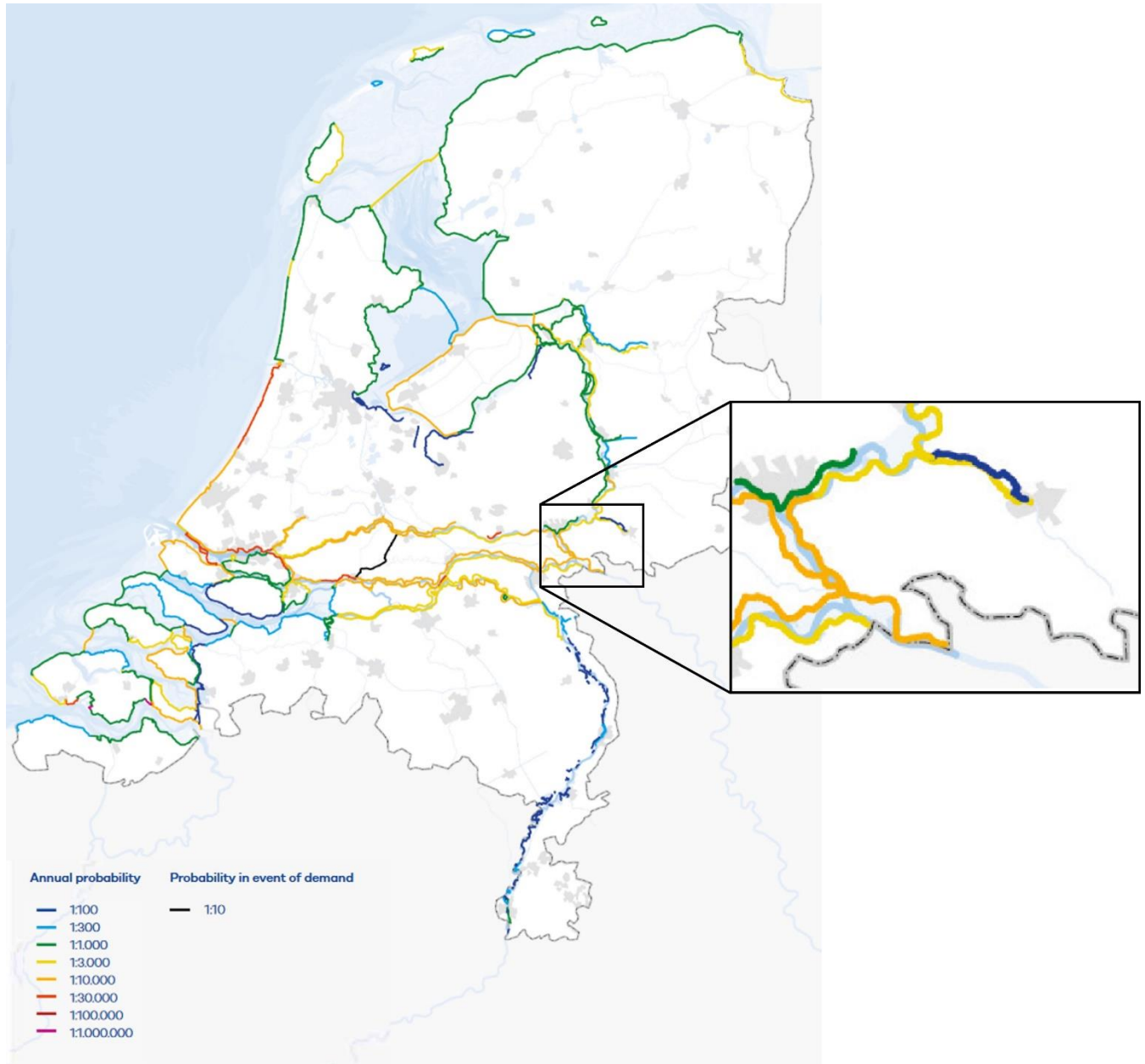


Figure 3 Annual probability of flooding for all primary dike segments in the Netherlands as part of the new flood risk approach. The close-up shows the dike segments and their corresponding probability of flooding in dike ring 48.

## 2.2 MODELLING DIKE BREACHES AND THEIR RESULTING INUNDATIONS

In order to implement measures that reduce the consequences of floods, knowledge about inundations is needed. This knowledge is often acquired through modelling. A first step in modelling of dike-breach induced floods is to select potential dike breach locations (Section 2.2.1). Secondly, if a dike fails at potential dike breach location, a dike breach is formed which will evolve over time. Several methods are available to model this evolution (Section 2.2.1). Water from the river will flow through the breach and will inundate the hinterland. Flooding of the hinterland is often described using the shallow water equations (Section 2.2.3).

### 2.2.1 Selection of dike breach locations

In literature, the selection of potential dike breach locations is generally done using three types of methods. Firstly, dike breach locations are selected based on expert judgement (e.g., de Bruijn et al., 2014; Huthoff et al., 2015). Moreover, preliminary model simulations are used to select dike breach locations. Roughly two types of preliminary simulations can be distinguished in literature. In the first type, the most vulnerable dike locations are selected based on a comparison between simulated peak water levels and the dike height (Curran et al., 2020; di Baldassarre et al., 2009; D’Oria et al., 2019) or a fragility function (Maranzoni et al., 2022). In the second type, inundation patterns are simulated using a 2D model. These simulations are used to find locations which would result in large overland flows (Bomers et al., 2019) or to group dike breaches which result in similar inundation patterns (Apel et al., 2009). Thirdly, the selection of dike breach locations can be based on data presented in other literature (e.g., Curran et al., 2019; Goeury et al., 2022; Mazzoleni et al., 2017).

When studying the sensitivity of the inundation pattern to dike breach location, dike breach locations need to be selected in such a way that all different inundation patterns in the study area are covered. Studies in which the selection is based on the expected inundation consequences or simulated inundations can give valuable information about the different inundation patterns which can occur in the study area or comparable areas. Thereby, it can give insight in the number and spacing of dike breach locations which need to be selected. Three of such studies will be discussed below, namely Arends and Bisschop (2014), de Bruijn et al. (2014) and Apel et al. (2009).

Arends and Bisschop (2014) researched the flood risk in dike ring 48 as part of the VNK project. Based on the simulations done in this project, they concluded that the primary flood defences in this dike ring can be divided into six dike sections. The final inundation extent and flood damage are almost independent of the exact breach location within each section. In other words, a dike breach at every location in a certain section will result in the same final inundation extent and flood damage. These sections are shown in Figure 4.

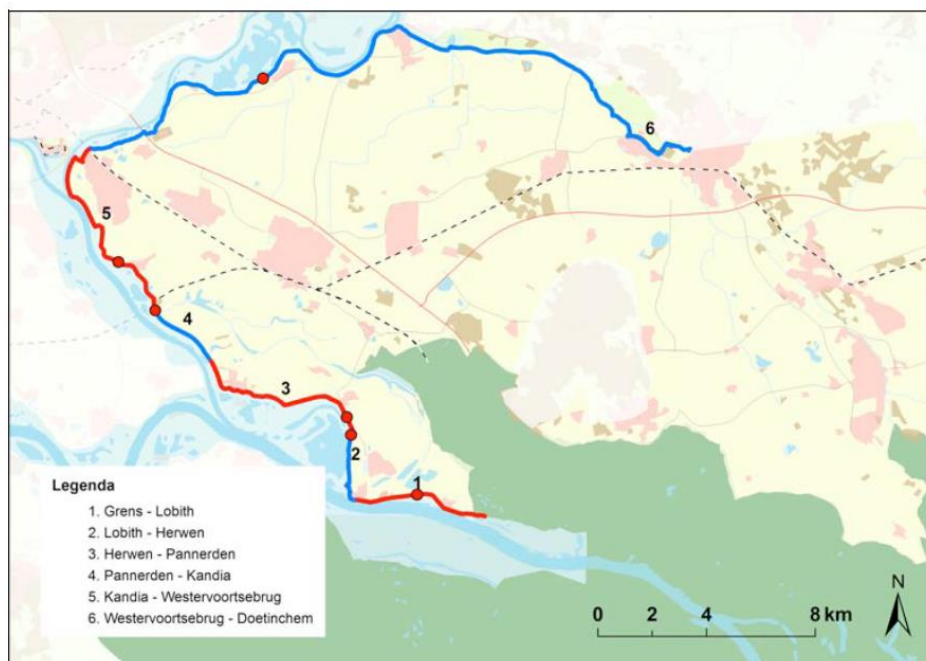


Figure 4 Dike sections where the final inundation extent is almost independent of the exact dike breach location in the section (Arends & Bisschop, 2014).

For their research, De Bruijn et al. (2014) researched the societal flood risk in the Netherlands including dike ring 48. For their research, they selected dike breach locations based on their expected consequences. If a breach is expected to have significantly different consequences from a neighbouring breach, an additional breach location was defined. For this assessment, they took land use, elevation and higher line elements into account. In their research, they came to the same sections as in the VNK report (Arends & Bisschop, 2014).

Apel et al. (2009) used 2D simulations to get a more manageable number of dike breach locations for the rest of their research. In these simulations, inundations were modelled every kilometre along the Rhine between Cologne and Rees. The dikes along this river stretch are almost 330 km long. The inundated areas were compared to each other and grouped according to their similarity. The resulting 43 representative dike breaches were then used in the rest of their research. Based on this research, it can be concluded that dike segments in the Lower Rhine area where inundation patterns are independent of the exact breach location within the segment are at least 1 km.

### 2.2.2 Modelling dike breach evolution

Dikes can fail in a variety of ways called failure mechanisms. The three most dominant failure mechanisms for river dikes are overtopping, macrostability (sliding inner slope) and piping (backward internal erosion) (VNK2 Project Office, 2012). In overtopping, a dike fails due to water which flows over the landward slope of the dike and progressively erodes the cover at this side of the dike (van Bergeijk et al., 2021; Vorogushyn et al., 2009). A dike fails due to macroinstability when the water pressure in the dike or the soil layers below the dike becomes too large. This causes the landward slope of the dike to become unstable and to slide (TAW, 2001). Another consequence of high water pressure in the soil layers below the dike is the formation of (horizontal) pipes below the dike. When these pipes reach the river, the flood defence will subside into the created cavities and fail (TAW, 1999).

If a dike fails, a breach will form and evolve over time. The formation and evolution of a dike breach subject to overtopping can be roughly divided in three phases (Kakinuma & Shimizu, 2014; Rifai et al., 2018; Schmitz et al., 2021; Zhao et al., 2015). In the first phase, the landside slope is eroded, the breach deepens towards the bottom of dike and breach opening begins to widen gradually. In the second phase, the breach opening begins to widen rapidly in the downstream direction. In the third phase, the rate of breach widening decreases leading to a continuing but slow breach expansion in the lateral direction (width of the breach). In literature, several dike breach models are used to describe the evolution of a dike breach. These dike breach models try to capture these described phases. A frequently used breach model, especially in Dutch studies (e.g., de Bruijn et al. (2014), van Mierlo et al. (2007), Courage et al. (2013) and Huthoff et al. (2015)), is the model of Verheij and Van der Knaap. In the dike breach model of Verheij and Van der Knaap, the evolution of a dike breach is split in a breach deepening and a breach widening phase.

Furthermore, in literature, breach evolution is often described by a linear function (Apel et al., 2006; Curran et al., 2020; Goeury et al., 2022; Meunier & Merwade, 2014; Vorogushyn et al., 2010, 2012). This choice for a simpler method is often made, because the prediction of dike breach growth is highly uncertain (Bomers et al., 2019; Meunier & Merwade, 2014). This makes that several models will give an overprediction or underprediction of the historical observed breach widths (Vorogushyn et al., 2010).

Another method which is frequently used to describe breach width over time is to assume a fixed breach width (Apel et al., 2009; D’Oria et al., 2019; Maranzoni et al., 2022; Mazzoleni et al., 2014, 2017). This means that breach evolution happens instantaneously after the initiation of the breach and the breach

will keep the fixed width over time. This choice is often made based on sensitivity analyses of for example Mazzoleni (2014) and Di Baldassarre (2009) which concluded that the breach development time had negligible effect on the outflow hydrographs.

### 2.2.3 Equations describing inundation flow

After a dike breach, water will flow through the hinterland behind the dike. This flow can be characterized as shallow flow. Shallow flow in this context means that the horizontal extent of the flow is much larger than the flow depth (Bates, 2022; Cheviron & Moussa, 2016). This is especially valid for inundations of the hinterland where water depths are no more than a few meters (Bates, 2022). The water in the hinterland moves due to two forcings. The first forcing is the change in static pressure gradient due to a difference in the water level. Water tends to flow from the location with a higher water level and thereby higher pressure to locations with a lower water level and thereby lower pressure. The second forcing is frictional resistance. Water flows along surfaces and experiences shear from these surfaces which causes energy losses and slows down the flow. To describe shallow flow of water subject to these two forcings, the shallow water equations are frequently used. These equations are derived by depth-averaging the Navier Stokes equations. This means that the vertical velocities and the vertical profile of the horizontal velocity components are neglected. Directly from this assumption it follows that there is a hydrostatic water pressure distribution. For a full derivation of the shallow water equations based on depth integration of Navier Stokes equations, the reader is referred to fluid dynamics textbooks.

The conservation of mass is described by the continuity equation :

$$\frac{\partial \zeta}{\partial t} + \frac{\partial uH}{\partial x} + \frac{\partial vH}{\partial y} = p \quad (2.1)$$

$$H(x, y, t) = \zeta(x, y, t) + b(x, y) \quad (2.2)$$

Where:

$H(x, y, t)$	water depth [m]
$\zeta(x, y, t)$	water surface elevation measured from the undisturbed water surface [m]
$b(x, y)$	bathymetry measured positive downward from the undisturbed water surface [m]
$u(x, y, t)$	depth-averaged flow velocity in the x-direction [m/s]
$v(x, y, t)$	depth-averaged flow velocity in the y-direction [m/s]
$p(x, y, t)$	source or sink term (e.g., precipitation) [m/s]
$t$	time [s]

The continuity equation describes that the changes in the water depth (first term) are balanced by the divergence of the volume in the x-direction (second term) and y-direction (third term). Moreover, water can flow in or out the system due to a source or sink term (fourth term).

Assuming that the Coriolis force and eddy viscosity are negligible, the conservation of momentum in both horizontal directions is described by:

$$\frac{\partial u}{\partial t} + u \frac{\partial u}{\partial x} + v \frac{\partial u}{\partial y} + g \frac{\partial \zeta}{\partial x} + \frac{c_f}{H} u |u| = 0 \quad (2.3)$$

$$\frac{\partial v}{\partial t} + u \frac{\partial v}{\partial x} + v \frac{\partial v}{\partial y} + g \frac{\partial \zeta}{\partial y} + \frac{c_f}{H} v |u| = 0 \quad (2.4)$$

Where:

$g$	gravitational acceleration (=9.81 m s <sup>-2</sup> )
-----	---

$c_f$  bottom friction coefficient [-]

The momentum equations represent a balance of the local inertia (first term), the convective inertia (second and third term), the hydrostatic pressure (fourth term) and the bottom friction (last term).

### 2.3 2D HYDRODYNAMIC MODELLING SOFTWARE

2DH hydrodynamic models are the most widely used models for simulating flood events (Ghostine et al., 2015; Hunter et al., 2007; Teng et al., 2017). In these models, flow is modelled in the two horizontal dimensions and the assumption is made that the water depth is small compared to the other two dimensions (Bates, 2022; Chevion & Moussa, 2016; Teng et al., 2017). There is a wide variety of 2D hydrodynamic modelling packages which numerically solve the 2D shallow water equations or approximations to these equations (Bates, 2022; Hunter et al., 2007; Jodhani et al., 2022; Mudashiru et al., 2021; Teng et al., 2017).

One of these modelling packages is 3Di, developed by a consortium of Nelen en Schuurmans, Deltares, TU Delft and Stelling Hydraulics, which will be used in this study. 3Di solves the full 2D depth-averaged shallow water equations including a subgrid method. This method accounts for high resolution information of the modelling domain. This includes information of the bathymetry and roughness. Furthermore, the subgrid technique does not significantly increase the computation costs while it strongly improves the accuracy of the simulation results (Casulli, 2009; Volp et al., 2013). This improvement in the accuracy is caused by the way spatial information of the modelling domain is considered in subgrid-based models compared to conventional models. In a conventional model, information of the modelling domain is averaged over the computational cells. If the computational cell size is increased, more and more spatial resolution is lost which causes a less accurate representation of the modelling domain and thereby of the simulated flow processes. In a subgrid-based model, spatial data is not averaged over the larger computational grid cells, but is incorporated in the model via the higher-resolution subgrid, so spatial resolution is not lost.

In its computations in the cloud, 3Di considers bathymetric and roughness variations which have a smaller scale than the computational cells. As a varying surface elevation in a computational cell is allowed, the computational cell can be partly wet, completely wet or completely dry as can be seen in Figure 5 (Volp et al., 2013).

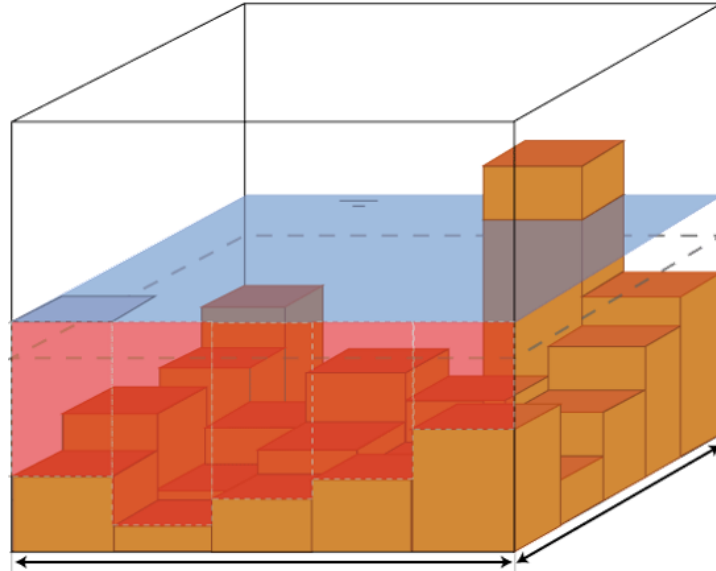


Figure 5 A schematic view a computational grid cell (large cube) with bathymetry (orange blocks) defined on the underlying subgrid where a part of the computational grid cell is dry. Figure edited from Nelen en Schuurmans (2022).

The model uses a structured, staggered computational grid. The computational cells are perfect squares where water levels are computed in the centres of these computational cells (blue dots in Figure 6) and the flow velocities at the cell edges (blue bars in Figure 6). At some locations, a finer resolution of the computational grid may be required due to, for example, more complex flow. In 3Di, the grid can be refined. For refining grid cells, 3Di uses a method called quad-tree refinement. In this method, the to be refined computational cells are divided by a factor 4 compared to the neighbouring cells (see right top corner in Figure 6) (Nelen & Schuurmans, 2022).

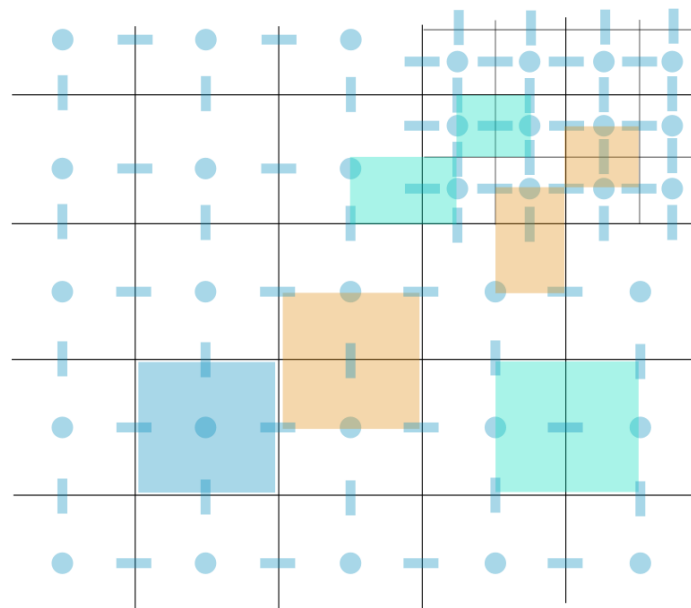


Figure 6 Structured, staggered 2D grid including a refinement which is used in 3Di. Water levels are defined at the cell centres (blue dots) and velocities at the cell edges (blue bars). The water level domain is indicated by blue areas, and the momentum domains by green and orange areas (Nelen & Schuurmans, 2022).

Roads and other higher line elements can have large effects on the inundation pattern in an area (de Bruijn et al., 2018; Prinsen et al., 2020). Therefore, it is important to properly schematize these objects. Although high resolution elevation is considered in 3Di, only higher line elements that are located at the computational cell edges are detected and will block the flow. The other higher line elements will leak which means that pixels downstream of the higher line elements will get wet while this is not expected. This happens because within a computational cell, all subgrid pixels that have a lower elevation than the uniform water level in the computational cell will get wet. In this way, line elements are bypassed. 3Di accounts for higher line elements within computational cells by defining obstacles which should be given explicitly to the model (green line in Figure 7). These obstacles are defined by a line segment and an elevation which are placed over a computational cell. For 2D flow links (blue dashed lines in Figure 7) that are crossed by the obstacle (thick red lines in Figure 7), the obstacle height is used instead of the ground elevation as the exchange level. This means that water will only flow to computational cells behind the obstacle if the water level in the computational cell in front of the obstacle is higher than the elevation of the obstacle.

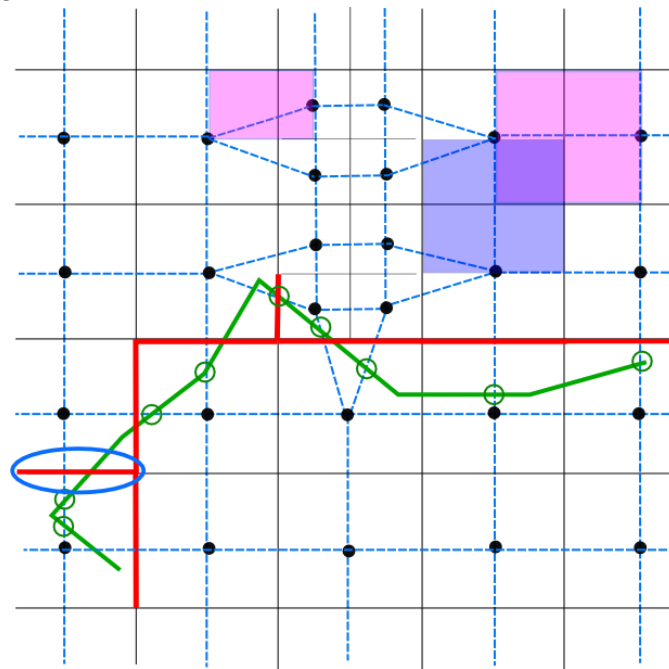


Figure 7 Example of a computational grid including local grid refinements and an obstacle. The momentum domains are indicated by the blue and pink planes. The drawn obstacle elements are given with a green line and the flow links with a dashed blue line. The flow links closed by the obstacle are indicated by a thick red line (Nelen & Schuurmans, 2022)

### 3. METHODOLOGY

---

In this chapter, the methodology which is used in this study to answer the research questions, is explained. A schematic representation of the method is shown in Figure 8. The method consists of seven steps, which can be summarized as follows:

1. In the first step, the model schematisation is set up which contains most information about the spatial domain. Missing key elements were added to the elevation raster and obstacles were defined. Based on the model schematisation, a hydrodynamic model is built by 3Di.
2. The final computational grid settings (overall grid size and grid refinements) were determined based on a sensitivity analysis. In this analysis, the effect of computational grid size on the inundation pattern and the computational time (wall-clock time) was determined. Based on the final grid settings, a computational grid is made within the hydrodynamic model.
3. Scenarios were defined to run simulations with the developed hydrodynamic model. Every scenario represents a dike breach at another location in the primary flood defence of the study area. 15 potential dike breach locations were selected based on the studies presented in Section 2.2.1. The dike breach locations are numbered according to the distance to the Dutch-German border along the primary dike. Furthermore, for all scenarios, the same initial and boundary conditions and inflow hydrograph were defined. This was done to minimize the number of uncertainties in the analysis and to keep the focus on the sensitivity of the inundation pattern to the dike breach location. The inflow hydrograph represents the inflow from the dike breach into the study area.
4. Every scenario is simulated using the set up 3Di hydrodynamic model. The simulation time of every simulation was 3 days based on advice of an expert at the waterboard (G. van den Houten, personal communication, May 20, 2023). According to this expert, the first three days of an inundation are the most important days for evacuation purposes as water tends to stop rising or already even falls and flows back to the river after around three days. The dike breach was initiated directly at the start of the simulation. The simulations are numbered after the corresponding dike breach locations. In the post-processing of the simulation results, three types of maps were generated, namely maximum inundation extent maps, arrival time maps and maximum water depth maps.
5. The maximum inundation extents of the different simulations were qualitatively compared. Based on the comparison, clusters of dike breaches which resulted in qualitatively similar inundation extents were made. These clusters were used in the quantitative part of the analysis.
6. For every cluster, the spatial sensitivity of the arrival times to the dike breach location in the cluster is analysed. As an indicator of this sensitivity, the Mean Absolute Difference (MAD) of the arrival times of the different simulations in the cluster was computed for every inundated location in the hinterland. In the computation of the MAD, every simulation is compared to every other simulation only once. If the MAD is higher than six hours at a certain location, the arrival time at this location is (very) sensitive to the dike breach location in the cluster. The six hours were based on advice of G. van den Houten (personal communication, May 20, 2023).
7. For every cluster, the spatiotemporal sensitivity of the maximum water depths to the dike breach location in the cluster is analysed. For every inundated location in the hinterland, the MAD of the maximum water depths at every day of the different simulations in the cluster was computed. The MAD served as an indicator for the sensitivity of the maximum water depths to the dike breach location. If the MAD is higher than 20 cm, the maximum water depth at this location and moment in time is (very) sensitive to the dike breach location in this cluster. The 20

centimetres were based on advice of G. van den Houten (personal communication, May 20, 2023).

The steps of the method are described in more detail in the following sections. Beforehand, the study area and the used data are introduced.

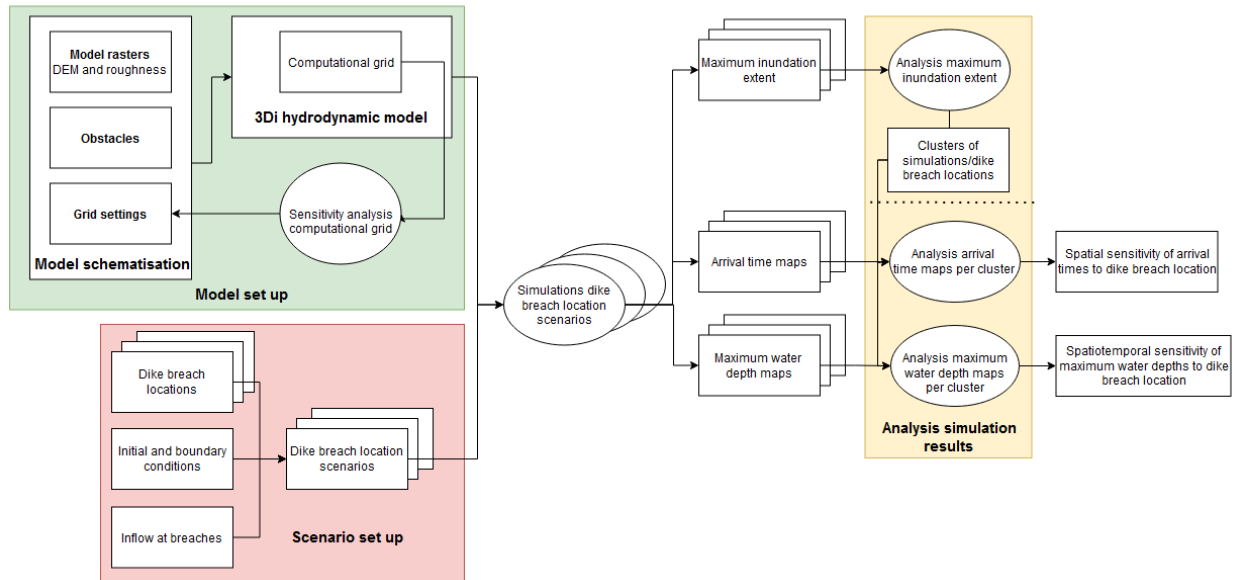


Figure 8 Flowchart of the used method

### 3.1 CHARACTERISTICS OF THE STUDY AREA

Dike ring 48 is used as the case study (Figure 9). This dike ring is mainly situated in the province of Gelderland in the Netherlands and is part of the management area of waterboard Rijn en IJssel. The other part of the dike ring is situated in Germany. The German part of the dike ring is not completely used as a study area, because it is expected that in case of a dike breach in the Dutch part, water will not flow east of Rees. This expectation is based on inundation maps presented in Arends and Bisschop (2014) and Prinsen et al. (2020) and the higher elevation in this area compared to the rest of the study area as can be seen in Figure 10. The dike ring is protected by primary dikes along the Rhine, Pannerdensch Kanaal, IJssel and Oude IJssel. After crossing the German-Dutch border, the Rhine bifurcates in the Pannerdensch Kanaal and the Waal. The Pannerdensch Kanaal flows roughly to the northwest and bifurcates into the IJssel and Nederrijn at Westervoort. The Oude IJssel is a tributary of the IJssel and flows into the IJssel at Doesburg.

Arends and Bisschop (2014) and Prinsen et al. (2020) thoroughly describe the main characteristics of dike ring 48. The most important characteristics of the study area that influence the inundation are the elevation, local obstacles, land use and waterbodies. The elevation in the area mainly ranges between 6 and 20 m+NAP. Yet, Montferland in the middle of the study area is a hilly area with an elevation up to 85 m+NAP. The elevation to the east of the Montferland and the German part of the study area is higher than to the west of the Montferland. The elevation in the study area can be seen in Figure 10. Major (elevated) infrastructure objects in the area are the highways A12/A3 and A18, the railway lines Arnhem-Zevenaar-Emmerich-Oberhausen, Zevenaar-Doetinchem-Winterswijk and the freight railway Betuweroute. Along the two highways in the area, several larger business areas are located. Furthermore, larger urban areas in the dike ring are Westervoort, Duiven, Zevenaar, Didam, Doetinchem and Emmerich am Rhein. Outside these urban areas, the land use in the dike ring is mainly agricultural

(livestock farming and arable farming). The study area also contains several large waterbodies. The most noteworthy waterbody is the Rijnstrangen area which contains a former course of the Rhine and is completely enclosed by dikes.

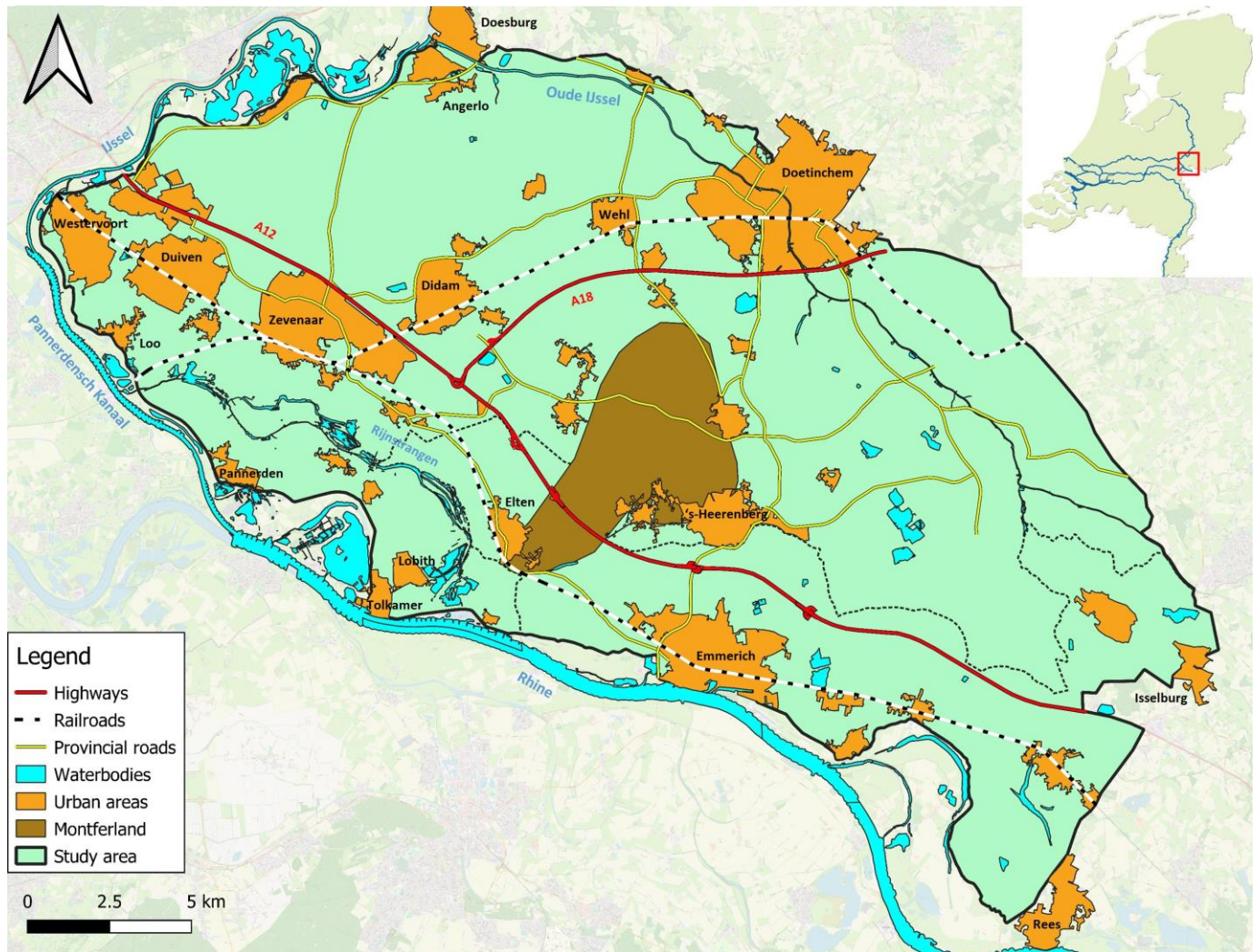


Figure 9 Map of study area: dike ring 48. The dotted line is the Dutch-German border.

### 3.2 DATA

In order to set-up an accurate hydrodynamic model in 3Di which can simulate inundation patterns, several datasets are needed. An overview of the used datasets is given below.

Firstly, for the elevation in the study area, two datasets were used. For the elevation in the Dutch part of the study area, a digital elevation model (DEM) of the Netherlands (AHN4: *Algemeen Hoogtebestand Nederland*) was utilized (PDOK, n.d.-a). The Dutch DEM has a resolution of  $0.5 \times 0.5 \text{ m}^2$ . For the German part of the dike ring, the DEM of the state North Rhine-Westphalia was used which has a resolution of  $1 \times 1 \text{ m}^2$  (Geodateninfrastruktur NRW, n.d.). In both DEMs, the ground elevation of buildings is used. The ground elevation is used as it is expected that in case of an inundation, water will enter the buildings and will fill the buildings. Therefore, using the roof level would result in an overprediction of the water level as the storage in the area is underpredicted. The DEM of the study area is shown in Figure 10.

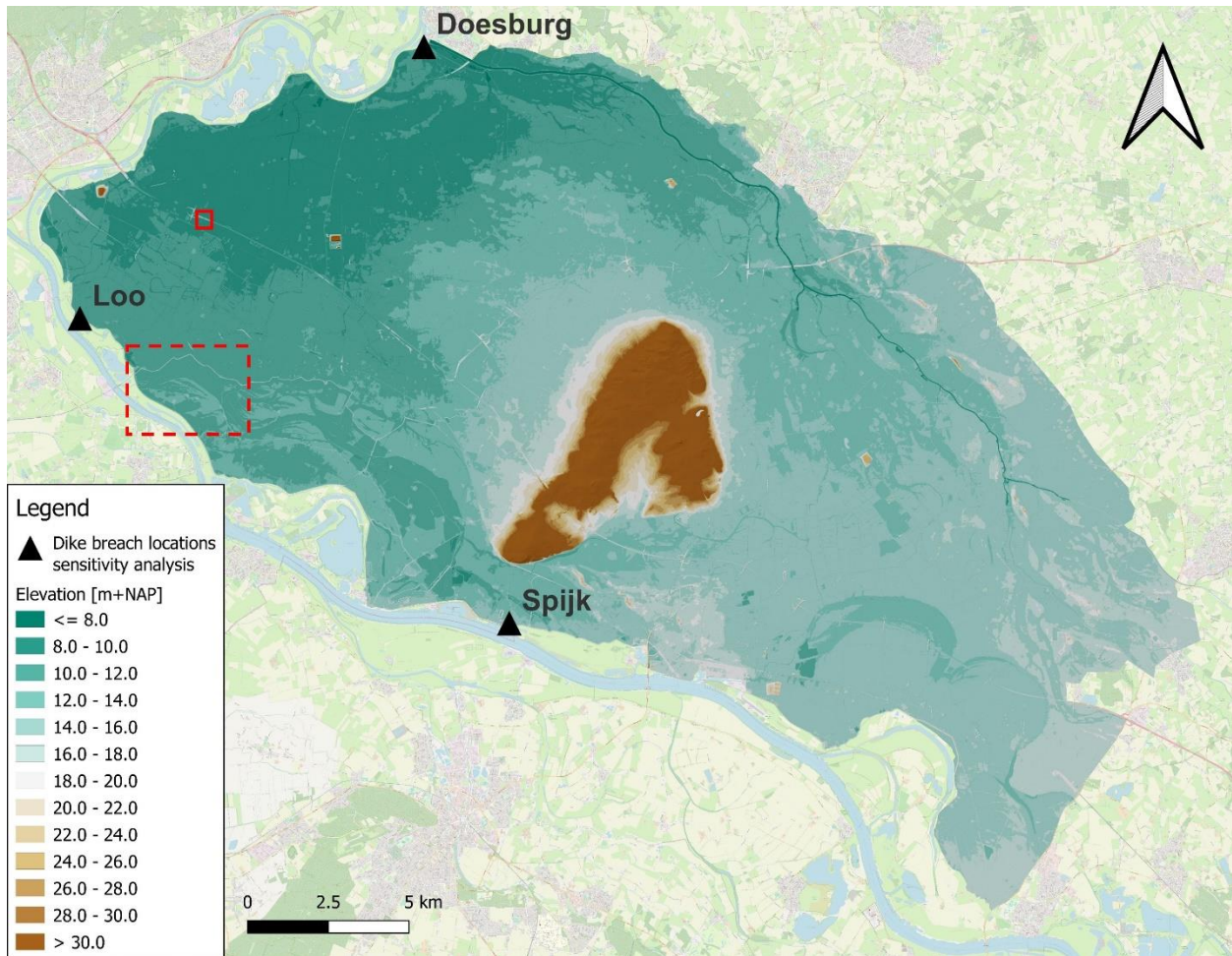


Figure 10 DEM of the study area and the dike breach locations that are used in the sensitivity analysis of the computational grid. In this DEM, the bottom elevation of the Oude IJssel and the underpasses in the obstacles are adjusted. The red boxes are the locations of the close-ups in Figure 11 (solid line) and Figure 12 (dashed line).

Secondly, land use data were used to determine the roughness coefficient as recommended by de Bruijn et al. (2018). For the Dutch part of the dike ring, the dataset LGN (Landelijk Grondgebruik Nederland) which is a map of the land use in the Netherlands was utilised (Wageningen Environmental Research, n.d.). The resolution of this land use map was  $0.5 \times 0.5 \text{ m}^2$ . For the German part of the study area, a map with land use was extracted from a global land cover map provided by European Space Agency (ESA, 2020). The resolution of this map is  $10 \times 10 \text{ m}^2$ . Next to a low resolution, another downside of this map is the low number of land use classes. This means that roads and houses felt in the same category while they have a different roughness. As no better options were available, this land use map was utilised. A conversion table was used to convert land use to Manning's roughness coefficient. This table can be found in Appendix A.

Both roads and underpasses are important for determining the location of the local obstacles and the openings in these objects. Therefore, a dataset of the Dutch physical environment (Basisregistratie Grootschalige Topografie, BGT) which contains the locations and dimensions of the underpasses and the location of the roads in the Netherlands was used (PDOK, n.d.-b). On top of this, the waterboard provided a dataset with additional underpasses which were not part of the BGT. Lastly, a graph of the daily measured water levels in the Oude IJssel was used to determine the initial water levels in the Oude IJssel (Waterschap Rijn en IJssel, 2023).

### 3.3 MODEL SET-UP

Within 3Di, a 2DH hydrodynamic model of the dike ring was developed to simulate dike breach-induced inundations. This model was based on a model schematisation which includes model rasters, 1D and 2D elements and several settings. Two model rasters were used, namely an elevation and a roughness raster. Two missing key elements were added to the elevation raster (Section 3.3.1). Furthermore, obstacles were defined which are 2D elements (Section 3.3.2). No 1D elements were added to the model schematisation. Settings about computational grid refinements and overall grid size were determined based on a sensitivity analysis (Section 3.3.3). In the hydrodynamic model, the computational grid is built based on these settings.

#### 3.3.1 Model rasters

To simulate flow in a two-dimensional plane, the model requires information about elevation and roughness in the area. To define the elevation in the area, the DEM of the Dutch and German part were combined. In order to keep the rasters manageable on the used computer, the DEM was defined on a resolution of  $2 \times 2 \text{ m}^2$ . Based on the land use maps, a roughness map was defined on the same resolution as the DEM.

Two key elements were added to the DEM, namely the Oude IJssel (waterway) and underpasses. The Oude IJssel was added to the DEM by lowering the elevation at all subgrid pixels of the Oude IJssel by 3.5 m which is the average depth of the Oude IJssel (Hoorweg, 2014). This adjustment was made to ensure that the storage of Oude IJssel was correctly incorporated. For all other waterbodies in the area, the elevation of the water level as present in the DEM was used as the bottom level. Based on the datasets with underpasses (BGT and dataset of the waterboard) and the DEM, the bottom elevation of underpasses with an unrealistic bottom level was adjusted. This adjustment of the elevation was done to enable flow of the water through the underpasses at the correct elevation and to avoid artificial blockage. The difference in elevation of an underpass before and after adjusting the bottom level of underpass in the DEM can be seen in Figure 11.

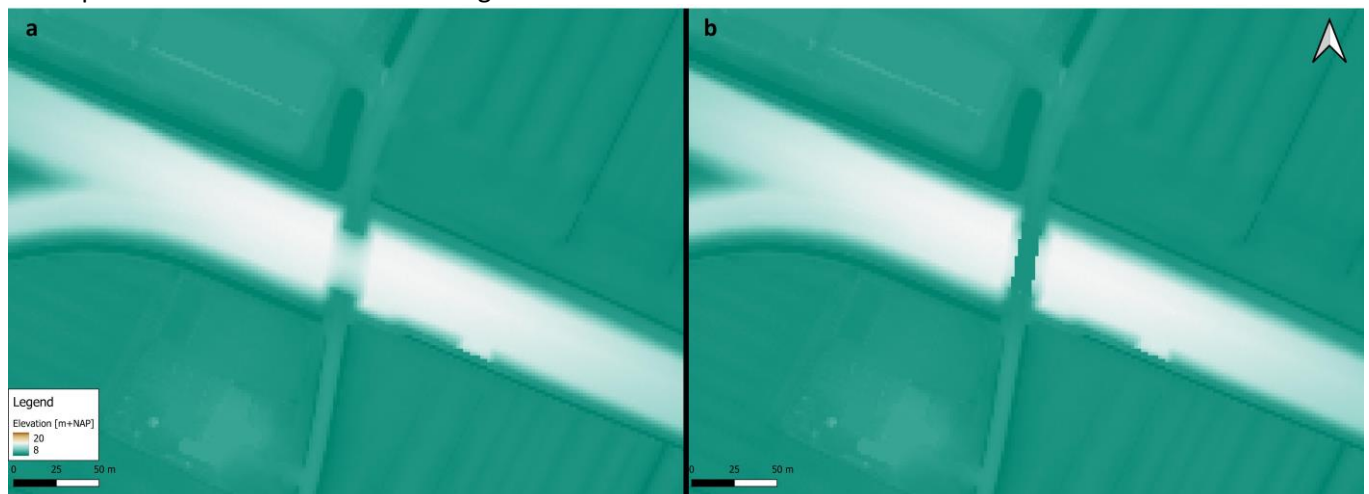


Figure 11 Example of an underpass (a) before and (b) after adjusting the bottom elevation of underpass in the DEM. The location of this close-up is shown as the red box with solid lines in Figure 10.

#### 3.3.2 Obstacles

As mentioned in Section 2.3, higher line elements should be explicitly given to the modelling software to prevent leakage. Therefore, the DEM was studied for higher line elements which were subsequently added as obstacles. Moreover, a tool within 3Di was used to detect leaking elements which were 0.5

metres higher than the surroundings area. It was assumed that this elevation difference is enough to block flow for a period and that smaller elevation differences do not significantly contribute to slowing down inundation. If these leaking elements were located on roads (found in the BGT) or small dikes, they were also added as flood obstacles. For all obstacles, it was assumed that they can only overflow and will not fail. A map with all obstacles can be found in Figure 47 in Appendix B.

### 3.3.3 Computational grid

A sensitivity analysis of the computational grid size was executed to determine the effect of the grid size on the inundation pattern and the computational time (wall-clock time). Based on the outcomes of this sensitivity analysis, the overall computational grid size and the grid refinements were determined. The sensitivity analysis was split into two phases. In the first phase, a simulation of a dike breach at Loo was run (for this location: see Figure 10). The dike breach was modelled as a point source with a constant discharge of 1000 m<sup>3</sup>/s and the simulation time was 3 days. A point source with a constant discharge was chosen to reduce the number of uncertainties in the comparison. The described scenario was run for different grid resolutions, namely 80×80 m<sup>2</sup> (Model 80), 100×100 m<sup>2</sup> (Model 100) and 160×160 m<sup>2</sup> (Model 160). As a reference, a simulation of this scenario was run with a grid size of 40×40 m<sup>2</sup>, because it is assumed that the model with the finest grid resolution produces the most accurate results. The differences in the water depths and arrival times between the grids and the reference simulation were analysed to determine the effect of the grid size on these variables. The results of this analysis are presented in Section 0. Based on this analysis and the computational time of the different grids, one of the three grids was selected which was further analysed in the second phase.

In the second phase, it was verified if the selected computational grid size also provided accurate results for inundation patterns at other locations. Simulations of a dike breach at Doesburg and at Spijk (for these locations: see Figure 10) with the same constant discharge as in the first phase were run. This flood event lasted 5 days, because this enabled the water to flow further inland than for a shorter event. In this way, the accuracy of the model results at locations deeper inland could also be determined. Based on the differences in the water depths and arrival times between the selected and the reference grid, the selected grid was locally refined. The results of this second phase can be found in Section 4.2.

Based on the results of the sensitivity analysis of the computational grid (see Chapter 4), the main part of the study area was assigned a grid resolution of 64×64 m<sup>2</sup>. The grid resolution in Montferland was kept coarser at 256×256 m<sup>2</sup> as it is expected based on the elevation of this area and the inundation maps presented in Arends and Bisschop (2014) and Prinsen et al. (2020) that this area will not be inundated. Furthermore, grid refinements were implemented near all underpasses based on their width. The computational grid was also refined near waterways in the study area which have embankments at both banks. The grid resolution near the underpasses and the waterways can be found in respectively Table 4 and Table 5 in Appendix C. A close-up of the final computational grid with grid refinements around De Keel and around underpasses in and openings between obstacles can be found in Figure 12. The location of this close-up can be found as the red box with dashed lines in Figure 10.

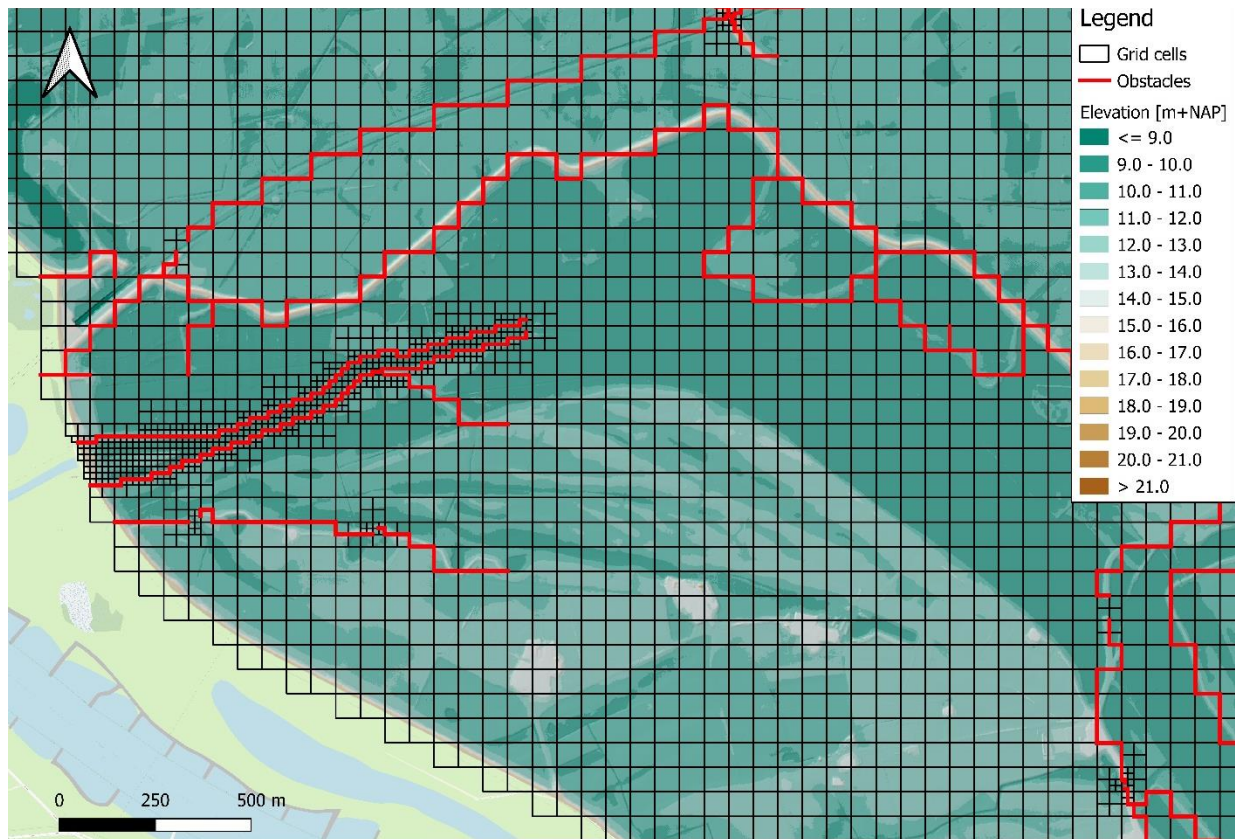


Figure 12 Close-up of the final computational grid with grid refinements around De Keel and around openings between and underpasses in obstacles. The location of this close-up can be found as the red box with dashed lines in Figure 10

### 3.4 SCENARIO SET UP

Scenarios were defined to run simulations with the developed hydrodynamic model. Every scenario represents a dike breach at another location in the primary flood defence of the study area. Potential dike breach locations were selected (Section 3.4.1). Furthermore, for all scenarios, the same inflow hydrograph (Section 3.4.2) and initial and boundary conditions (Section 3.4.3) were defined. After definition of the scenarios, the scenarios were simulated in the cloud using the set up hydrodynamic model. The length of every simulation was 3 days and the dike breach was initiated directly at the start of the simulation. This simulation length was chosen based on the advice of an expert at the waterboard (G. van den Houten, personal communication, May 20, 2023). He stated that the first three days of an inundation are the most important days for evacuation purposes as water tends to stop rising or already even falls and flows back to the river after around three days. The simulations were numbered after the corresponding dike breach locations. So, simulation 2 corresponds to dike breach location 2.

#### 3.4.1 Selected dike breach locations

For this study, a set of potential dike breach locations is selected based on the studies of Arends and Bisschop (2014), de Bruijn et al. (2014) and Apel et al. (2009) which were introduced in Section 2.2.1. Arends and Bisschop (2014) and de Bruijn et al. (2014) found that the primary dikes around the study area can be divided into six dike sections. The final inundation extent and flood damage are almost independent of the exact breach location within each section. Furthermore, based on the study of Apel et al. (2009), it can be concluded that dike segments in the Lower Rhine area where inundation patterns are independent of the exact breach location within the segment are at least 1 km long.

Based on these studies, the decision was made to include at least two potential dike breach locations per dike section which were defined by Arends and Bisschop (2014). This was done in order to cover all potential inundation patterns at least twice. As the first four dike sections are shorter, a dike breach location was selected every two kilometres in these four sections. Yet, the fifth and sixth dike section are longer. Therefore, in the fifth and sixth dike section, the dike breach locations were spaced four kilometres apart. The resulting dike breach locations are shown in Figure 13. The dike breach locations are numbered according to the distance to the Dutch-German border along the primary dike. So, dike breach location 2 is 2 km away from the Dutch-German border.

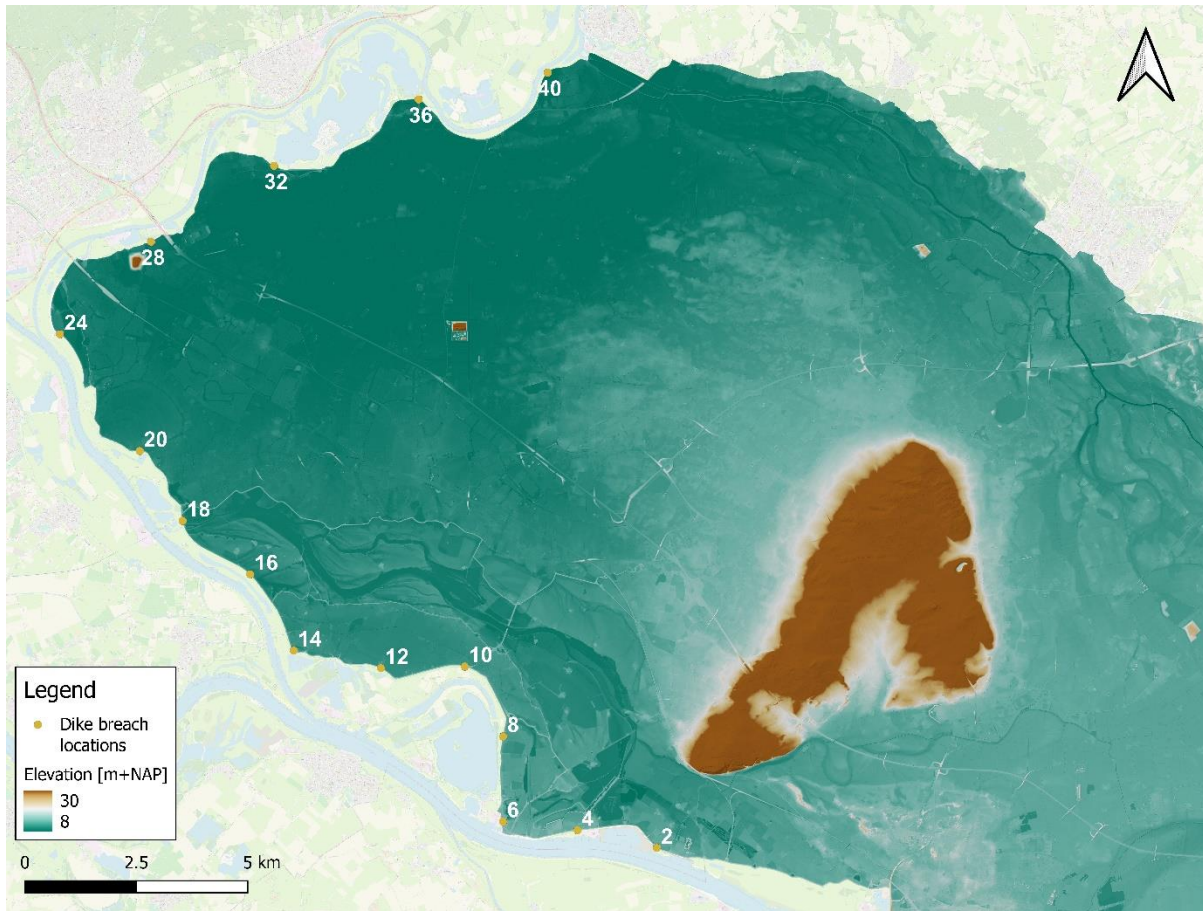


Figure 13 Selected dike breach locations. The dike breach locations are numbered according to the distance to the Dutch-German border along the primary dike.

### 3.4.2 Schematisation breaches and inflow hydrograph

All breaches were schematized as a point source with an imposed inflow hydrograph. The choice was made to use the same inflow hydrograph for every dike breach location, because using a breach model with a water level boundary condition would have added extra uncertainties to the analysis. This used inflow hydrograph can be found in Figure 14. The inflow hydrograph only covers three days as this is the simulation length.

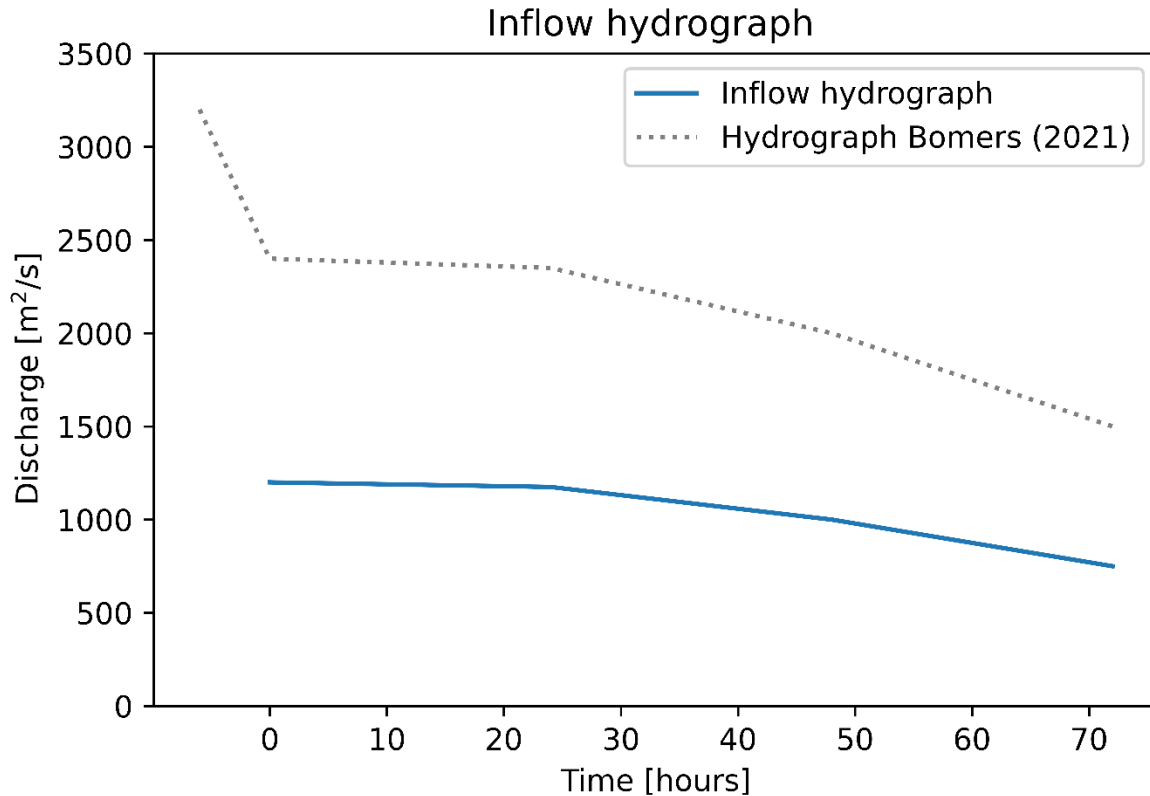


Figure 14 Inflow hydrograph used at every dike breach location in this study and a part of the breach outflow hydrograph used in Bomers (2021)

The used inflow is based on a hydrograph as presented in Bomers (2021) of which a part is shown in Figure 14. Bomers simulated the outflow hydrograph of potential dike breaches in the Lower Rhine area using a hydrodynamic model. One of the simulated dike breaches was in the western part of the study area. To obtain the outflow hydrograph of this breach, Bomers (2021) used a constant breach width of 150 metres. However, this is quite wide for breaches in the Lower Rhine area based on historical data of Verheij and Van der Knaap (2003) and Apel et al. (2008). Bomers et al. (2019) combined these two datasets and determined that the average breach width in these datasets was 75 m. Therefore, in this study, the discharge of the presented outflow hydrograph is halved as the width is two times smaller than in Bomers (2021). This is in accordance with modelling results of Tadesse and Fröhle (2020) which showed that by halving the breach width, the breach discharge was also approximately halved. Furthermore, the initial sharp peak in the data of Bomers (2021), which can be seen in Figure 14, was not used. This peak was not present in other literature which simulated dike breach outflow in the same region (e.g., Mooijaart, 2023; Prinsen et al., 2020). The used inflow hydrograph in this study resulted in almost the same cumulative inflow volume after three days for a similar breach width as in Prinsen et al. (2020) (275 Mm<sup>3</sup> vs. 280 Mm<sup>3</sup>). Using the initial peak in the data of Bomers (2021) would have resulted in a cumulative inflow volume of 300 Mm<sup>3</sup> after 3 days.

### 3.4.3 Initial and boundary conditions

For most of the study area, it is assumed that at the start of the simulation, the surface is dry which means that no parts of the study area initially flooded. Moreover, it is assumed that the soil is completely saturated which means that no water can infiltrate into the soil. For the Oude IJssel, initial water levels were prescribed which can be found in Table 6 in Appendix B.

The boundaries of the model domain were closed boundaries. This means that no water will flow to the dike ring 49 which is the dike ring to the north of dike ring 48. Furthermore, this means that it is assumed that all outlets from the dike ring to the Rhine, Pannerdensch Kanaal and IJssel are closed and therefore do not discharge water to these waterways.

### 3.5 ANALYSIS OF THE SIMULATION RESULTS

During all simulations, the water levels in every computational grid cell and at every timestep were stored. After every simulation, the stored water levels were post-processed during which water depth maps were generated. The water depth is computed as the difference between the water level and the surface elevation. As the surface elevation (DEM) is defined on the subgrid, the water depth is also computed per subgrid pixel. Based on the computed water depths, arrival time maps were generated for every simulation. The arrival time in these maps is defined as the first instance in time when a subgrid pixel is inundated. In post-processing, a pixel is indicated as inundated when the water depth is  $1 \times 10^{-4}$  m. After post-processing, three types of maps were analysed. Firstly, for each simulation, maps with the maximum inundation extent were analysed. As no water can flow out of the study area due to the prescribed initial (no infiltration) and boundary conditions, water keeps flowing into the study area due to the prescribed discharge hydrograph. Therefore, the maximum inundation extent is the final inundation extent at the end of day 3. Secondly, the arrival time maps were analysed. The last type of maps which were analysed were three maps with the maximum water depths at  $t = 1, 2$  and 3 days. These analyses are discussed in the sections below.

#### 3.5.1 Analysis maximum inundation extent

The first step in the analysis was to qualitatively compare the maximum inundation extent of the different simulations by visual inspection. Based on the comparison, clusters of simulations with qualitatively similar inundation extents were made. These clusters are selected for the quantitative analysis of the arrival times and maximum inundation water depths.

#### 3.5.2 Analysis arrival times

The objective of this part of the quantitative analysis is to determine the spatial sensitivity of the arrival times to the dike breach location in a certain cluster. The clusters were determined in the qualitative part of the analysis and include simulations with qualitatively similar inundation extents. The differences in the arrival times of the different simulations in the cluster at a certain location are an indicator for the sensitivity of the arrival time at this point. Differences in arrival times tend to become significant when they are close to or larger than six hours. According to G. van den Houten (personal communication, May 20, 2023), the safety region makes evacuation plans based on the expected arrival times of the flood in the area. The safety region is a public body in the Netherlands which is tasked with regulating and administering emergency services during crisis situations. In their evacuation plans, the safety region uses intervals of six hours. This means that people who live in areas which will be flooded in the first six hours will be evacuated together in the first six hours. People who live in areas which will be flooded in the second six hours will be evacuated together afterwards. Therefore, if differences in arrival times between the different simulations at one location become larger than six hours, people at this location will certainly be evacuated either too early or too late.

To quantify the differences in the arrival times, the Mean Absolute Difference (MAD) of the arrival times of all simulations in a certain cluster was computed. The MAD at a certain location gives an indication of the sensitivity of the arrival time at this location. If, at a certain location in the inundated area, the MAD is lower than six hours, there is no small average difference in the arrival time of the different

inundations at this location. If there is a small average difference, arrival times at this location will be almost the same for all compared inundations. This means that the arrival time at this location is not (very) sensitive to the dike breach location in this cluster. If the MAD is higher than six hours, this means that the arrival time at this location is (very) sensitive to the dike breach location in this cluster.

The used equation of the MAD is as follows:

$$MAD_x = \frac{\sum_{N_j} \sum_{N_k} |T_{x,j} - T_{x,k}|}{\frac{1}{2} N_j (N_j - 1)} \quad (3.1)$$

Where:

- $T_{x,j}$  arrival time at point  $x$  of the inundation caused by dike breach location  $j$  [s]
- $N_j$  number of all dike breach locations in a cluster
- $J$  all dike breach locations in a cluster
- $N_K$  number of dike breach locations in set  $K$
- $K$  set with all dike breach locations in cluster which are further away from the Dutch-German border than dike breach location  $j$

This equation can be explained using an example. One of the clusters contains four dike breach locations with qualitative similar maximum inundation extents: dike breach location 2, 4, 6 and 8. In this case, dike breach location 2 is the closest to the Dutch-German border,  $J = \{2,4,6,8\}$  and  $N_j = 4$ . Furthermore, if  $j = 2$ , then  $K = \{4,6,8\}$ , if  $j = 4$ , then  $K = \{6,8\}$ , if  $j = 6$ , then  $K = \{8\}$  and if  $j = 8$ , then  $K = \{\}$ . This means that in fact the sum of all cells above the main diagonal in the following matrix is calculated. In this way, the arrival time of each simulation is compared to the arrival time in every other simulation in the cluster only once.

		$K$			
		2	4	6	8
$J$	2	-	$ t_{x,2} - t_{x,4} $	$ t_{x,2} - t_{x,6} $	$ t_{x,2} - t_{x,8} $
	4	-	-	$ t_{x,4} - t_{x,6} $	$ t_{x,4} - t_{x,8} $
	6	-	-	-	$ t_{x,6} - t_{x,8} $
	8	-	-	-	-

Equation 3.1 was based on the equation of the Mean Absolute Error (MAE). The MAE is often used in literature to compare simulated variables (e.g., water depth) between two different models or between a model and measurements (e.g., Kadir et al., 2019; Papanicolaou et al., 2010; Pasquale et al., 2014; Pinos & Timbe, 2019). The equation of MAE was adjusted for this study to be able to compare results of multiple simulations at one location instead of comparing the results of two simulations at multiple locations.

### 3.5.3 Analysis maximum water depths

The objective of this part of the quantitative analysis is to determine the spatiotemporal sensitivity of the maximum water depth for the dike breach location in a certain cluster. The differences in the maximum water depths of the different simulations in the cluster at a certain moment in time and location are an indicator for the sensitivity of the maximum water depth at this point in time and space. According to G. van den Houten (personal communication, May 20, 2023), differences in maximum water depths tend to become significant when they are close to or larger than 20 cm. To quantify the differences in the maximum water depths, the MAD of the water depths of all simulations in a certain cluster was computed. This was done at three moments in time, namely at the end of day 1, day 2 and day 3. The MAD at a certain location and moment gives an indication of the sensitivity of the maximum water depth at this location and moment. If, at a certain location and moment in time, the MAD is lower than 20 cm,

the maximum water depth at this location and moment is not (very) sensitive to the dike breach location in this cluster. However, if the MAD is higher than 20 cm, the maximum water depth at this location and moment in time is (very) sensitive to the dike breach location in this cluster. The same type of equation as for computing the MAD for arrival times was used to calculate the MAD for the water depths:

$$MAD_{x,t} = \frac{\sum_{N_j} \sum_{N_k} |h_{x,t,j} - h_{x,t,k}|}{\frac{1}{2} N_j (N_j - 1)} \quad (3.2)$$

Where:

$h_{x,t,j}$  water depth at point  $x$  at moment  $t$  of the inundation caused by dike breach location  $j$  [m]

## 4. RESULTS OF THE SENSITIVITY ANALYSIS OF THE COMPUTATIONAL GRID

In Figure 15, an impression of the inundation patterns of simulated dike breaches at Loo and Spijk using the reference model is given. These simulations were used in the sensitivity analysis of the computational grid.

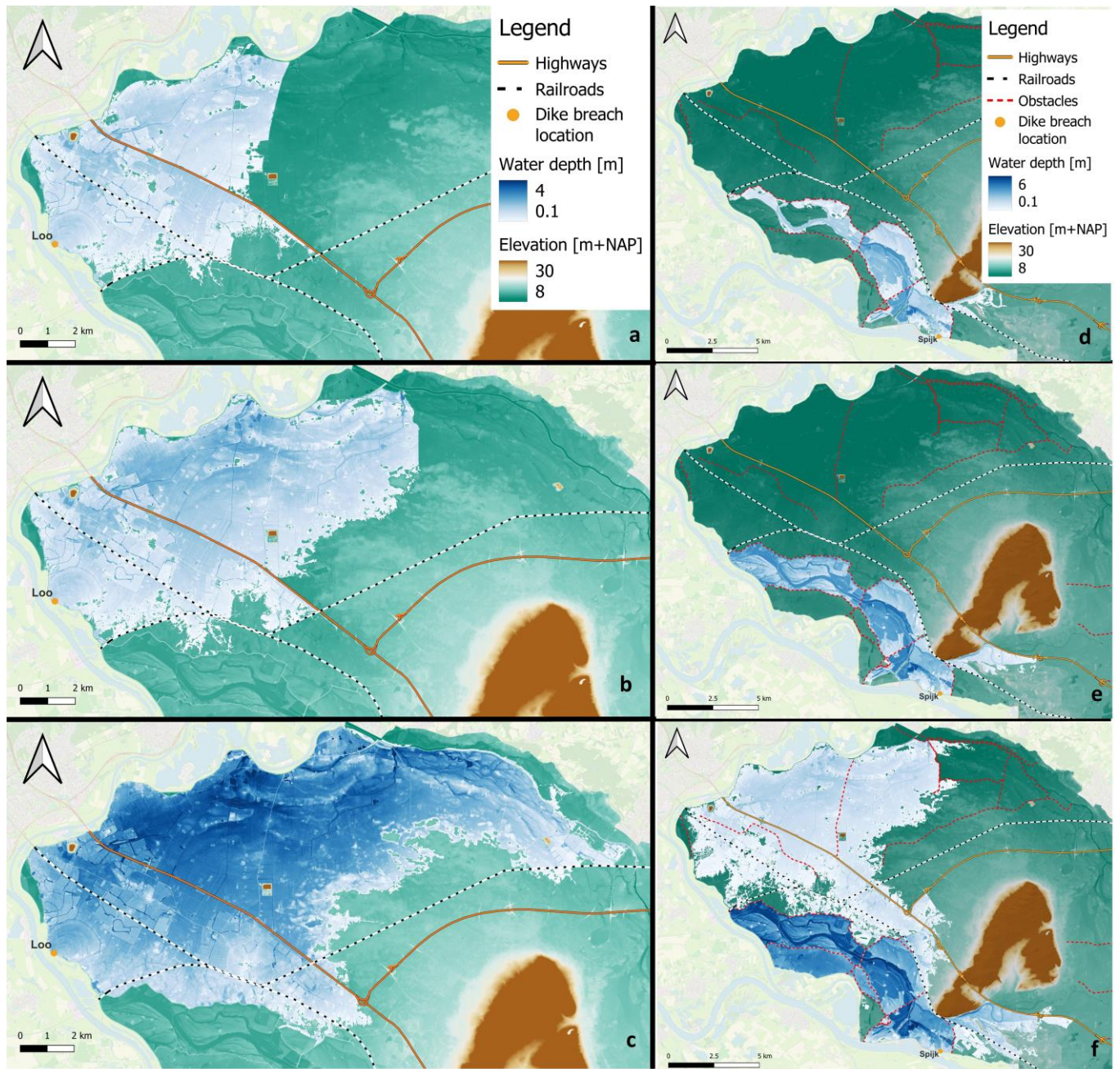


Figure 15 Inundation patterns of inundations starting at Loo (a-c) and at Spijk (d-f). Inundation water depths are shown after 12 hours (a and d), 1 day (b and e) and 3 days (c and f). These inundation patterns are simulated using the reference model.

#### 4.1 FIRST PHASE: DIKE BREACH AT LOO

The computational time of the simulations performed with the different grid sizes in the first phase can be found in Table 1.

Table 1 Computational time of three-day simulations performed with the different grid sizes for a dike breach at Loo. Computational time is based on calculations of 3Di in the cloud.

	Grid size [m <sup>2</sup> ]	Computational time [h]
Reference model	40×40	16.40
Model 80	80×80	3.61
Model 100	100×100	2.68
Model 160	160×160	1.00

In Figure 16a, differences in the water depth after 12 hours between model 80 and the reference model are shown. Positive differences (blue) indicate that the water depth in model 80 is larger than in the reference model. In Figure 16b, differences in the water depth after 12 hours between model 160 and the reference model are shown. It can be seen in Figure 16 that in general, the differences in water depth between grids with a lower resolution and the reference grid are small (below 10 cm). Moreover, after 1 day, differences in water depths between coarser grids and the reference grid tend to get even smaller. Furthermore, the red and blue colours mean that respectively more and less volume of water flows to these areas in the reference model compared to the coarser models. This indicates that the grid size impacts the volumes of water which flow to the different parts of the study area.

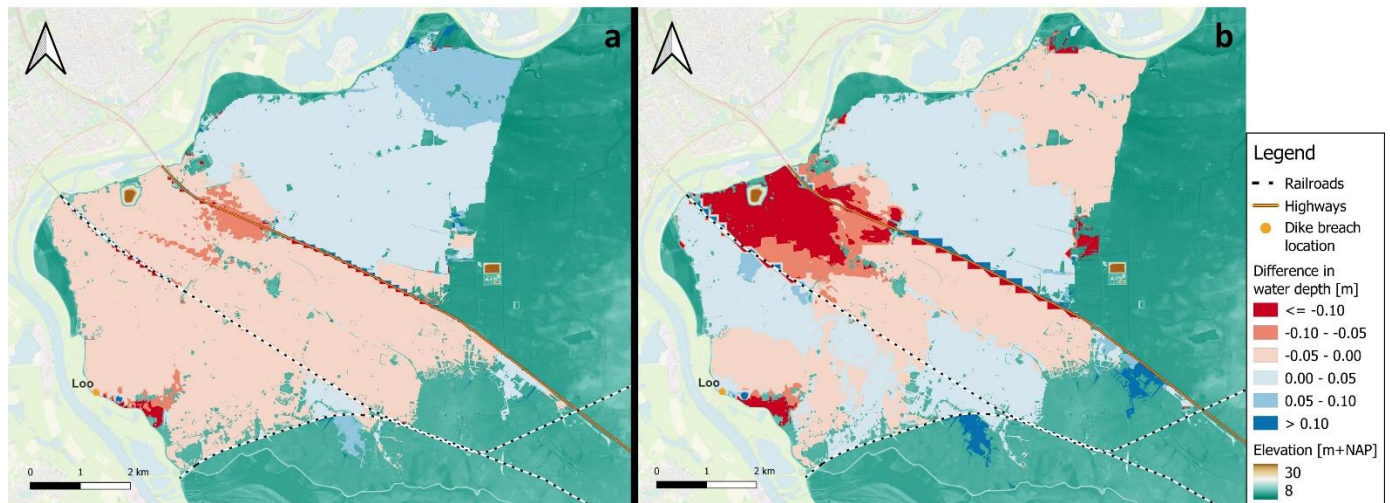


Figure 16 Differences in water depth between a grid with resolution of (a) 80×80 m<sup>2</sup> and 40×40 m<sup>2</sup> and (b) 160×160 m<sup>2</sup> and 40×40 m<sup>2</sup> after 12 hours. Positive differences (blue) indicate that the water depth in the grid with a resolution of 80×80 m<sup>2</sup> or 160×160 m<sup>2</sup> is larger than in the reference grid.

In Figure 17a, the differences in arrival times between model 80 and the reference model are shown. Positive differences (blue) indicate that the water arrives later in model 80 than in the reference model. In Figure 17b, the differences in arrival times between model 80 and the reference model are shown. As can be seen in Figure 17, the differences in the arrival times in a major part of the inundated area are small (well below 1 hour) especially when comparing model 80 with the reference model. Yet, at the edges of the inundated area, differences are larger.

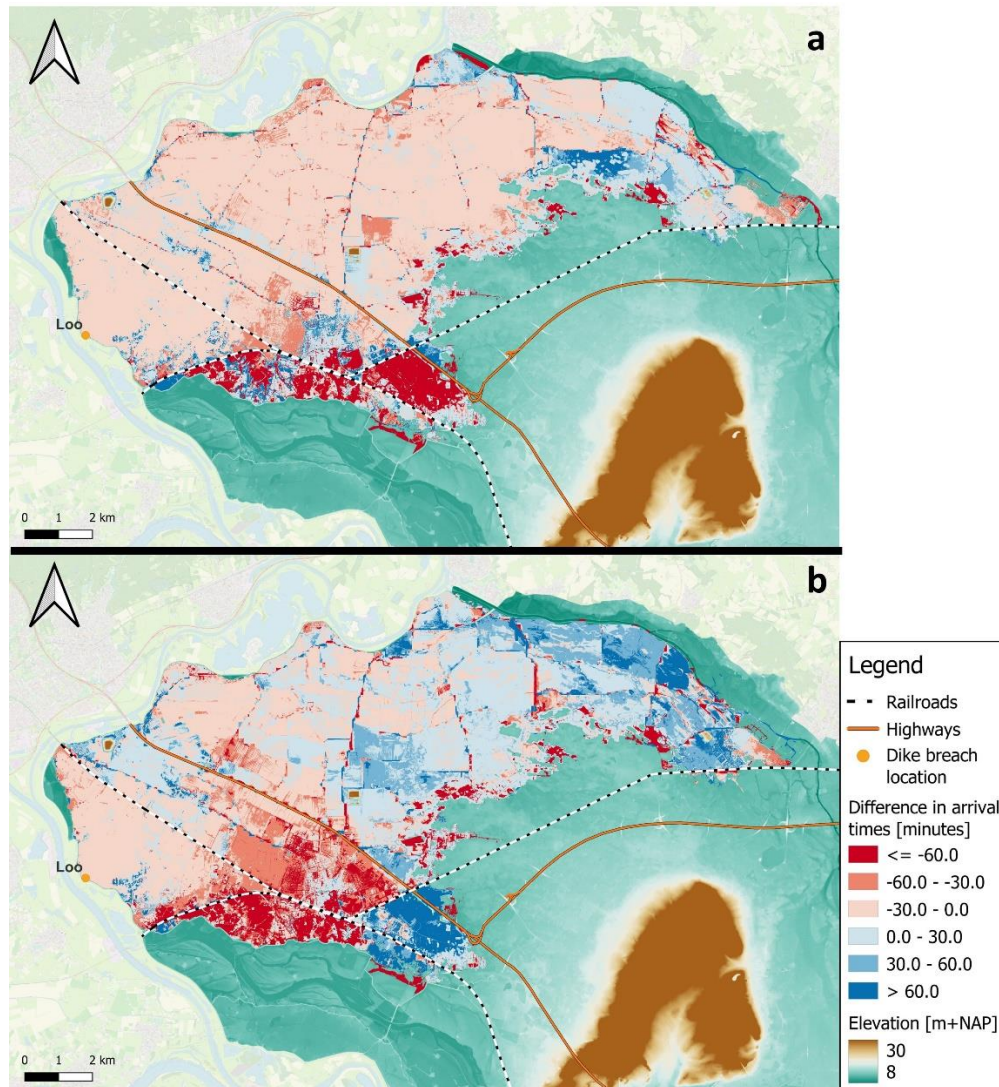


Figure 17 Differences in arrival times between the grid with resolution of (a)  $80 \times 80 \text{ m}^2$  and  $40 \times 40 \text{ m}^2$  and (b)  $160 \times 160 \text{ m}^2$  and  $40 \times 40 \text{ m}^2$ . Positive differences (blue) indicate that the water arrives later in the grid with a resolution of  $80 \times 80 \text{ m}^2$  or  $160 \times 160 \text{ m}^2$  than in the reference simulation.

Based on the first phase of the sensitivity analysis, model 80 was selected. The results of the simulation with this computational grid showed the most agreement with the reference model as differences in water depths were very small and the area with large differences in the arrival times was smaller than in the other grids. Furthermore, the computational time of model 80 for a flood event of 3 days was still acceptable as can be seen in Table 1. Lastly, although differences in water depth and arrival times between model 100 and the reference model were not significantly larger than between model 80 and the reference model, this grid was not chosen, as model 100 cannot be refined further. This is caused by the requirement in the modelling software that an even number of subgrid pixels should be located on the edge of a computational grid cell.

## 4.2 SECOND PHASE: DIKE BREACHES AT DOESBURG AND SPIJK

The computational time of both the reference model and selected model (model 80) for the five-day simulation at both breach locations can be found in Table 7 in Appendix E. The differences in the water depth and arrival times between model 80 and the reference model for the dike breach location at

Doesburg were qualitative similar to the results of the dike breach at Loo, described in the previous section.

However, for the breach location at Spijk, differences in water depth and arrival times between model 80 and the reference model were much larger than at Loo. In Figure 18a, the differences in water depths at the end of the first day between model 80 and the reference model are shown. In Figure 19a, the differences in water depths at the end of the first day between model 80 and the reference model are shown. As can be seen in Figure 18a and Figure 19a, differences in water depths after 1 day ranged from 0.4 m up to 2 m while differences in arrival times ranged up to 12 hours. Analysis of the results and the elevation of the obstacles showed that the largest differences could be attributed to differences in the exchange level or schematisation of the openings in the obstacles. For example, in model 80, some openings in the Rijnstrangen area were either closed or had a higher exchange level which causes higher water levels in front of an opening and later arrival times behind the opening. Therefore, all openings in the obstacles were refined to  $40 \times 40 \text{ m}^2$  in model 80. This adjusted computational grid is referred to as adjusted grid 1.

To assess the effect of these refinements on the differences in the water depths and arrival times, a dike breach at Spijk with a similar discharge as in the previous phases of the sensitivity analysis was simulated. The computational time of this simulation can be found in Table 2. In Figure 18b, the differences in water depth after 1 day between adjusted grid 1 and the reference model are shown. As can be seen in Figure 18b, the differences in water depth became significantly smaller and are mostly below 0.1 m. Yet, large differences can still be observed at the east of the inundated area. At this location, water from the reference model arrives much earlier than water in adjusted grid 1. This is probably caused by an obstacle in the computational grid of the reference model which does not extend completely to the edges of the model domain. This means that water can flow around the obstacle which may result in earlier arrival times.

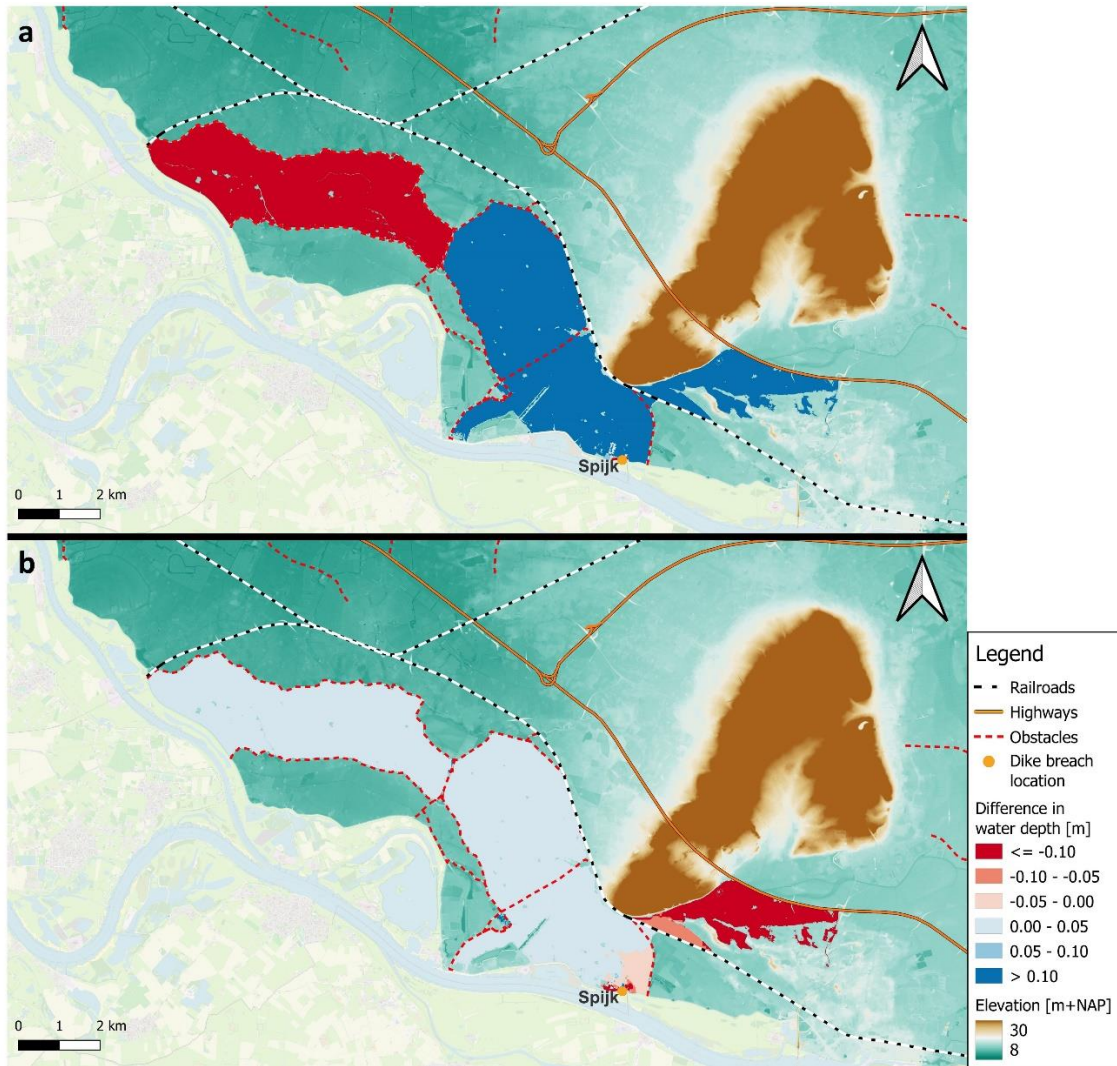


Figure 18 Differences in water depths after 1 day between (a) model 80 and the reference model and (b) adjusted grid 1 and the reference model. In model 80, no openings/underpasses in this area are refined while in adjusted grid 1, all openings/underpasses are refined.

In Figure 19b, the differences in water depth after 1 day between adjusted grid 1 and the reference model are shown. As can be seen in Figure 19b, differences in arrival times became also smaller and are mostly below 1 hour. This decrease in the differences in water depth and arrival times can be attributed to the importance of obstacles and thereby openings for guiding the flow in the Rijnstrangen area, because flow in this area is strongly confined by a lot of (small) embankments. Refining all obstacles instead of all openings to  $40 \times 40 \text{ m}^2$  did not further decrease the differences in water depth or arrival times. Yet, the computational time increased as can be seen in Table 2.

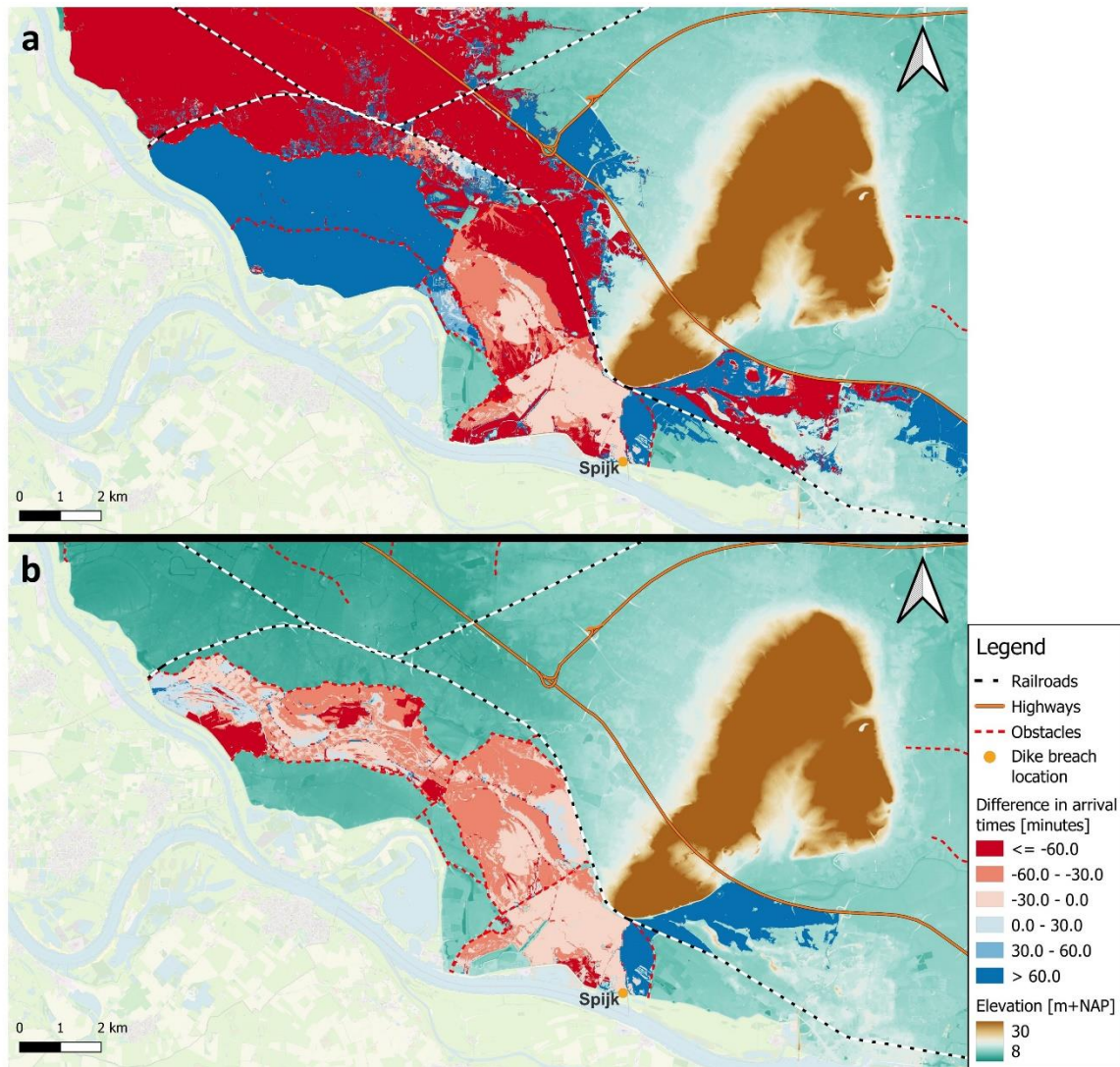


Figure 19 Differences in arrival times between (a) model 80 and the reference model and (b) adjusted grid 1 and the reference model. In model 80, no openings/underpasses in this area are refined while in adjusted grid 1, all openings/underpasses are refined.

A shortcoming of using a computational grid with a grid size of  $80 \times 80 \text{ m}^2$  is that this grid cannot be refined far enough to properly schematize small underpasses ( $< 20 \text{ m}$ ). This is caused by the requirement in the modelling software that an even number of subgrid pixels should be located on the edge of a computational grid cell. Therefore, a similar scenario as for adjusted grid 1 and 2 was simulated with two other computational grids which overcame this problem. The grid sizes and computational time of these adjusted grids 3 and 4 can be found in Table 2. Results of the simulations with these grids showed that the resulting water depths and arrival times in adjusted grid 4 showed more agreement with the reference model than in adjusted grid 3. Furthermore, the grid around narrow underpasses (width  $< 10 \text{ m}$ ) was properly schematized in adjusted grid 4 contrary to adjusted grid 3. Therefore, based on this sensitivity analysis, the main part of the study area was assigned a grid resolution of  $64 \times 64 \text{ m}^2$  and around underpasses in obstacles, the grid was refined.

Table 2 Computational time of one-day simulation at Spijk with the reference model and several adjusted grids

<b>Name</b>	<b>Grid size major part study area [m<sup>2</sup>]</b>	<b>Refinements [m<sup>2</sup>]</b>	<b>Computational time [h]</b>
Reference model	40×40	-	4.18
Adjusted grid 1: all openings/underpasses refined	80×80	40×40	1.00
Adjusted grid 2: all obstacles refined	80×80	40×40	1.73
Adjusted grid 3: all openings/underpasses refined	96×96	48×48 24×24 12×12	0.98
Adjusted grid 4: all openings/underpasses refined	64×64	32×32 16×16 8×8	1.89

# 5. RESULTS

## 5.1 MAXIMUM INUNDATION EXTENT

The simulations of dike breaches at the different dike breach locations result in two distinct types of maximum inundation extents after 3 days. The maximum inundation extents of the simulations 2-18 are overlaid in Figure 20. Here, the greyish/greenish area is inundated in simulations 2-18. Differences in the maximum inundation extent are visible in areas I, II and III. Area I (blue) is only inundated in simulations 10-18, area II (orange areas) only in simulations 2-8 and area III (purple area) only for dike breach locations 2 and 4. Yet, these areas are only limited in surface area compared to the greyish, inundated area. Therefore, it can be concluded that dike breaches at locations 2-18 lead all to a similar maximum inundation extent. In the rest of this report, this cluster of dike breach locations and simulations will be referred to as Cluster South.

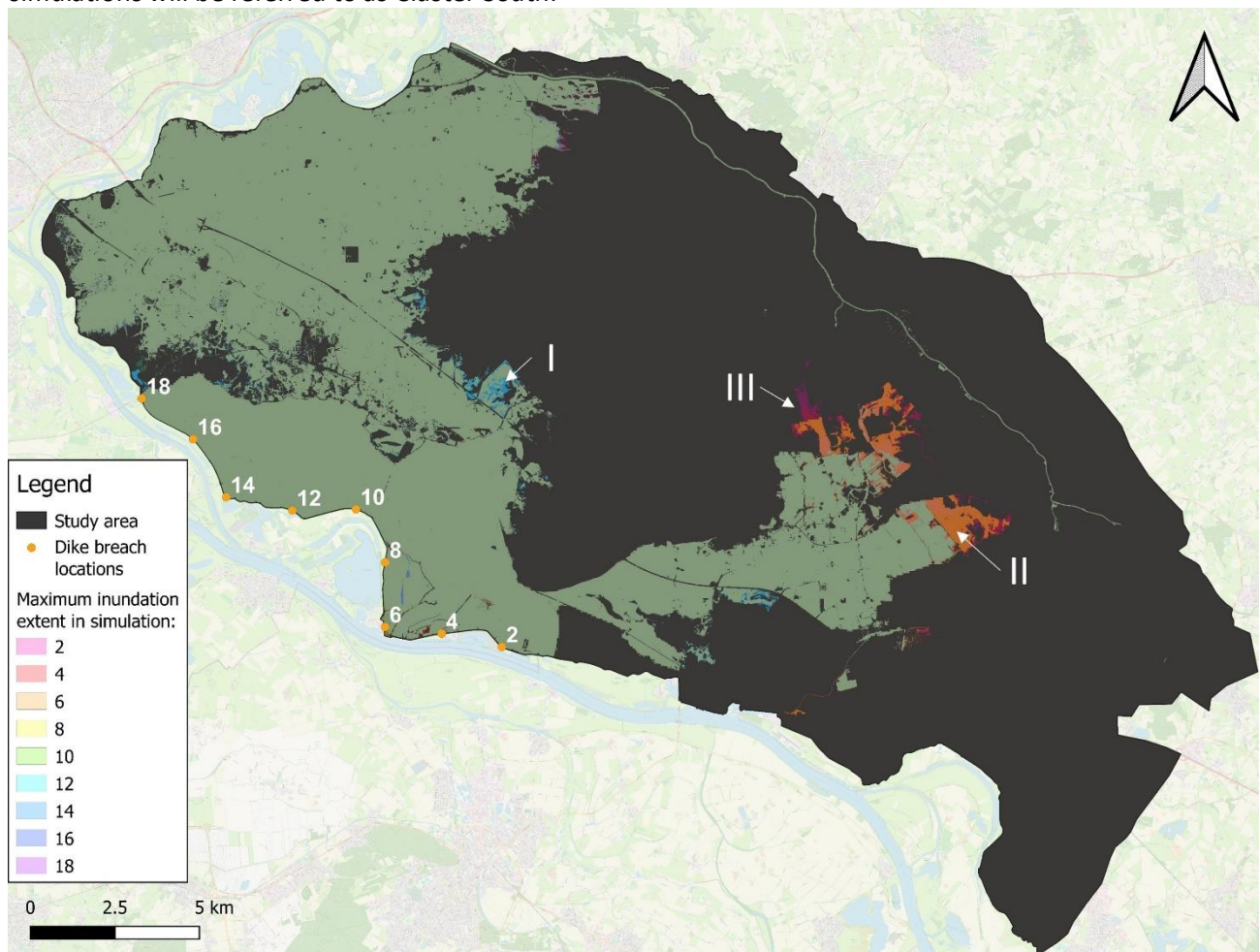


Figure 20 Overlay of maximum inundation extents after 3 days of simulations 2-18 (Cluster South). Green/grey is inundated in all simulations. Area I (blue) is only inundated in simulations 10-18, area II (orange areas) only in simulations 2-8 and area III (purple area) only for simulations 2 and 4.

In Figure 21, the maximum inundation extents of simulations 20-40 are overlaid. Here, the greenish area is inundated in simulations 20-40. As can be seen in Figure 21, area IV (orange area) is only inundated in simulation 24. Again, the surface area of this part of the inundated area of dike breach location 24 is limited compared to the greenish area. Therefore, it can be concluded that dike breaches at locations 20-40 lead all to a similar maximum inundation extent. In the rest of this report, this cluster of dike breach locations and simulations will be referred to as Cluster South.

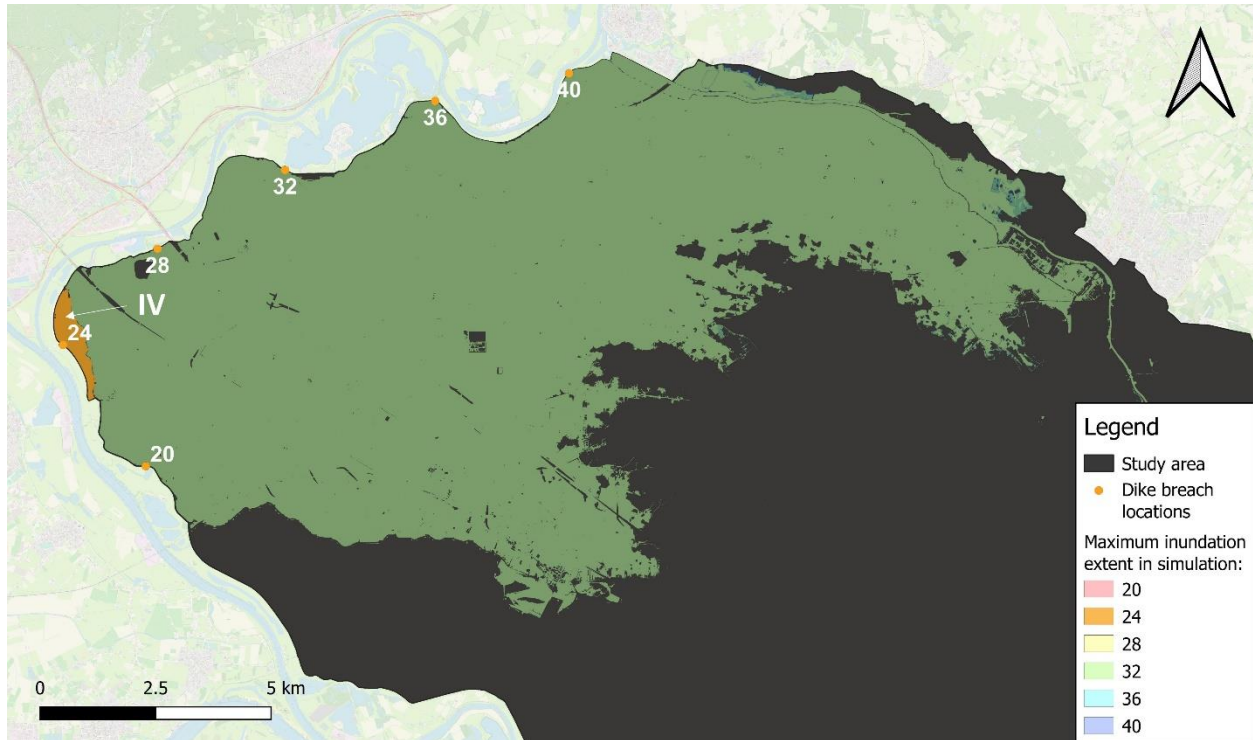


Figure 21 Overlay of maximum inundation extents after 3 days of simulations 20-40 (Cluster North). The greenish area is inundated in all simulations. Area IV (orange) is only inundated in simulation 24.

The main reason that all dike breaches in Cluster South lead to the same maximal inundation extent and dike breaches in Cluster North result in another maximum inundation extent is the regional dike along the Rijnstrangen area. The Rijnstrangen area is almost completely enclosed by a regional dike which is in the north of the area up to 5 metres higher than the surrounding area. This dike forms a large barrier for water flowing from the higher south-eastern part to the lower-lying northern part of the study area. In the east, the Rijnstrangen area is enclosed by the railway from Arnhem to Emmerich and by the higher lying grounds of Montferland. At the lowest point (in the northeast; see arrow in Figure 22) of this obstacle, water still has to rise 2 metres to flow to the lower-lying part of the study area. This means that water from the dike breaches south of the regional dike (Cluster South) should first completely fill the Rijnstrangen area in such a way that the water will rise with 2 metres at the lowest point of the barrier. If this has happened, water will always flow in a similar pattern to the north-western part of the study area, which is the lowest lying part. Due to the high regional dike and consequently filling of the Rijnstrangen area, all dike breaches in Cluster South lead to a similar maximum inundation extent. In case of a dike breach to the north of this regional dike (Cluster North), water will flow to the north-western part of the study area, which is the lowest lying part. Furthermore, after this part of the study area is filled, water will distribute over the other areas. However, water will not rise to such a level that it can flow over the regional dike around the Rijnstrangen area. This means that dike breaches in Cluster

North lead to a similar maximum inundation extent which is different from the maximum inundation extent of breaches in Cluster South.

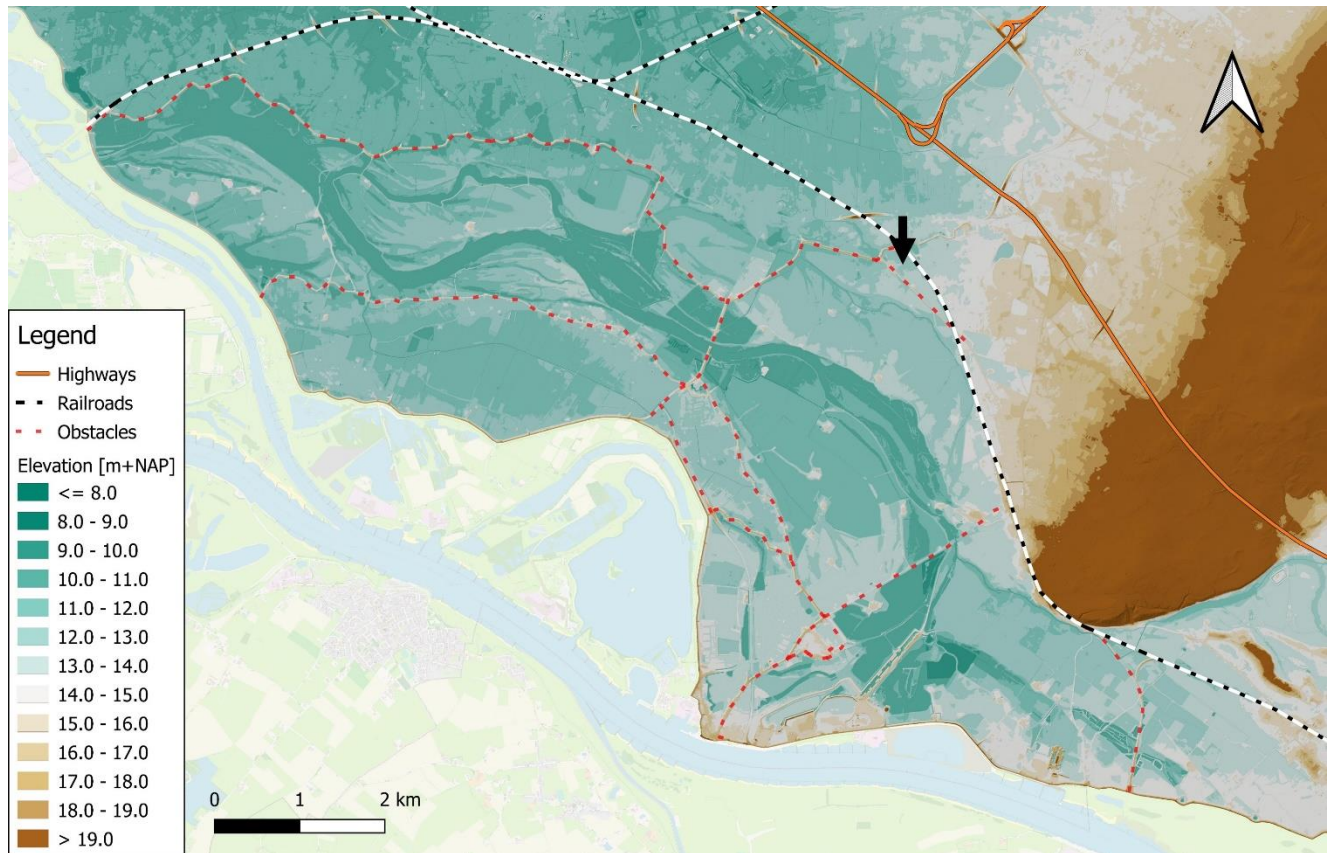


Figure 22 Close-up of the DEM in and around the Rijnstrangen area. The Rijnstrangen area is the area between the parallel obstacles (regional dikes). The arrow indicates the location where water will first flow out of the Rijnstrangen area to the northern part of the study area.

In the next sections, the sensitivity of the arrival times and maximum water depths for the dike breach location is discussed per cluster. The discussed sensitivity is the sensitivity of the arrival times or maximum water depth to the dike breach location within one of the clusters. At the same location, sensitivities may be different when considering the other cluster.

## 5.2 CLUSTER SOUTH

In Figure 23, the dike breach locations in this cluster are again shown. The dike breach locations are numbered with black numerals. Furthermore, the relevant part of the DEM which is covered by final inundation extent of all simulations in this cluster is shown. Moreover, the water level points where water level graphs of the simulations in this cluster will be compared are presented. These points are numbered with white numerals. Lastly, the local obstacles are represented by the white dashed lines. Areas between these obstacles will be referred to as compartments. These compartments are numbered with black Roman numerals.

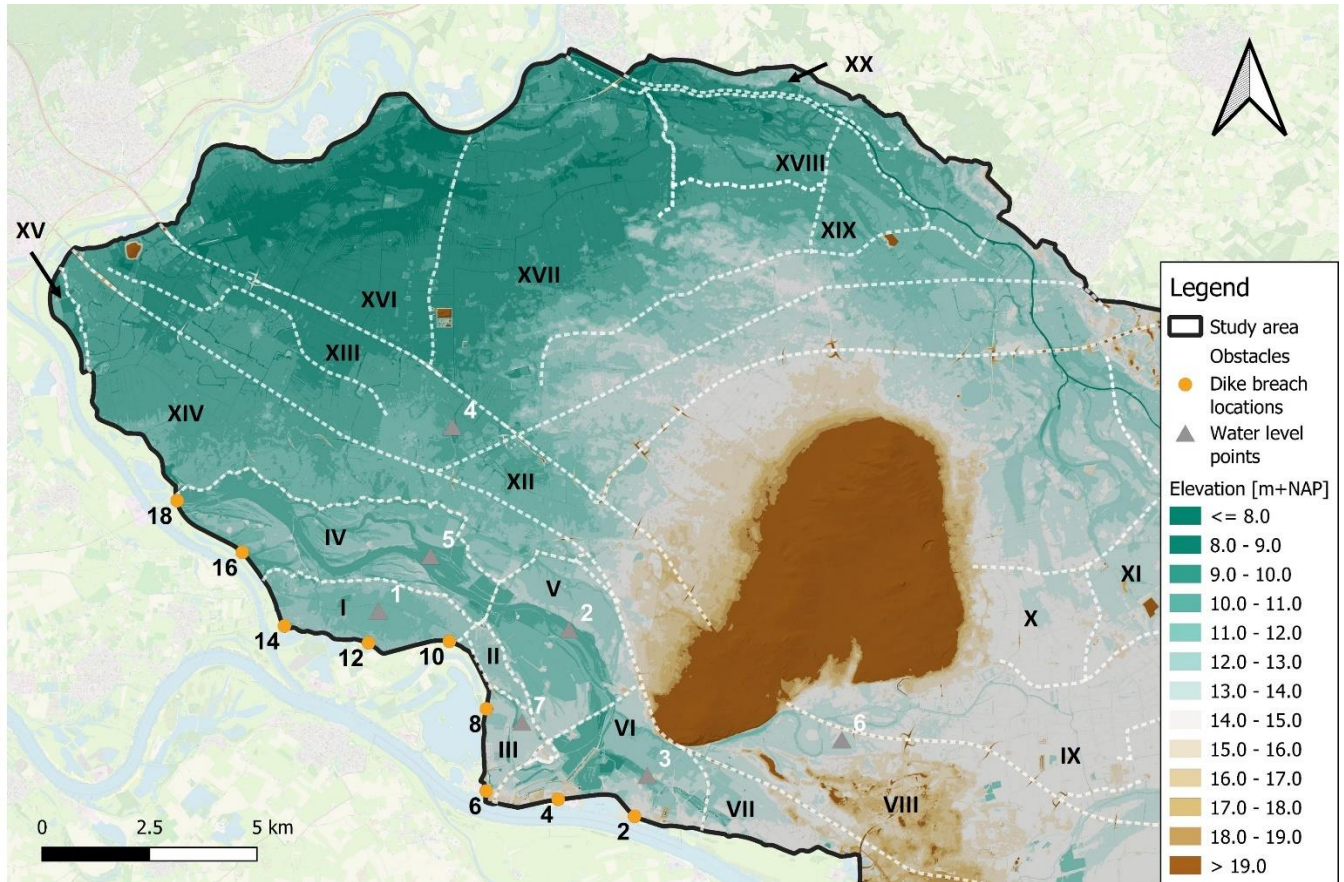


Figure 23 Relevant part of the DEM for Cluster South with relevant water level points where water level graphs will be compared. White dashed lines represent local obstacles. Areas between local obstacles are compartments and are numbered with black Roman numerals. Water level points and dike breach locations are numbered with respectively white and black numerals.

### 5.2.1 Arrival times

In Figure 24, the MAD of the arrival times for Cluster South is shown. In general, if the MAD is low, the arrival time at this location is not (very) sensitive to the location of the dike breach in this cluster of dike breach locations. If the MAD is high, the arrival time at this location is (very) sensitive to the location of the dike breach in Cluster South. Specifically, the sensitivity of the arrival time to the dike breach location becomes significant when the MAD is close to or larger than six hours as was explained in Section 3.5.2. Based on this criterion, it can be seen in Figure 24 that the sensitivity of the arrival times is significant in compartments I, II, III, VI, VIII and IX. The location of these compartments can be found in Figure 23. Furthermore, at some locations in compartments IV and V, the arrival times are also significantly sensitive to the dike breach location in this cluster. In all other compartments, the arrival times are not significantly sensitive to the dike breach location in this cluster.

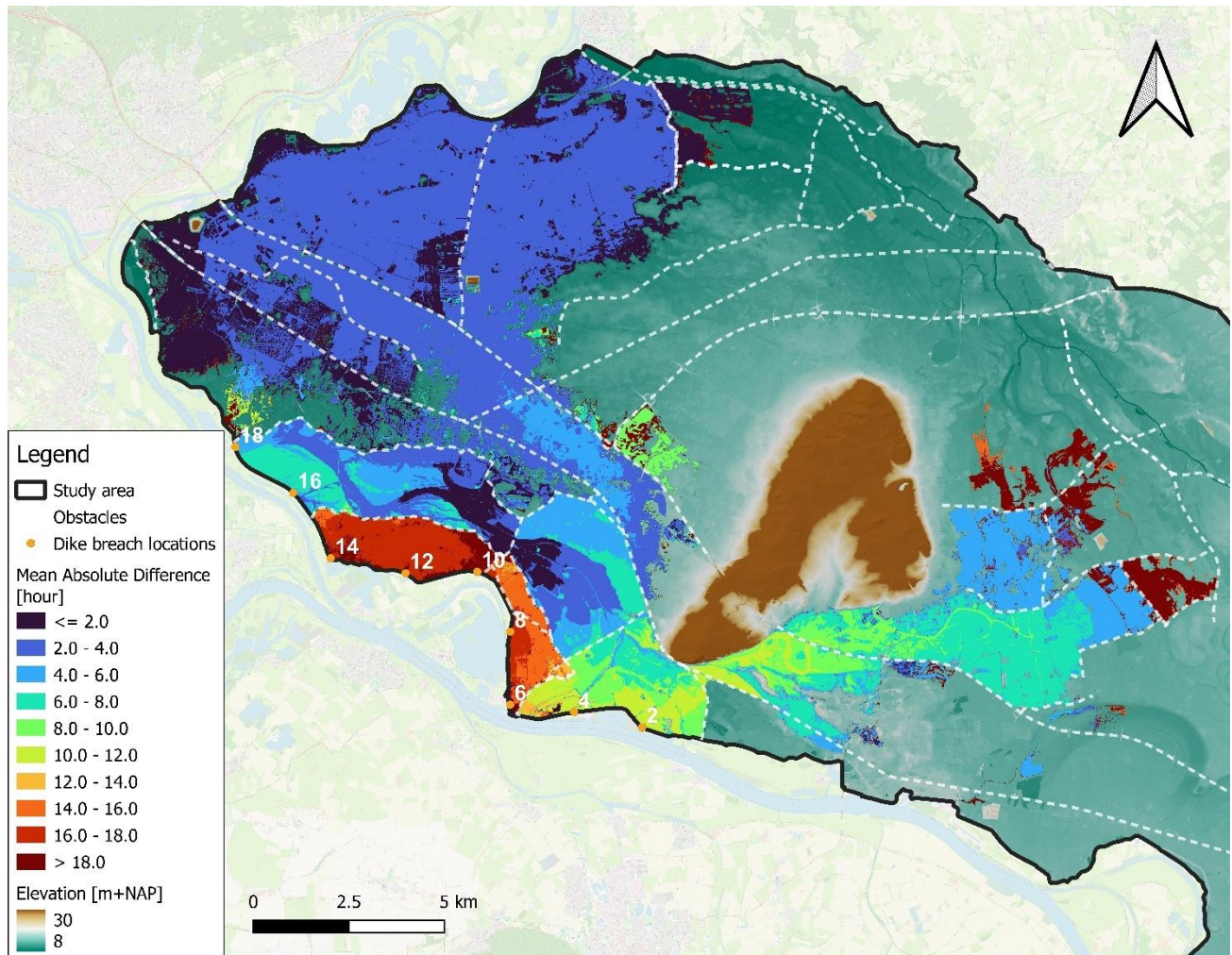


Figure 24 MAD of the arrival times for Cluster South. White dashed lines represent local obstacles.

As can be seen in Figure 24, the arrival times in compartments I, II and III (orange-red areas) are very sensitive to the dike breach location in this cluster. As already mentioned, the sensitivity of the arrival times in these compartments is significant. These compartments are enclosed by high regional dikes as can be seen in Figure 22. Floods which start in one of these compartments will immediately inundate this compartment. The regional dikes block inundations starting at dike breach locations outside these compartments from arriving in these compartments. These inundations will only arrive in these compartments if an opening in the regional dikes is found or when the water levels have risen high enough in the Rijnstrangen area. These later arrival times can also be seen in Figure 25 in which the water level graphs of the different simulations at water level point 1 (see Figure 23 for the location of this point) are shown. Inundations in simulations 10 to 14 all immediately flood this compartment as these inundations start in this compartment. The inundations in all other simulations will arrive at least a day later in this compartment due to the high regional dike.

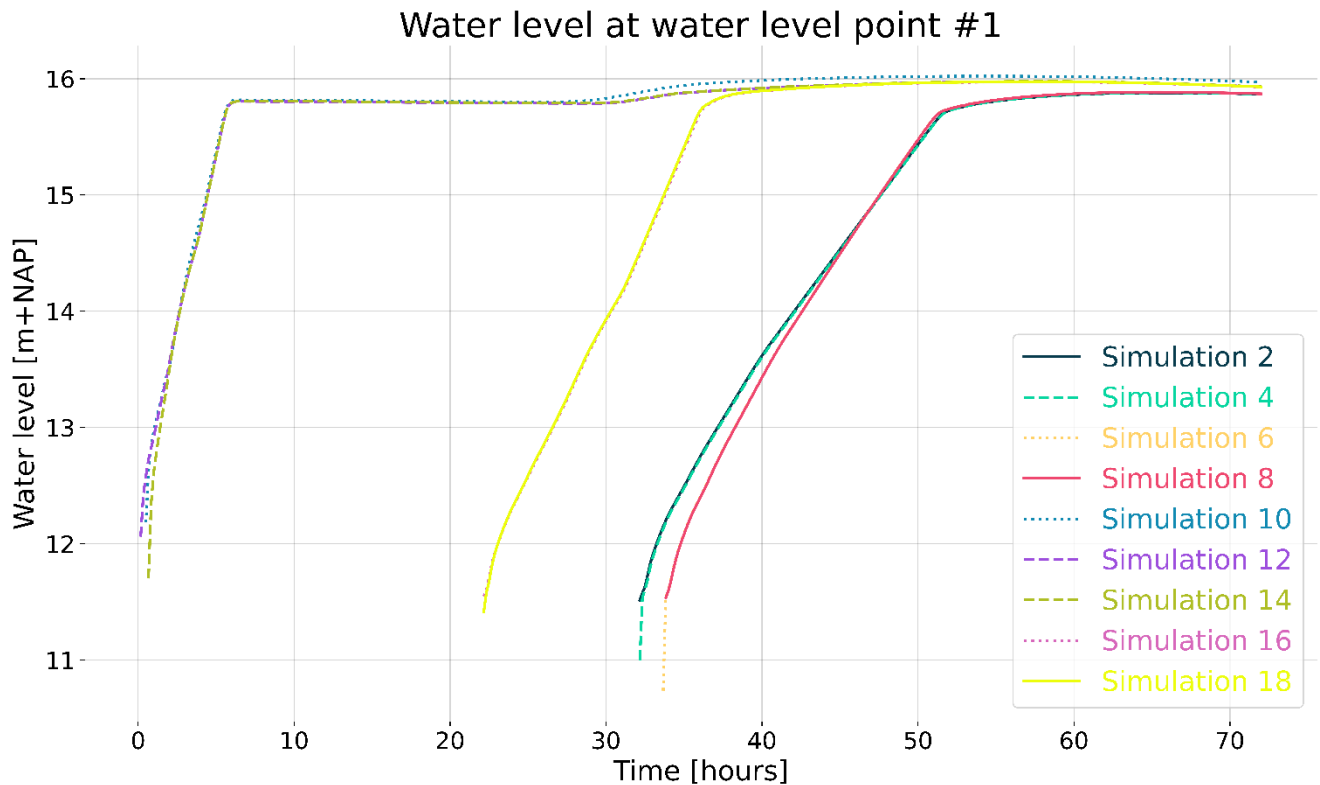


Figure 25 Water level in simulations 2 to 18 (Cluster South) at water level point 1

Furthermore, as can be seen in Figure 24, the arrival times in compartments IV and V (the Rijnstrangen area) are not very sensitive to the dike breach location in Cluster South. As already mentioned, the sensitivity of the arrival times at most locations in these compartments is not significant. These compartments are centrally located and lower lying with respect to most dike breach locations as can be seen in Figure 23. Due to its lower elevation, the inundations in most simulations will flow to this area early in the flood event. Moreover, due to its central location with respect to most dike breach locations, most inundations will arrive in this area at approximately the same time. This can be seen in water level graphs at water level point 2 (see Figure 23) which are shown in Figure 26. Inundations in simulations 2-8, 16 and 18 arrive at almost the same time, very early, at this water level point. Inundations in simulations 10 to 14 arrive only 2 hours later, because these inundations are temporarily blocked by the high regional dikes around the compartment where these inundations start. Variations in the sensitivity in the Rijnstrangen area can be mainly attributed to the location with respect to all dike breach locations and the elevation of the location. For example, arrival times at higher parts of this area which are less centrally located (closer to some dike breach locations than others) are more sensitive to the dike breach location.

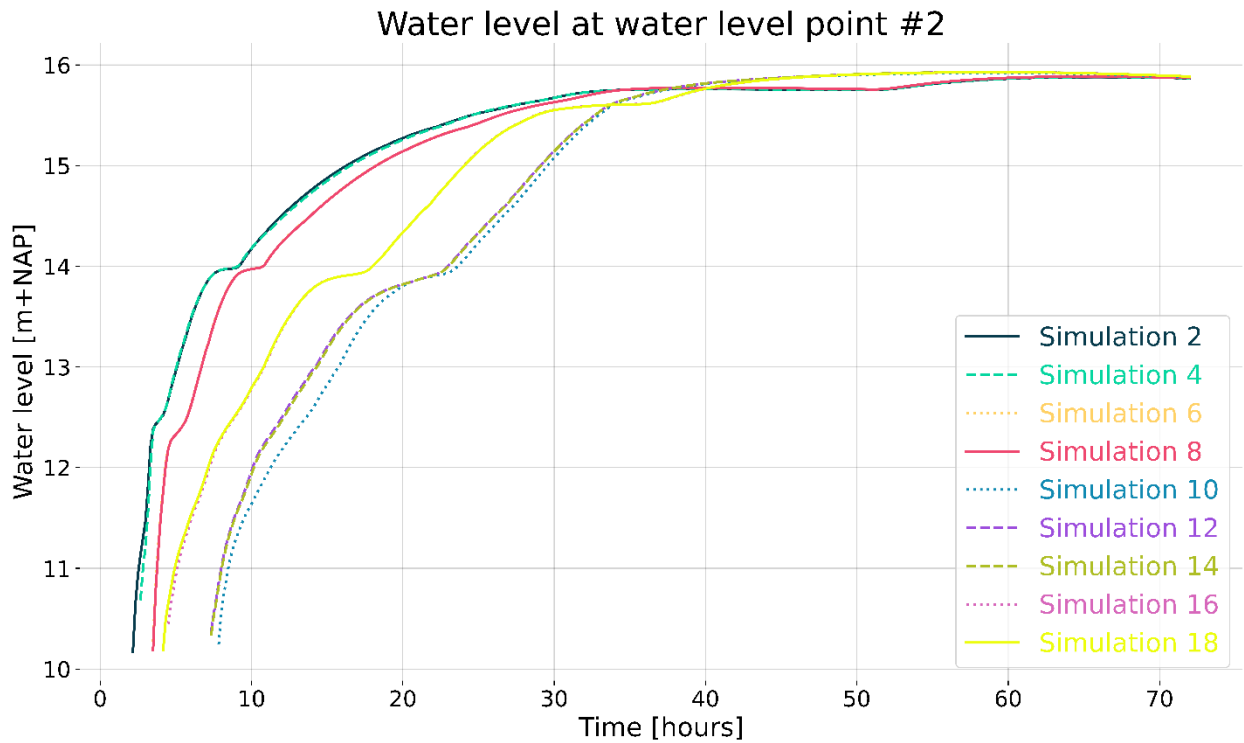


Figure 26 Water level in simulations 2 to 18 (Cluster South) at water level point 2

As can be seen in Figure 24, arrival times in compartment VI (yellow-green area) are more sensitive to the dike breach location in Cluster South. This sensitivity is also significant as the MAD is higher than six hours. This is mainly caused by its less central location and its higher elevation with respect to compartment IV and V (Rijnstrangen area) as can be seen in Figure 23. Compartment VI is closer to dike breach locations 2 and 4 and in a lesser extent to dike breach locations 6 and 8 than to dike breaches 10 to 18. This already causes differences in the arrival times to occur in this area. These differences are increased as inundations in simulations 10 to 18 need to overcome an elevation difference between compartments IV and V (Rijnstrangen area) and a large part of this compartment (VI). Overcoming an elevation difference takes more time as the water level in the complete lower-lying area in front of the higher elevated area needs to rise. These differences in arrival times can also be noticed in the water level graphs of the different simulations at water level point 3 (see Figure 23) which are shown in Figure 27. Inundations in simulations 2 and 4 arrive at this location very early in the flood event as these dike breach locations are closest to this area. Five hours later, inundations in simulations 6 and 8 arrive in this area. Inundations in simulations 16 and 18 arrive 12 hours after the start of the flood event. Again, inundations in simulations 10 to 14 arrive latest as they first need to flow over the regional dike.

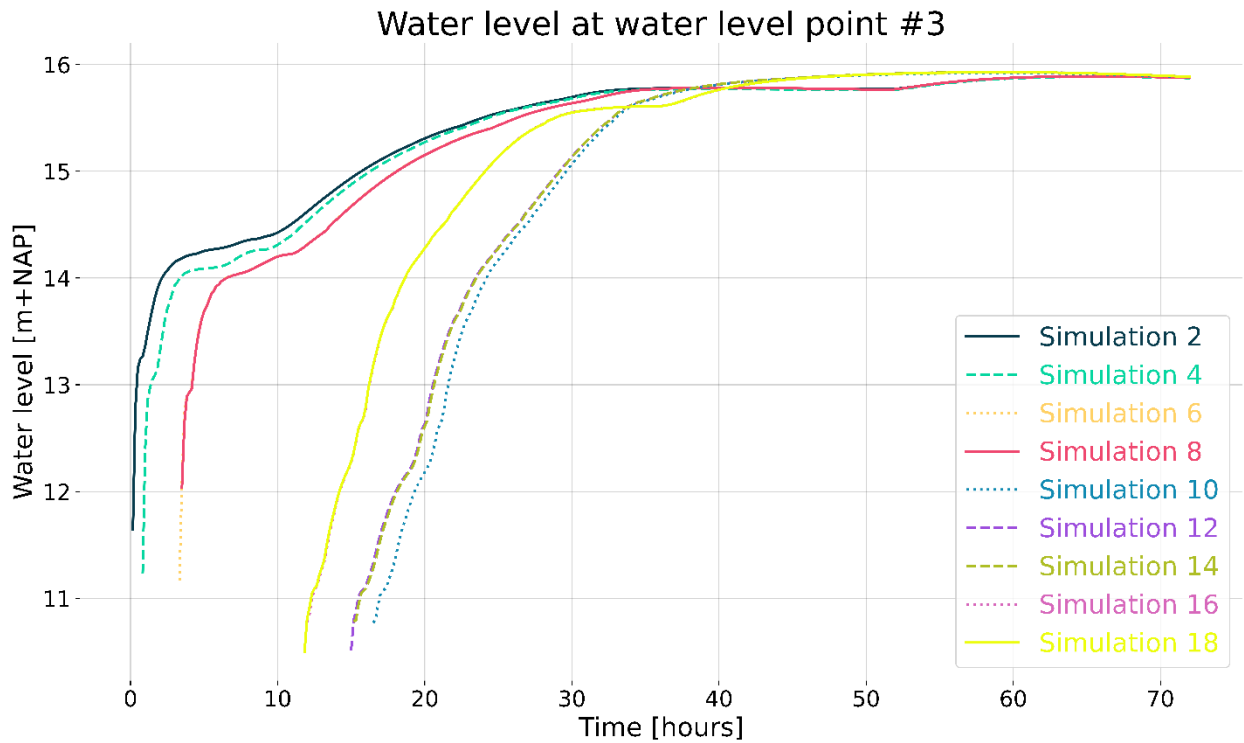


Figure 27 Water level in simulations 2 to 18 (Cluster South) at water level point 3

The sensitivity of the arrival times to the dike breach location in this cluster gradually decreases in compartments VIII and IX although it remains still significant. Major contributors to this decrease are the gradual increase in the elevation in this area as can be seen in Figure 23. During all simulations, the water level in the lower parts of this area need to rise in order to overcome the elevation differences. This causes a later arrival time of all inundations and less spread in the arrival times. The dark brown areas directly to the north and east of the just discussed area coincide with the areas II and III in Figure 20. This means that in these areas, the inundations at several dike breach locations do not arrive. This causes the arrival times in this area to have a very high sensitivity.

As can be seen in Figure 24, the arrival times in compartments XII, XIII, XIV, XVI and XVII are not very sensitive to the dike breach location in Cluster South. Furthermore, the sensitivity of the arrival times is not significant in these compartments as the MAD is lower than 6 hours. This is mainly caused by its lower elevation compared to the rest of the inundated area as can be seen in Figure 35 and by compartments IV and V (Rijnstrangen area) which serve as bathtubs. As already mentioned in Section 5.1, the water level in the complete Rijnstrangen area needs to rise to a certain level for water to flow over the lowest point of the dike around the Rijnstrangen area (arrow in Figure 22). This requires a certain volume of water which is the same in all simulations. Due to the same outflow hydrograph, which was used as boundary condition in this study, this volume is reached at approximately the same time for the inundations in all simulations. Yet, there will be differences in the time in which this volume is reached. For example, inundations in simulations 10 to 14 will need more time to completely fill the Rijnstrangen area as they first need to fill the compartment where they are start. This can also be seen in water level graphs at water level point 4 which are shown in Figure 28. After the inundations have flown over the regional dike around the Rijnstrangen area, water will always flow in a similar pattern to the north-western part of the study area, which is the lowest lying part of the study area.

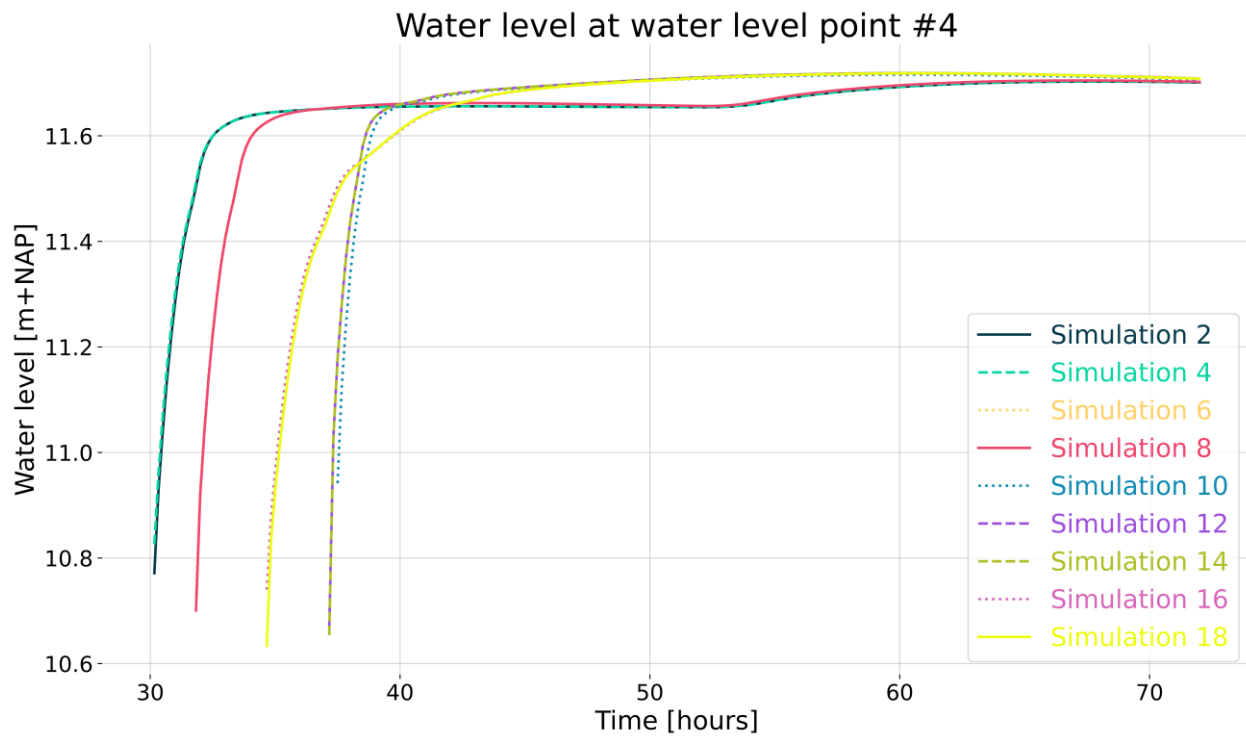


Figure 28 Water level in simulations 2 to 18 (Cluster South) at water level point 4

In the very dark blue parts in compartments XIII, XIV, XVII and XVIII in Figure 24, the arrival times are almost not sensitive to the dike breach location in Cluster South. This is mainly caused by the elevation of this area and its position with respect to the dike breach locations. These areas are sufficiently distant from all dike breach locations to prevent the area from inundating at the start of the flood event. Combined with the higher elevation of these areas, inundations in the different simulations will first fill the lower-lying areas before they arrive at these higher elevated, more distant areas.

#### 5.2.2 Maximum water depths at day 1

In Figure 29, the MAD of the maximum water depth at day 1 of the flood event for Cluster South is shown. The sensitivity of the maximum water depth to the dike breach location becomes significant when the MAD is close to or larger than 20 cm. Based on this criterion, it can be seen in Figure 24 that the sensitivity of the maximum water depths is significant in almost all compartments.

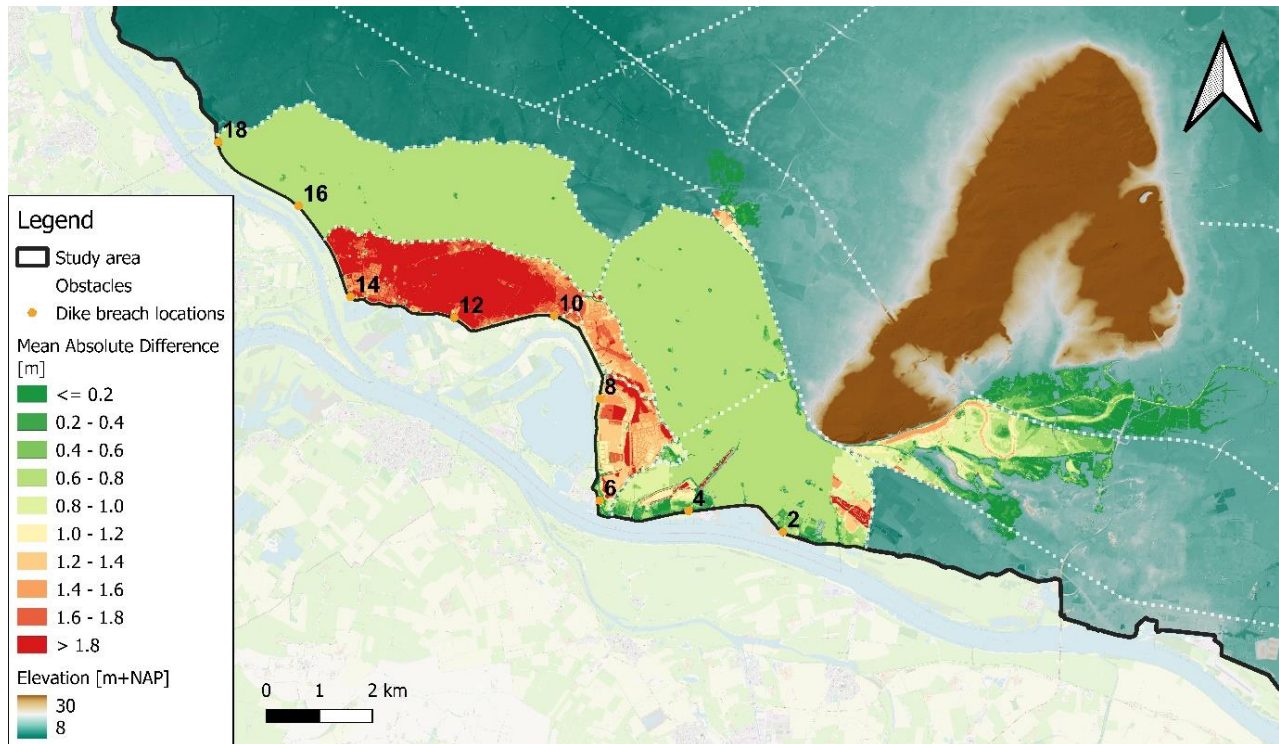


Figure 29 MAD of maximum water depths at day 1 for Cluster South. White dashed lines represent local obstacles.

As can be seen in Figure 29, the maximum water depths at day 1 in compartments I, II and III are very sensitive to the dike breach location. As already mentioned, these compartments are enclosed by high regional dikes. This means that the inundations which start in these areas will arrive very early in these compartments as can be seen in Figure 25. Moreover, water from these inundations will have risen to a higher level at the end of the first day to flow over the regional dikes. The inundations in the other simulations arrive after 1 day in these areas due to high dikes which block their flow as can be seen in Figure 25. Thereby, water levels of these inundations are zero.

Moreover, as can be seen in Figure 29, the maximum water depths at day 1 in the compartments IV and V (Rijnstrangen area) are slightly sensitive to the dike breach location compared to the sensitivity in compartments I to III. In Figure 30, the water level graphs at water level point 5 (see Figure 23 for the location of this point) are shown. It can be seen in Figure 30 that the spread in arrival times is small, so this cannot explain the sensitivity of the maximum water depths in this area to the dike breach location. However, at the end of day 1, the spread in the water levels is relatively large. This is mainly caused by the change in the rise rate in the inundations in simulations 2 to 8.

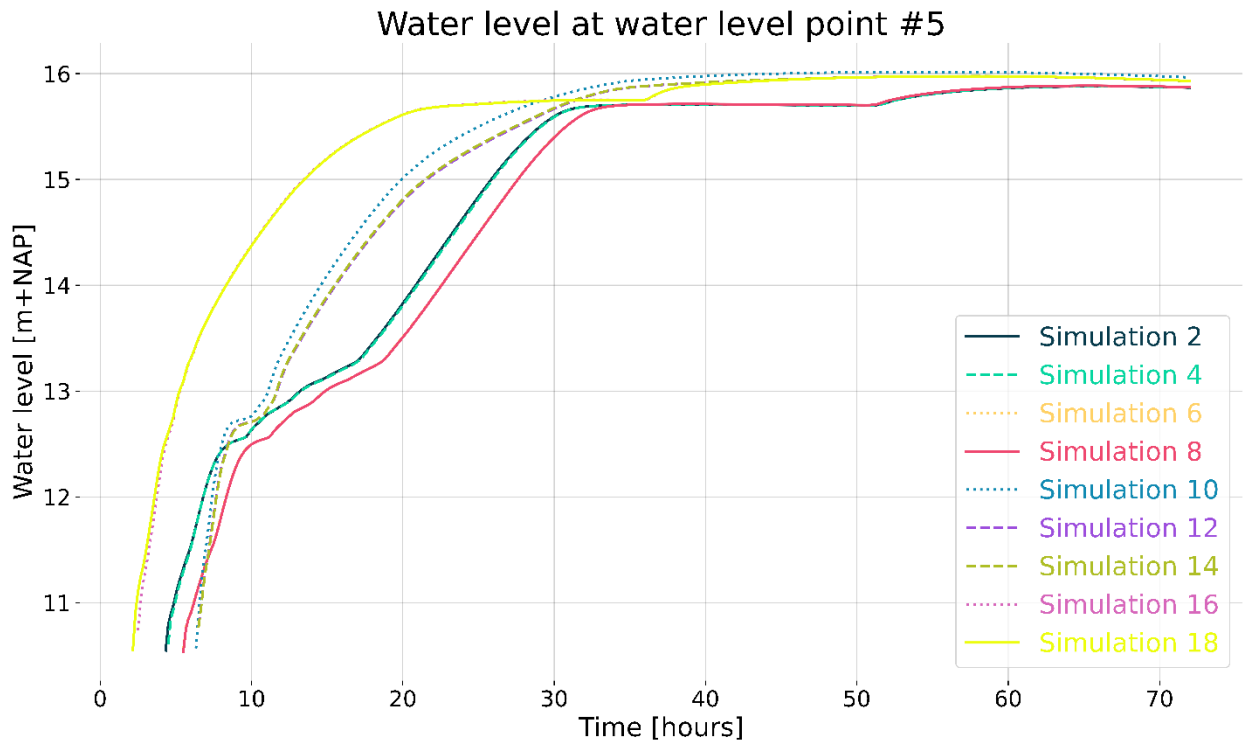


Figure 30 Water levels in simulations 2 to 18 (Cluster South) at water level point 5

This change in rise rate may be attributed to stronger flow to compartment VIII between 10 and 20 hours after the start of the flood event for these inundations as can be seen in Figure 31. Here, the water level graphs at water level point 6 (see Figure 23 for the location of this point) are shown. As can be seen in Figure 31, the inundations in simulations 2 to 8 rises quickly at this water level point in compartment VIII between 10 and 20 hours.

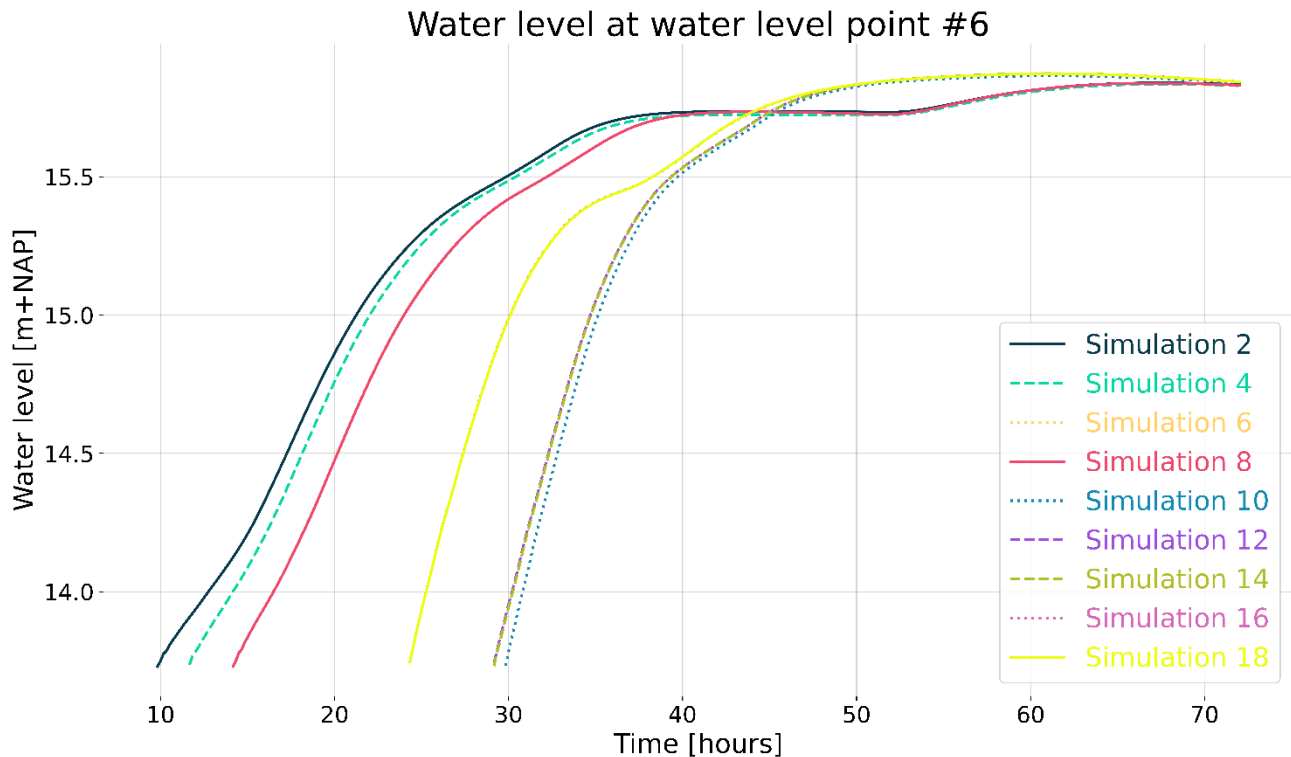


Figure 31 Water levels in simulations 2 to 18 (Cluster South) at water level point 6

In the area at the eastern edge of the inundated area, the maximum water depths at day 1 are almost insensitive to the dike breach location in Cluster South as can be seen in Figure 29. In this area, the sensitivity is also not significant. This is mainly caused by the distance to the dike breach locations. Just before the end of day 1, inundations in simulations 2 to 8 arrived in this area as the dike breach locations 2 to 8 are closest to this area. Due to this late arrival, the water depths of these inundations are low. Moreover, inundations in simulations 10 to 18 did not arrive in this area before the end of the first day. This means that the water depth of these inundations is zero. Due to the low water depths in the other simulations (2-8), the average difference in the water depth of all inundations is small. Therefore, the sensitivity of the maximum water depth is small.

### 5.2.3 Maximum water depths at day 2

In Figure 32, the MAD of the maximum water depths at the second day of the flood event for Cluster South is shown. As can be seen in Figure 32, the water depths are only significantly sensitive to the dike breach locations in compartments I, II and III and parts of compartments XVI and XVII. In these areas, the MAD is higher than 20 centimetres.

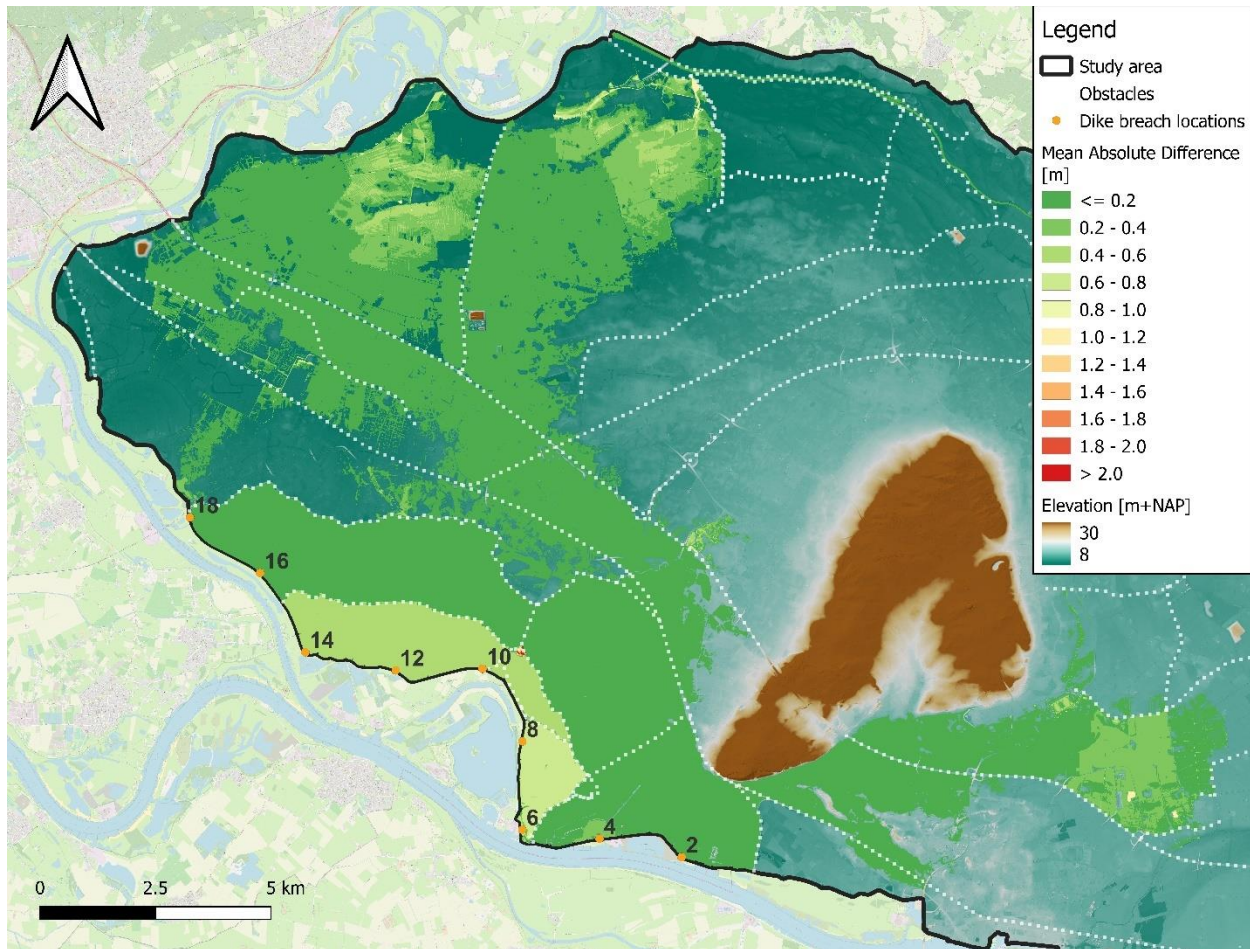


Figure 32 MAD of maximum water depths at day 2 for Cluster South. White dashed lines represent local obstacles.

As can be seen in Figure 32, the maximum water depths at the second day in almost the complete inundated area are insensitive to the dike breach location. Although there may be differences in the arrival times of the inundations at the different dike breach locations, all inundations have flooded the complete area halfway the second day. When the area is completely flooded, the water will rise in the area which is almost independent on the dike breach location. This can be seen in for example in the water level graphs in Figure 26 and Figure 27. This process is comparable to filling a bathtub. After a bathtub is filled with thin layer of water, the water level in the complete bathtub will rise with the same rate. This happens irrespective of the location of the tap.

Furthermore, the maximum water depths in the compartments I, II and III are still quite sensitive to the dike breach location. As already mentioned, the inundations which do not start in these compartments arrive later due to the high regional dikes around these compartments. Due to this later arrival, water depths at the end of day 2 are still not the same in all simulations.

At the edges of the inundated area in the northern part of the study area, the water depths at day 2 are quite sensitive (light green areas). This is mainly caused by the distance to the dike breaches. These areas are later reached by inundations starting at dike breach locations which are further away from these areas, or which are temporarily blocked. For example, inundations in simulations 10 to 18 arrive later in these areas than inundations in simulations 2 to 8 due to the blockage of the regional dikes. Subsequently the water depths in these latter simulations will be higher than in the former simulations.

#### 5.2.4 Maximum water depths at day 3

In Figure 33, the MAD of the maximum water depths at the third day of the flood event for the first set of dike breach locations is shown. As can be seen in Figure 32, the maximum water depths are still only significantly sensitive to the dike breach location in compartment III, because the MAD is higher than 20 centimetres. In the rest of the study area, the maximum water depths are not significantly sensitive to the dike breach location.

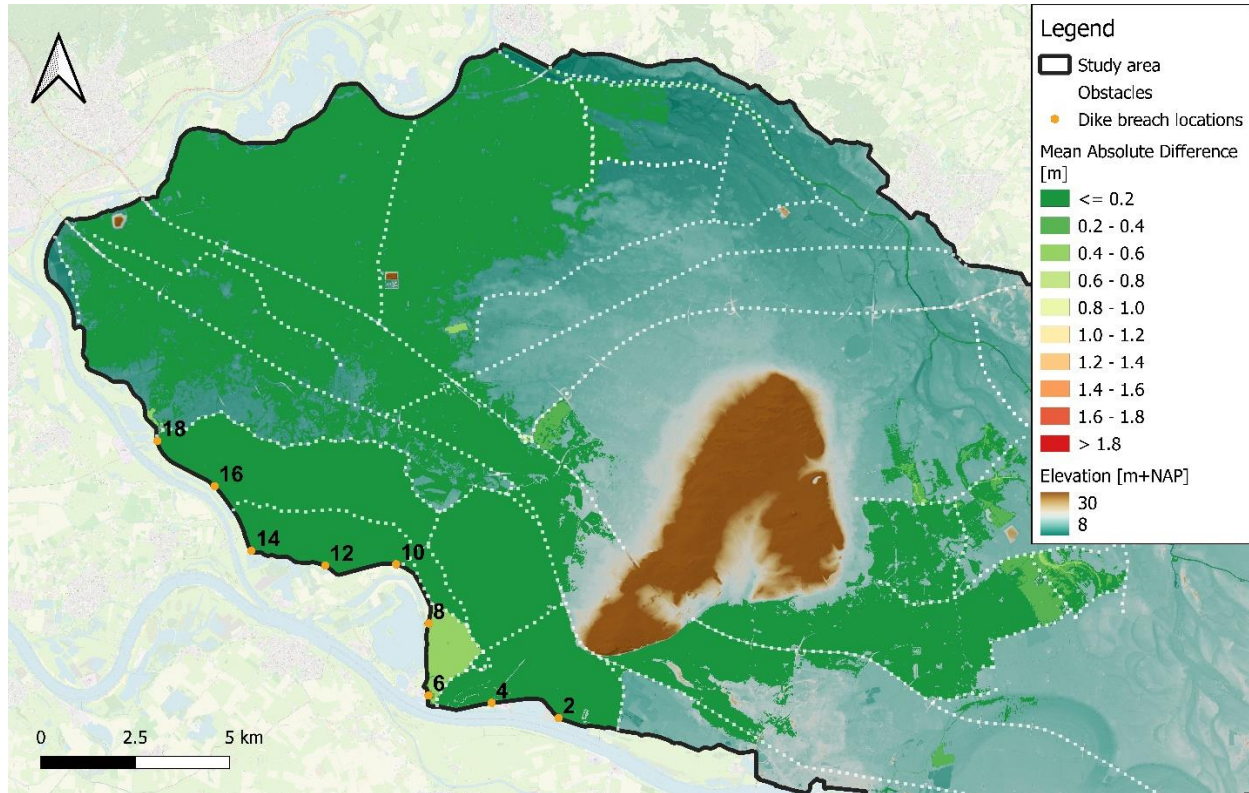


Figure 33 MAD of maximum water depths at day 3 for Cluster South. White dashed lines represent local obstacles

As can be seen in Figure 33, the maximum water depths at the third day in almost the complete inundated area are insensitive to the dike breach location in Cluster South. The reason for this insensitivity is already explained in the previous section.

Furthermore, the maximum water depths at the third day in the compartment III are still quite sensitive to the dike breach location in Cluster South. As was already mentioned in the previous two sections, this compartment is enclosed by high regional dikes which causes later arrival times of the inundations which do not start in this compartment. However, this does not completely explain the sensitivity of the maximum water depths at day 3 in this area. As mentioned in the previous section, inundations in simulations 2 to 8, 16 and 18 also arrive late in compartment I and II which are the compartments directly to the north of compartment III. Yet, the maximum water depths at day 3 in compartments I and II are not sensitive to the dike breach location as can be seen in Figure 33 and in Figure 25. Apparently, in compartment III, water depths do not increase as fast as in compartments I and II. This can also be seen in the water level graphs at water level point 7 which are shown in Figure 34. Inundations in simulations 2, 4 and 10 to 18 arrive much later in this compartment than inundations in simulations 6 and 8 which start in this compartment. The water levels of the former simulations do not rise as fast and high as the water levels in the latter simulations. Furthermore, when comparing Figure 34 to Figure 25, it becomes

clear that in compartment III, water levels of inundations that do not start in this compartment do not rise as high and fast as in compartment I.

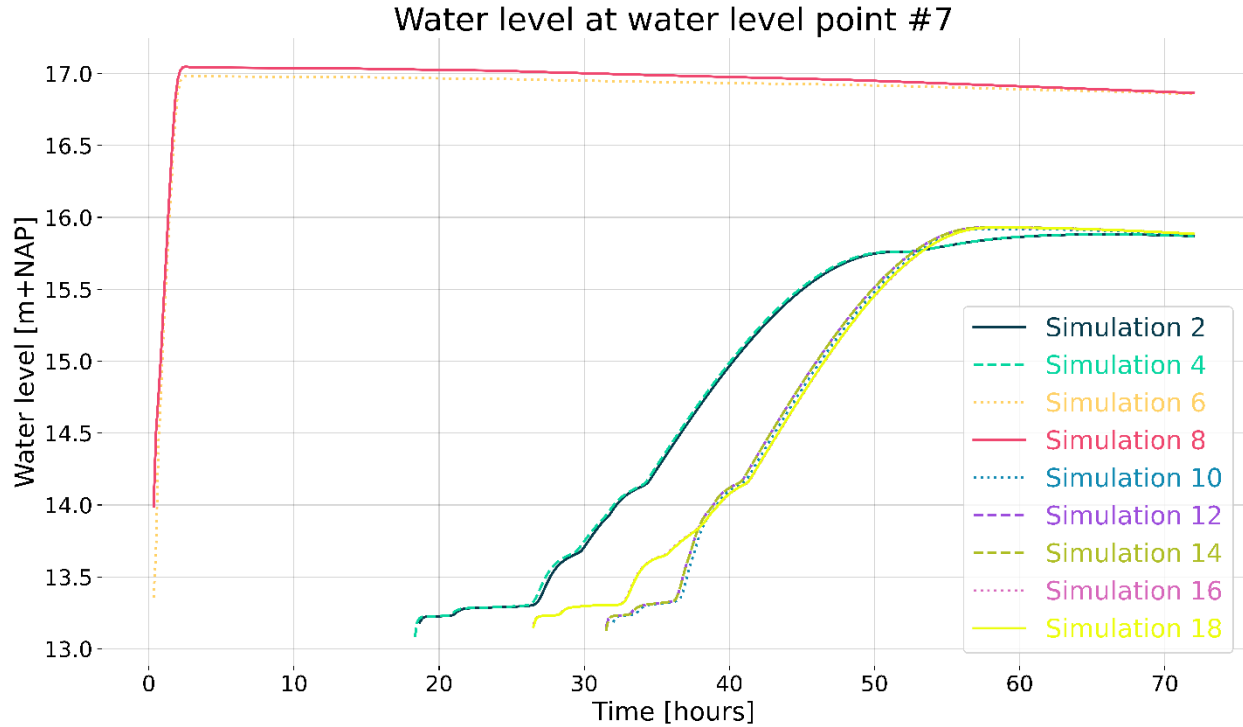


Figure 34 Water levels in simulations 2 to 18 (Cluster South) at water level point 7

### 5.3 CLUSTER NORTH

In Figure 35, the dike breach locations in this cluster are again shown. The dike breach locations are numbered with black numerals. Furthermore, the relevant part of the DEM which is covered by final inundation extent of all simulations in this cluster is shown. Moreover, the water level points where water level graphs of the simulations in this cluster will be compared are presented. These points are numbered with black numerals. Lastly, the local obstacles are represented by the white dashed lines. Areas between these obstacles will be referred to as compartments. These compartments are numbered with black Roman numerals.

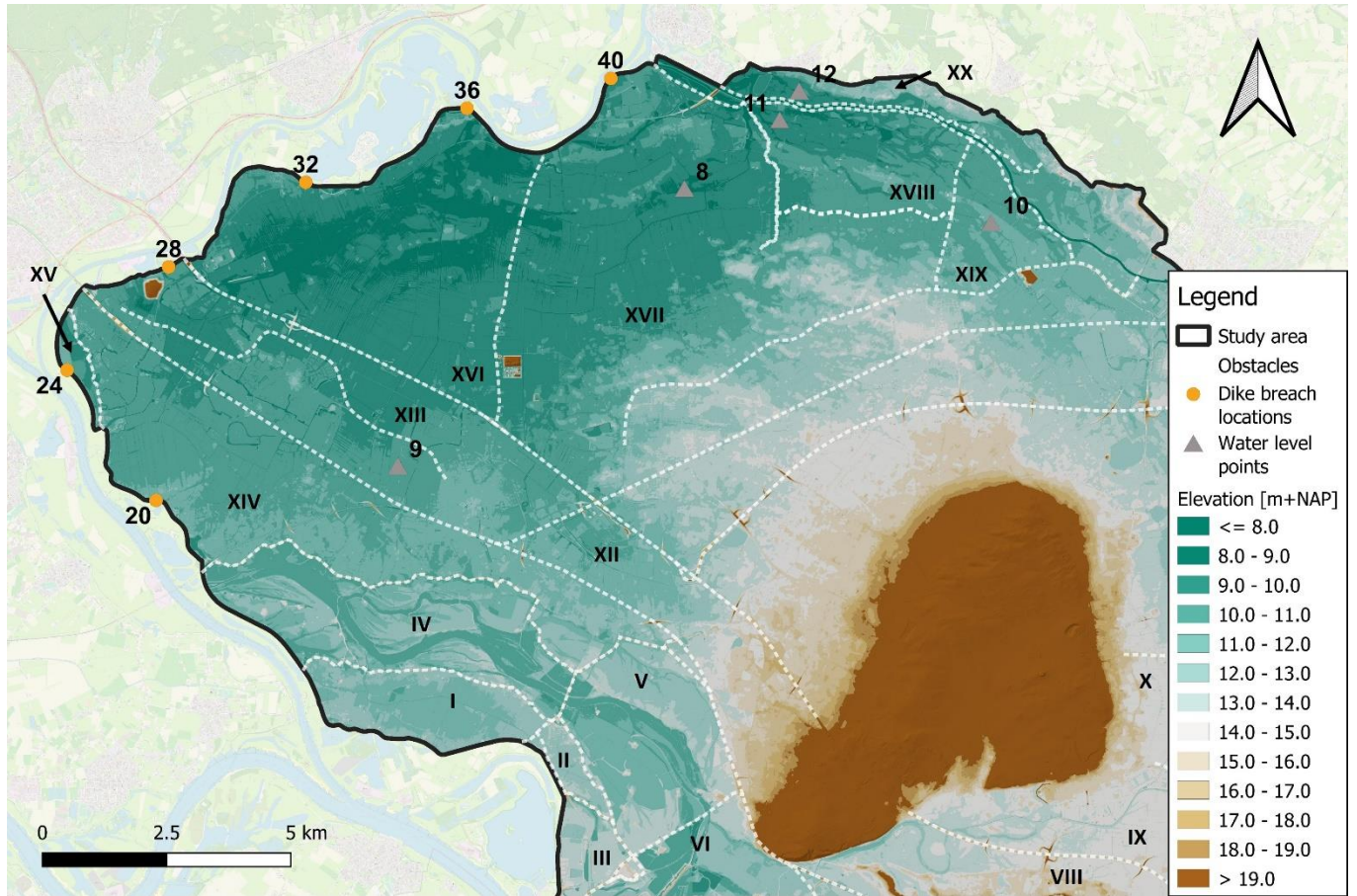


Figure 35 Relevant part of the DEM for Cluster North with relevant water level points where water level graphs will be compared. White dashed lines represent local obstacles. Areas between local obstacles are compartments and are numbered with black Roman numerals. Water level points and dike breach locations are numbered with black numerals.

### 5.3.1 Arrival times

In Figure 36, the MAD of the arrival times for Cluster North is shown. The sensitivity of the arrival time to the dike breach location becomes significant when the MAD is close to or larger than six hours as was explained in Section 3.5.2. Based on this criterion, it can be seen in Figure 36 that the sensitivity of the arrival times is significant in compartments XIV and in large part of compartments XIII, XVII and XVIII. The location of these compartments can be found in Figure 35. In all other compartments, the arrival times are not significantly sensitive to the dike breach location in this cluster.

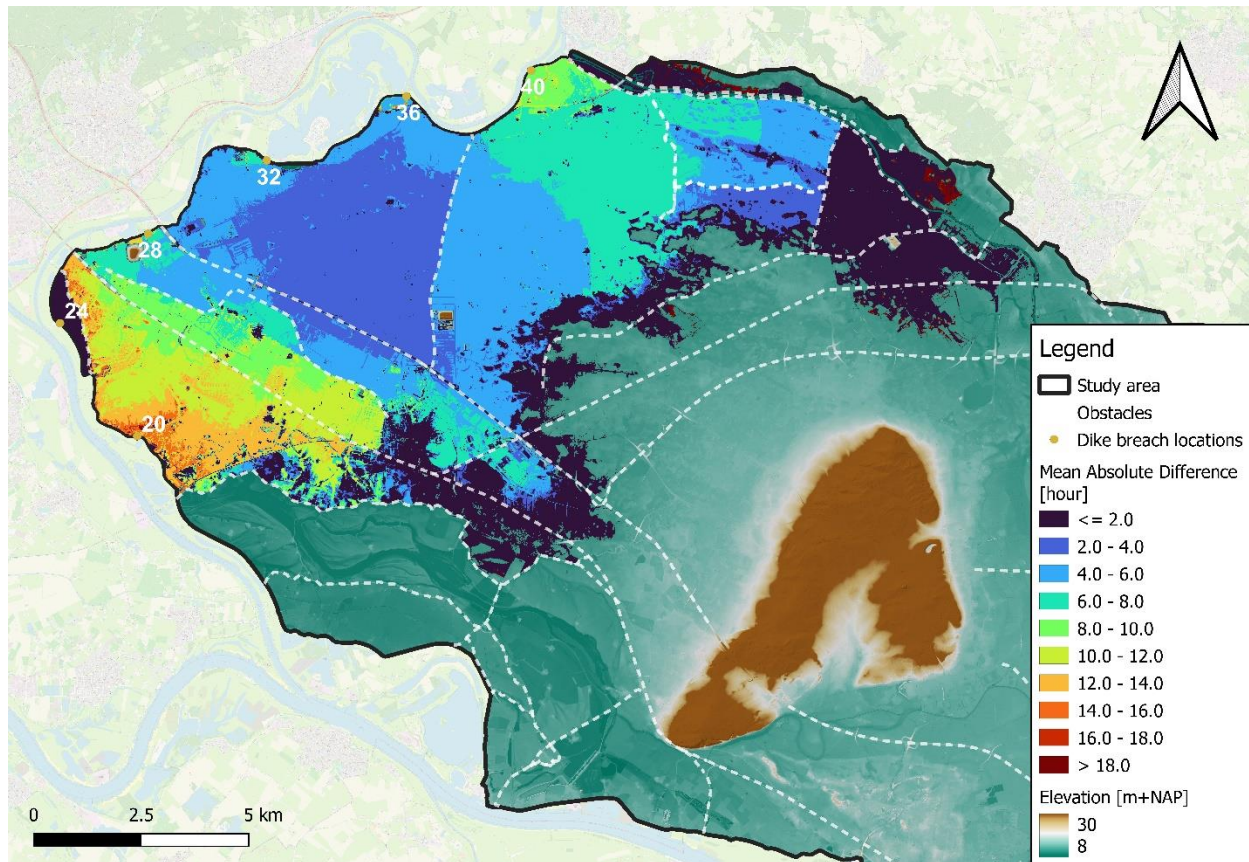
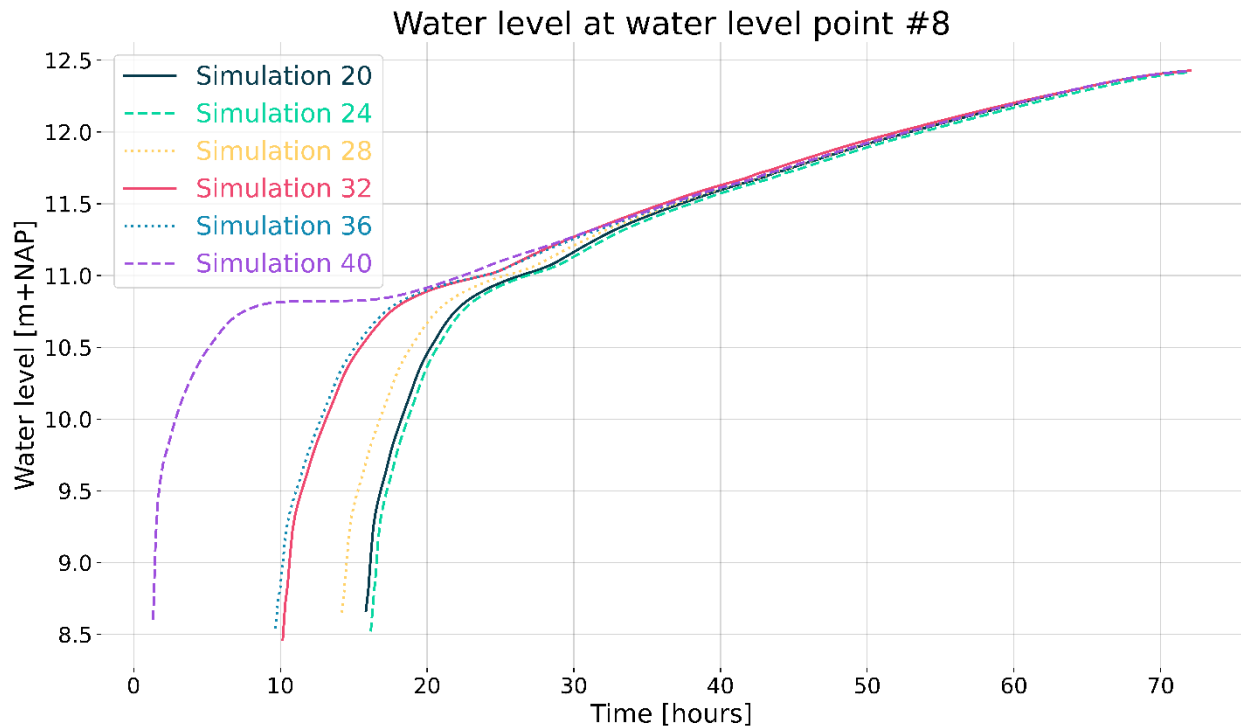


Figure 36 MAD of arrival times for Cluster North. White dashed lines represent local obstacles.

As can be seen in Figure 36, the arrival times in compartment XVI are only slightly sensitive to the dike breach location in Cluster North. Furthermore, the sensitivity is insignificant as the MAD is well below 6 hours. This compartment is the lowest part of the study area as can be seen in Figure 35 and is centrally located relative to the dike breach locations. Due to its lower elevation compared to all dike breach locations, the inundations in most simulations will be directed to this area early in the flood event. Moreover, due to its central location with respect to most dike breach locations, most inundations will arrive in this area at approximately the same time, within 12 hours after the dike breach.

Furthermore, in the area directly around this compartment (light blue area), the arrival times are slightly more sensitive to the dike breach location although still not significantly sensitive. These areas are less centrally located with respect to the dike breach locations in Cluster North. This means that these areas are reached earlier by inundations starting from dike breach location which are closer to these areas than from dike breach locations which are further away. For example, compartment XVII is reached earlier by an inundation in simulation 32 to 40 than in simulation 20 to 28. This shows that the location of an area with respect to the dike breach locations in Cluster North largely determines the sensitivity of the arrival times to the dike breach location. This can also be seen in the light-green area in compartment XVII. This area is even less centrally located which is also reflected in a higher sensitivity of the arrival times in this area to the dike breach location. These differences in the arrival times in this area can also be seen in the water level graphs of the different simulations at water level point 8 (see Figure 35 for the location of this point) which are shown in Figure 37. Here, it can be seen that inundation in simulation 40 already arrives at this point after 2 hours. The inundations in simulations 32 and 36 arrive at this point 8 hours later. Five hours later, the inundations in simulations 20 to 28 arrive at this location.



*Figure 37 Water levels in simulations 20 to 40 (Cluster North) at water level point 8*

Furthermore, as can be seen in Figure 36, the arrival times in compartment XIV and part of compartment XIII are very sensitive to the dike breach location in Cluster North. In these green-orange areas in Figure 36, the arrival times are also significantly sensitive to the dike breach location in this cluster.

Compartment XIV is at the same relative position to the dike breach locations as the light-green area in compartment XVII. However, the sensitivity of the arrival times to the dike breach location is higher in compartment XIV. This is mainly caused by the higher elevation in compartment XIV compared to the light-green area in compartment XVII as can be seen in Figure 35. In Figure 38, graphs of the water levels at water level point 9 are shown. As can be seen in Figure 38, inundations in simulations 20 to 28 arrive very early in the flood event at this water level point, as these simulations start in or close to this compartment. Around 20 hours, inundations in simulations 32 to 40 arrive in this area (see Figure 38). Due to the higher elevation, inundations in simulation 32 to 40 first need to fill the lower-lying area in compartments XIII, XVI and XVII until the water level has risen high enough to flow to the higher elevated area in compartment XIV.

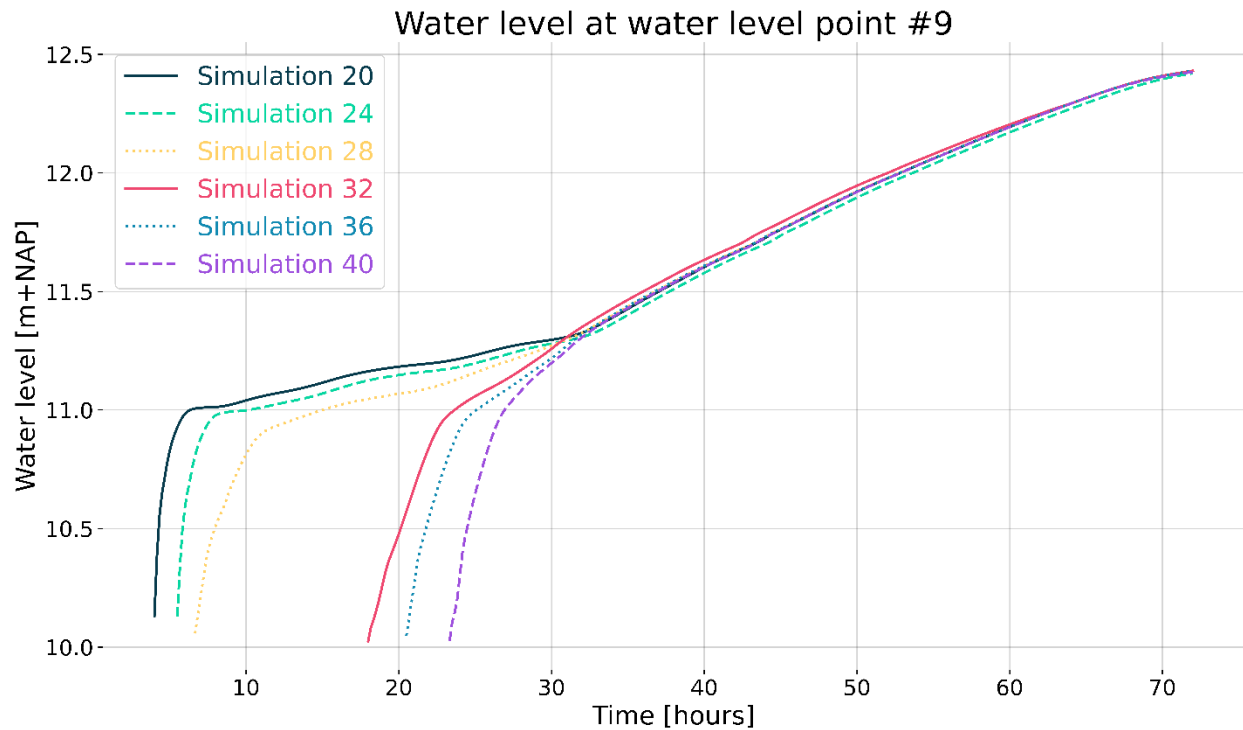


Figure 38 Water levels in simulations 20 to 40 (Cluster North) at water level point 9

At the edges of the inundated area (darker blue), the arrival times are less sensitive to the dike breach location in Cluster North. The sensitivity is also not significant. This is mainly caused by the elevation of this area and its position with respect to the dike breach locations. These areas are sufficiently distant from all dike breach locations to prevent from inundating at the start of the flood event. Combined with the higher elevation of these areas as can be seen in Figure 35, inundations in all simulations will first fill the lower-lying areas before they arrive at these higher elevated, more distant areas. For filling the lower-lying areas, the same amount of water is needed in all simulations. Furthermore, the inflow is the same in all simulations due to the use of the same inflow hydrograph. This means that filling the lower-lying areas in front of the more elevated areas will take the same amount of time in all simulations. In Figure 39, the water level graphs of the inundations in all simulations in Cluster North are shown for water level point 10. As can be seen in Figure 39, all inundations arrive relatively later in the flood event at this location.

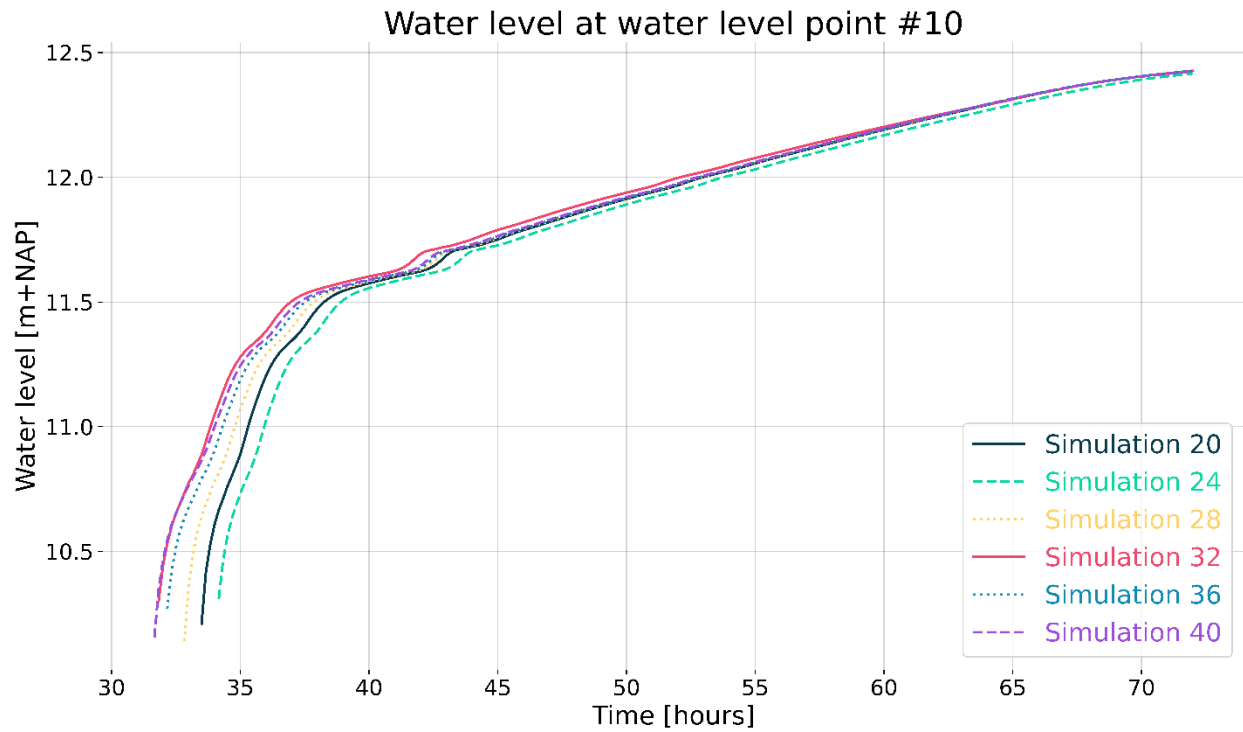


Figure 39 Water levels in simulations 20 to 40 (Cluster North) at water level point 10

### 5.3.2 Maximum water depths at day 1

In Figure 40, the MAD of the maximum water depths at the first day of the flood event for Cluster North is shown. The sensitivity of the maximum water depth to the dike breach location becomes significant when the MAD is close to or larger than 20 cm. Based on this criterion, it can be seen in that the sensitivity of the maximum water depths is significant in almost all compartments with the exception of compartments XVI and a large part of compartment XVII.

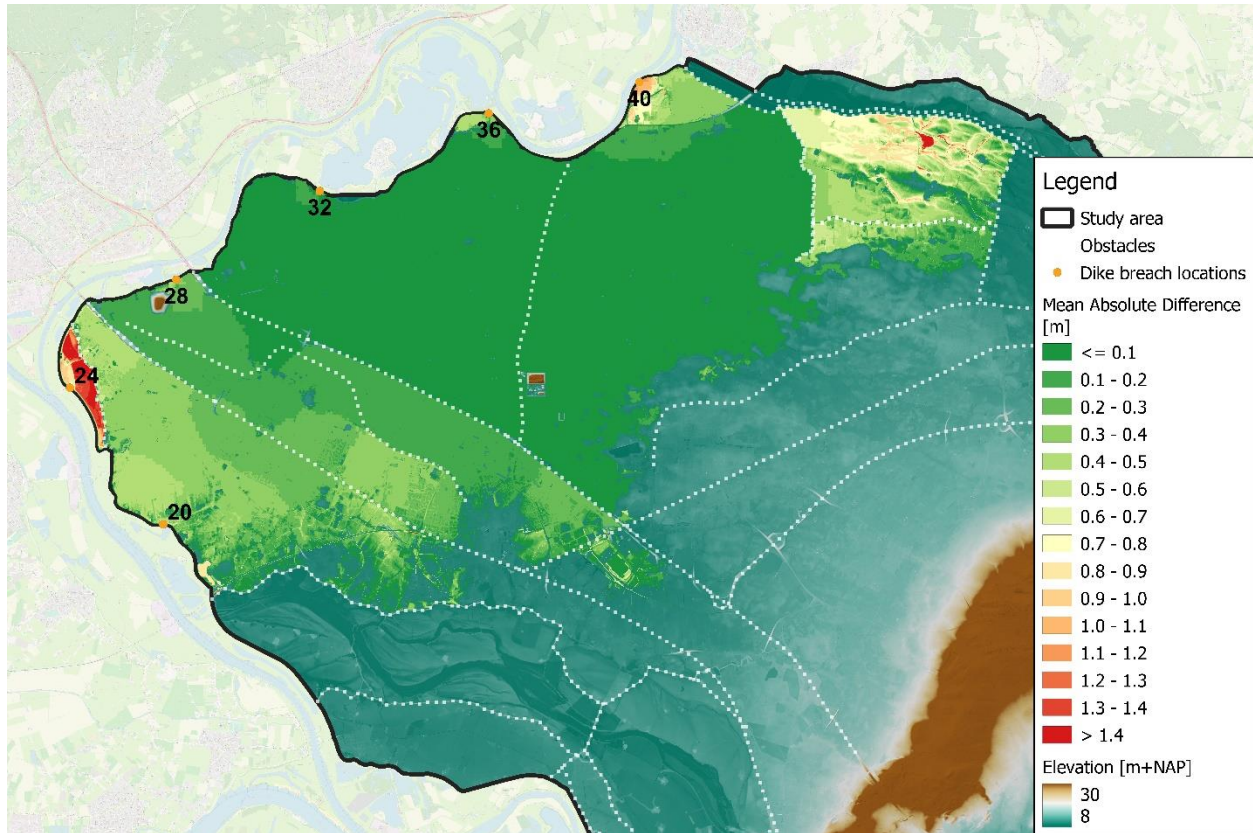


Figure 40 MAD of maximum water depths at day 1 for Cluster North

As can be seen in Figure 40, the maximum water depths at the first day in compartments XVI and XVII are almost not sensitive to the dike breach location in Cluster North. Although there may be differences in the arrival times of the inundations in the different simulations, all inundations have flooded the complete area before the end of the first day. When the area is completely flooded, the water will rise in the area which is almost independent on the location where the inundation starts (i.e., dike breach location). This can also be seen in Figure 37.

The maximum water depths in compartment XV are very sensitive to the dike breach location in Cluster North. Moreover, the maximum water depths are significantly sensitive. This is caused by the high water depths in this area for the inundation in simulation 24 while the inundations in all other simulations do not arrive in this area.

In compartments XIII and XIV, there is a gradual increase in the sensitivity of the maximum water depth to the dike breach location in Cluster North. The maximum water depths are also significantly sensitive in these compartments. The gradual increase in the sensitivity is caused by the gradual increase in elevation as can be seen in Figure 35. Furthermore, the area is more in the proximity of dike breach locations 20 to 28 than of dike breach locations 32 to 40. As already mentioned, this causes later arrival times of inundations in simulations 32 to 40. These later arrivals cause that the maximum water depth after the first day is not as high for the inundations in simulations 32 to 40 than in the simulations 20 to 28.

Moreover, as can be seen in Figure 40, maximum water depths at the first day in compartment XVIII are quite sensitive to the dike breach location in Cluster North. The sensitivity is also significant as the MAD

in the complete compartment is higher than 20 centimetres. At the west side, the compartment is bordered by two small embankments which temporarily block the flow. Furthermore, this part of the study area is closer to dike breach 40 and more distant from dike breach locations 20 to 28. As can be seen in Figure 41, this causes the water level west of the embankments to be risen high enough to flow over the embankments earlier in case of simulation 40. The inundations in simulations 32 and 36 arrive ten hours later while inundations in simulations 20 to 28 arrive just before the end of the first day. These later arrival times around the end of the first day cause the maximum water depths to be different for the different simulations. This can also explain the higher sensitivity of the maximum water depths at the end of the first day to the dike breach locations in this compartment.

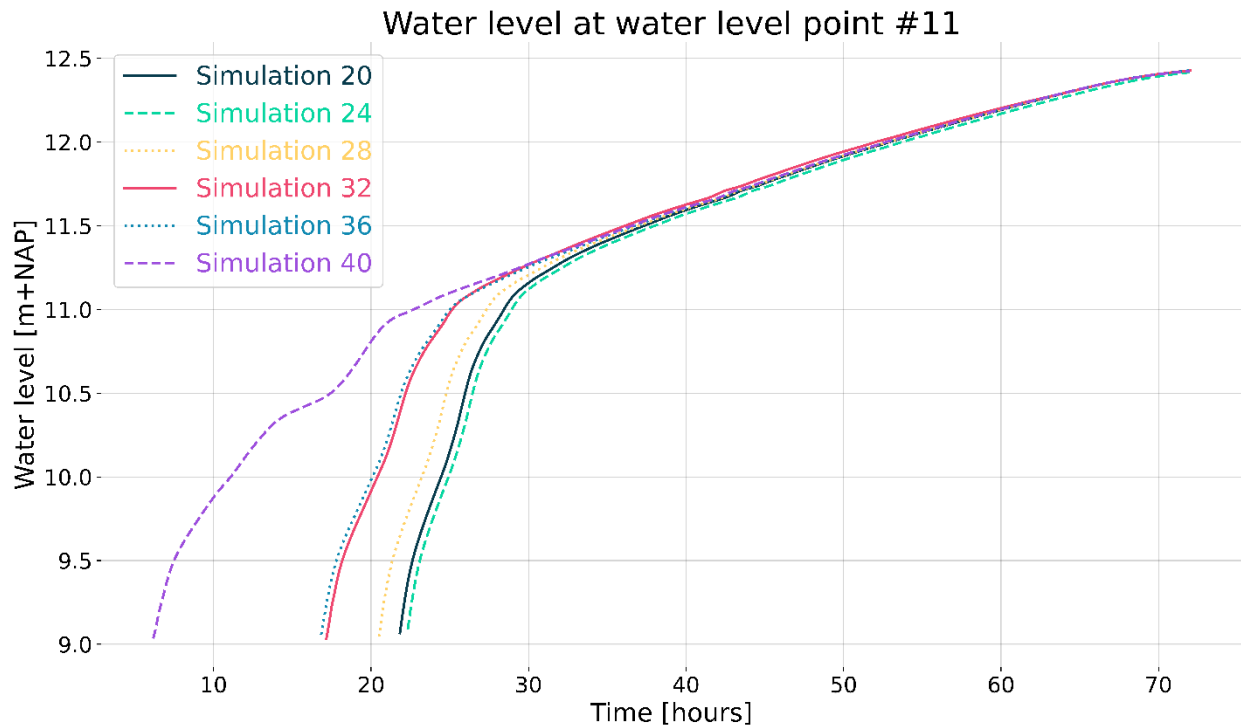


Figure 41 Water levels in simulations 20 to 40 (Cluster North) at water level point 11

### 5.3.3 Maximum water depths at day 2

In Figure 42, the MAD of the maximum water depths at the second day of the flood event for Cluster North is shown. As can be seen in Figure 42, the maximum water depths are still only significantly sensitive to the dike breach location in compartment XV, because the MAD is higher than 20 centimetres. In the rest of the study area, the maximum water depths are not significantly sensitive to the dike breach location.

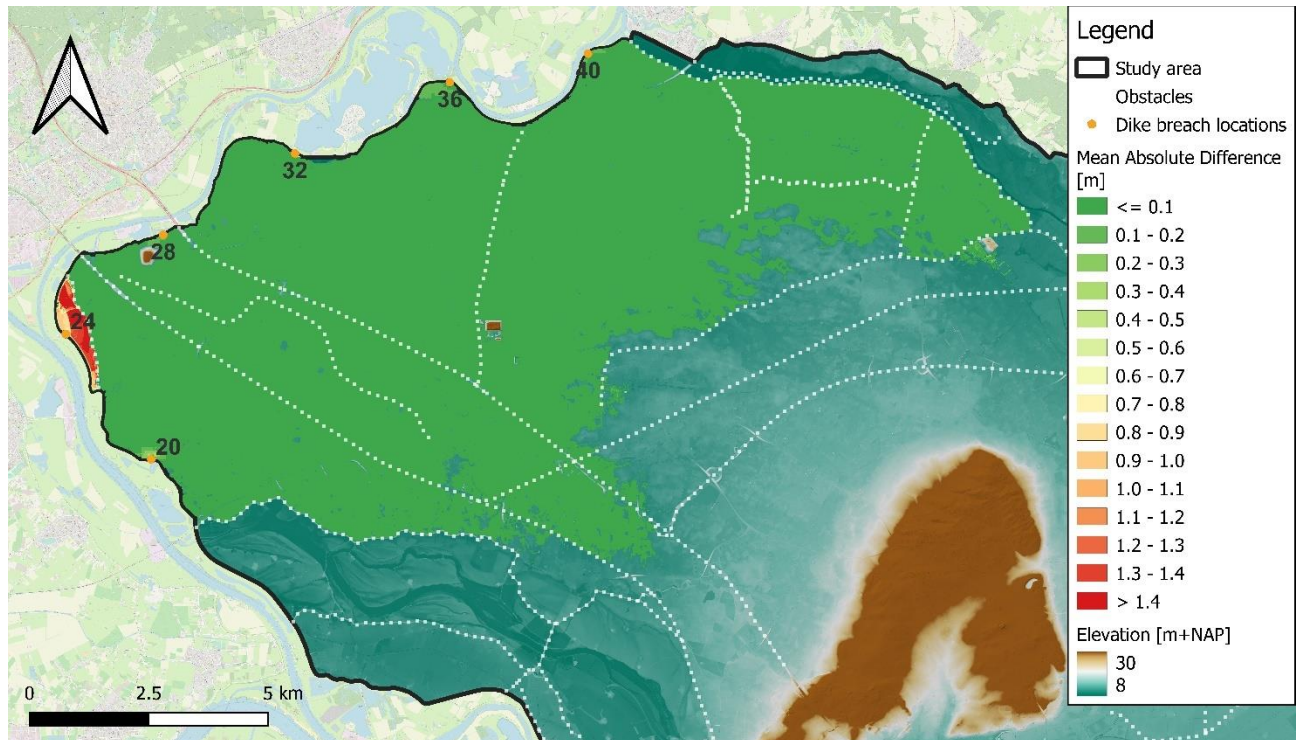


Figure 42 MAD of maximum water depths at day 2 for Cluster North

As can be seen in Figure 42, the maximum water depths at day 2 in almost the complete inundated area are insensitive to the dike breach location in Cluster North. In the first day, the low-lying part of the study area is reached by the inundations in all simulations of Cluster North. When the area is completely flooded, the water will slowly and almost equally rise in the complete area which almost independent on the dike breach location. This causes differences in the water level between the different simulations to diminish as can be seen in Figure 37, Figure 38, Figure 39 and Figure 41. In these figures, it can be seen that water levels in the different simulations tend to converge before the end of the second day. Yet, the maximum water depths in compartment XV are still very sensitive to the dike breach location. The reason for this very high sensitivity is already explained in the previous section.

#### 5.3.4 Maximum water depths at day 3

In Figure 43, the MAD of the maximum water depths at the third day of the flood event for Cluster North is shown. Here, it can be seen that the maximum water depths are only significantly sensitive to the dike breach location in compartment XV and XX, because the MAD is higher than 20 centimetres. In the rest of the study area, the maximum water depths are not significantly sensitive to the dike breach location.

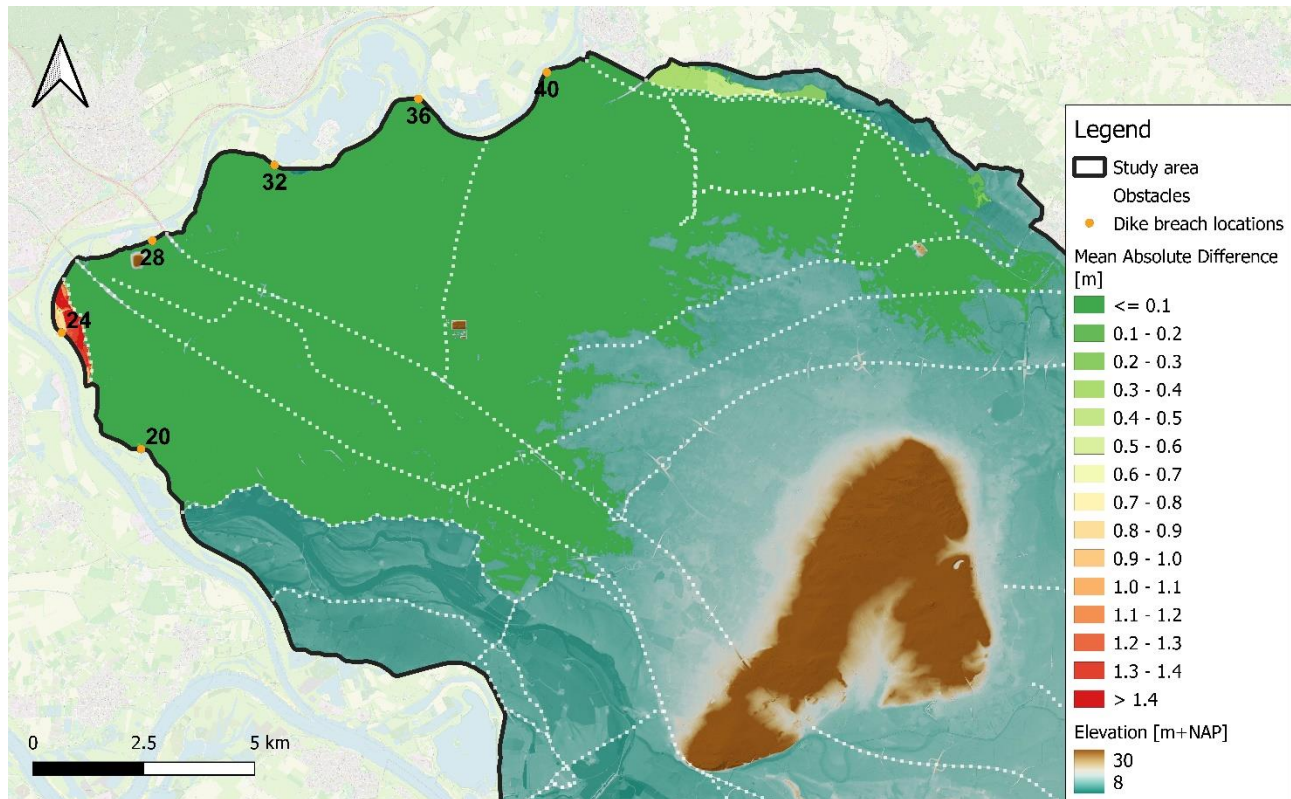


Figure 43 MAD of maximum water depths at day 3 for Cluster North

As can be seen in Figure 43, the maximum water depths at day 3 in almost the complete inundated area are still insensitive to the dike breach location. Furthermore, the maximum water depths in compartment XV are still very sensitive to the dike breach location. The reason for both sensitivities is already explained in the previous sections. The maximum water depths at day 3 in compartment XX are quite sensitive to the dike breach location. This compartment is located behind two dikes along the Oude IJssel and is only reached by the inundations in all simulations just before the end of the third day. However, as this compartment is closer to dike breach 40, the inundation in simulation 40 arrives earlier in this compartment. The inundations in simulations 20 and 28 to 36 arrive an hour later while the inundation in simulation 24 arrives completely at the end of day 3 as can be seen in Figure 44. These differences in arrival times combined with high rise rate of the water cause the differences in the water depths at the end of day 3 to be quite large.

### Water level at water level point #12

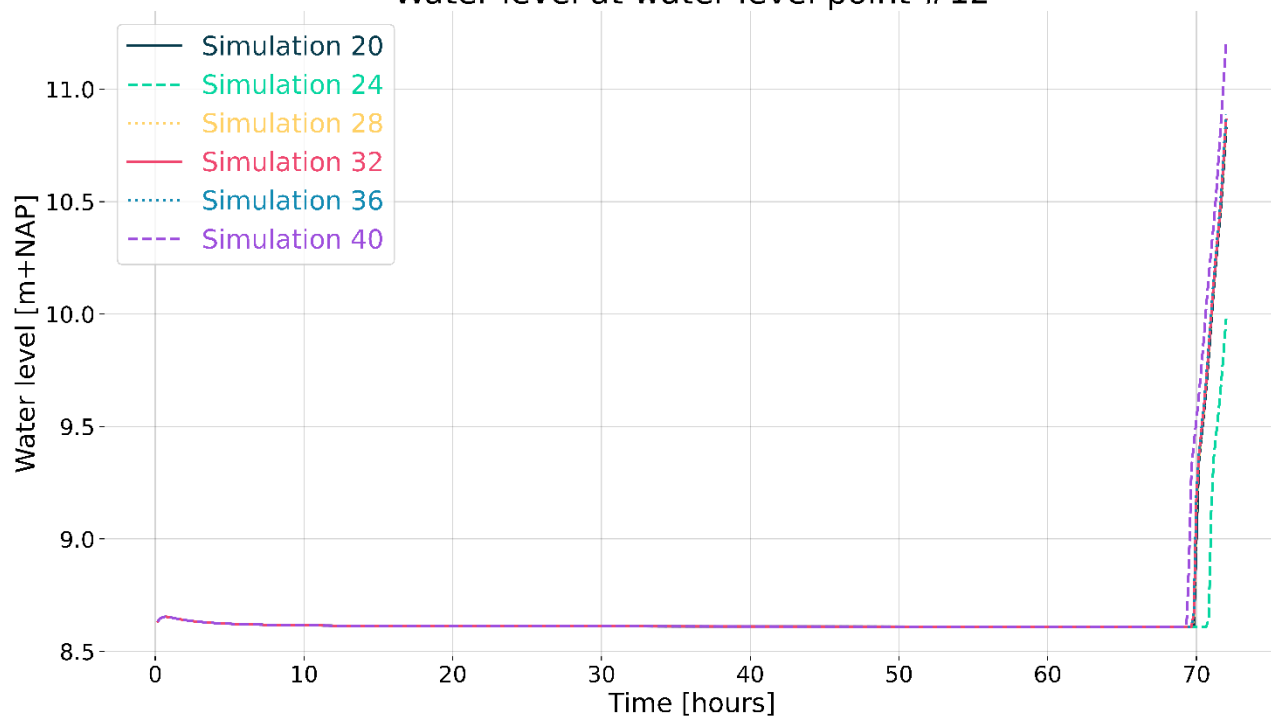


Figure 44 Water levels in simulations 20 to 40 (Cluster North) at water level point 12

# 6. DISCUSSION

---

## 6.1 MAIN FINDINGS

### 6.1.1 Sensitivity analysis of the computational grid

The first phase of the sensitivity analysis of the computational grid showed that larger computational cells can be used without a significant effect on the water depths. For the arrival times, differences between coarser grids and a 40×40 m<sup>2</sup> grid are predominantly small although the differences at the edges of the inundated area are larger. Both these observations are in accordance with a modelling study of Volp et al. (2013) and Yu and Lane (2006b) who found that using a subgrid, the dependence of hydrodynamic results on the grid resolution decreased. However, these observations contradict with modelling studies which used conventional hydrodynamic models (e.g., Alipour et al., 2022; Caviedes-Voullième et al., 2012; Mooijaart, 2023; Yu & Lane, 2006a). In these studies, significant influence of the grid size on simulated hydrodynamics was found. This difference between subgrid-based models and conventional models is probably caused by the way the elevation is considered in both types of models as was explained in Section 2.3.

The second phase of the sensitivity analysis showed that properly schematizing openings/underpasses in obstacles is important to accurately simulate arrival times and water depths. Not properly schematizing these model elements is especially a problem in areas where water is strongly confined between obstacles (e.g., dikes). In this type of areas, underpasses or openings in obstacles play a crucial role in guiding the water through an obstacle. This limits the water level in the area in front of the obstacle and decreases the arrival time behind the obstacle. Therefore, it may be necessary to refine the computational grid around openings and underpasses in coarser grids to ensure consistency with a finer grid. It is not necessary to refine the computational grid along all obstacles. This will not result in a more accurate simulation of the water depths and arrival times while it increases the computational time of a simulation.

### 6.1.2 Analysis of the maximum inundation extent

In the qualitative analysis of the maximum inundation extent of all simulations, two distinct maximum inundation extents were found. This means that the primary dikes around the study area can be divided into two dike sections where the final inundation extent is almost independent of the exact dike breach location in the section. This seems to contradict with results of the VNK study (Arends & Bisschop, 2014) which found that the dike could be divided into six sections (see also Figure 4). These sections were also used by de Bruijn et al. (2014). However, the section in Arends and Bisschop (2014) do not only result in the same inundation extent, but in the same flood damage too. For flood damage, other factors which matter are flow velocity, order of arrival and water depths. These factors were not considered in the determination of the two sections in this study. As these factors are more spatially variable than the final inundation extent, clustering dike breach locations with the same flood damage and inundation extent will result in smaller clusters and thereby more dike sections. The two dike sections where the final inundation extent is almost independent of the exact dike breach location in the section are much longer than 1 km. This is in accordance with the study of Apel (2009). Based on the research of Apel (2009), it can be concluded that dike segments in the Lower Rhine area where inundation patterns are independent of the exact breach location within the segment are at least 1 km.

Furthermore, the analysis of the maximum inundation extent showed that the regional dike around the Rijnstrangen area causes the distinction between both inundation extents. The regional dike forms a barrier for flow from south to north and the other way around. Due to this dike, floods due to dike breaches south of the dike will fill the Rijnstrangen area. These inundations will only flood the area north of dike when water in this compartment is high enough to flow over the sides of the regional dike. Inundations starting at dike breach locations north of the dike will not flood the area south of the regional dike as water will not rise high enough to flow over the dike in the simulated flood event. If this dike breaches, the inundation extent and pattern of many inundations will be completely different.

For evacuation planning and early warning systems, it is important in the case of high discharge event to at least determine in which of the two dike sections it is most probable a dike will breach. The differences in the resulting inundation pattern are so large that an incorrect determination of the dike breach in the incorrect dike section can result in a mistimed evacuation and potentially high loss of life. For example, all inundations arrive in the compartments in the north of the study area (XVI and XVII). However, the inundations in Cluster North will arrive at least 12 hours earlier which also means that water depths will be higher earlier in the flood event. If it was forecasted that a dike breach would happen in Cluster South, people would not be evacuated based on early warning but on their own perception. This can result in up to six times more casualties (Alonso Vicario et al., 2020).

#### 6.1.3 Analysis of the arrival times

The quantitative analysis of the sensitivity of the arrival times for the dike breach location within each cluster showed that the spatial variability in this sensitivity is mainly caused by three factors, namely the elevation, the presence of higher line elements and the distance to the dike breach locations.

Firstly, in lower-lying areas and centrally located areas, which are in the proximity of most dike breaches, the sensitivity of the arrival times to the dike breach location is insignificant. An example of this type of area is compartment XVI in Figure 36. Due to the lower elevation, the inundations starting at most dike breach locations will be directed to these areas early in the flood event as water tends to flow to the lowest location. Moreover, due to the central location, most inundations will arrive in these areas at approximately the same time.

Secondly, arrival times in lower-lying and less centrally located areas are slightly more sensitive to dike breach location compared to the arrival times in the lower-lying areas and centrally located areas. In both type of areas, water of all inundations is directed to these areas due to its low elevation. Yet, in less centrally located areas, some inundations will arrive earlier as the dike breach locations where these inundations started are closer to the area. This causes more spread in the arrival times which makes the arrival times in these areas more sensitive. In these lower-lying and less centrally located areas, the sensitivity of the arrival times tends to be insignificant. Yet, if the location becomes even less central, arrival times will become significantly sensitive to the dike breach location. An example is the difference in the sensitivity of the arrival times in compartment XVII in Figure 36. The west side of this compartment is more centrally located than the east side. This causes a difference in the sensitivity of the arrival times between the west and east side. Furthermore, the arrival times are significantly sensitive to the dike breach location in the east side of this compartment.

Thirdly, the arrival times in higher lying and less centrally located areas are significantly sensitive to the dike breach location. Furthermore, the arrival times are more sensitive than in areas which are lower lying. This type of higher-lying and less centrally located areas is closer to some breaches than others which already causes differences in the arrival times to occur in these areas. These differences are

increased as inundations which are not induced in this type of areas must overcome an elevation difference.

However, if these elevated areas are located at the edges of the lower areas and further away from all dike breach locations, arrival times will be almost insensitive to the dike breach location. These areas are sufficiently distant from all dike breach location to prevent from inundating at the start of the flood event. Combined with the higher elevation of these areas, inundations at the different dike breach locations will first fill the lower-lying areas before they arrive at these higher elevated, more distant areas.

Lastly, arrival times in small compartments which are completely enclosed by obstacles without large openings and underpasses are significantly sensitive to the dike breach location. Inundations which start in these areas will immediately flood this type of compartments. The inundations starting at all other dike breach locations will arrive much later in this type of compartments due to obstacles around the area. An example of these areas are compartments I, II and III in Figure 24.

#### 6.1.4 Analysis of the maximum water depth

The sensitivity of maximum water depths to dike breach location varies over time. In the period directly after the arrival of the first inundation, maximum water depths are most sensitive to dike breach location. From this point in time, the water depth of the first inundation starts rising while the water depth of the inundations in all other simulations is still zero, because the inundations in these simulations did not arrive yet. So, if there is a large spread in the arrival times of the inundations in the different simulations, the difference in the water levels between the inundations in the various simulations will be larger as well. This means that in areas where arrival times are sensitive to the dike breach location, the maximum inundation water depths are most sensitive to dike breach location. Furthermore, in these areas, maximum inundation water depths tend to be sensitive for a longer period.

This can clearly be seen in Cluster South. In compartments I, II and III, the arrival times are significantly sensitive. Furthermore, the water depths are significantly sensitive on day 1 and day 2. Only on day 3, the water depths in these compartments are not significantly sensitive anymore. The arrival times in compartments IV, V and VI are less sensitive than in compartment I, II and III although in large parts of these compartments the arrival times are significantly sensitive. The maximum water depths in these compartments are also less sensitive in absolute sense compared to the maximum water depths in compartment I, II and III. Moreover, the maximum water depths are only significantly sensitive on day 1. On day 2 and day 3, the maximum water depths in these compartments are not sensitive to the dike breach location anymore. In the compartments north of the Rijnstrangen area (> XI), the arrival times are even less sensitive to the dike breach location in Cluster South. In these compartments, the maximum water depth is always almost insensitive to the dike breach location. This shows that in areas where the arrival times are more sensitive to the dike breach location, the maximum water depths are more sensitive and for a longer period of time.

In general, after all inundations arrived, water depths tend to get less sensitive over time especially if the rise rate of water level for the later arriving inundations is high. So, the sensitivity of the maximum water depth decreases over time. However, in certain specific cases, water depths tend to become temporarily more sensitive as can be seen in Figure 30. This is the case when the rise rate of the later arriving inundations decreases. This can be caused by an increasing flow of these inundations to other compartments. Due to this decrease in rise rate, maximum inundation water depths can also be sensitive

to dike breach location in areas where arrival times are only slightly sensitive to the dike breach locations.

The analysis of the sensitivity of the arrival times and maximum water depths showed that both sensitivities vary over space and sensitivity of the maximum water depth also varies over time. This is in accordance with a study of Savage et al. (2016). They concluded that the sensitivities of the inundation pattern to several other model inputs are variable in time and space.

Some locations in the hinterland where arrival times and maximum water depths are significantly sensitive, larger urban areas are situated. For example, Westervoort, Duiven and Zevenaar are situated in compartment XIII and XIV while Pannerden and Tolkamer are situated in respectively compartment I and III. In these areas, it is important to accurately determine the arrival times and water depths to timely evacuate all inhabitants of these areas and thereby to prevent a large loss of life. To correctly determine the arrival times and water depths in these urban areas, it should be known with more accuracy where a dike will breach in case of an extreme discharge event due to the significant sensitivity of the inundation pattern in these areas. For evacuation purposes, hydrodynamic simulations of dike breaches are often performed in advance. During the extreme flood event, the results of these simulations are used to decide on the evacuation. To accurately predict water depths and arrival times in these urban areas, at least one dike breach should be simulated per dike section. These dike sections are shown in Figure 45. A dike breach at any location in a certain section will result in the same final inundation extent, similar arrival times and maximum water depths. These sections were determined based on the water level graphs as presented in Sections 5.2 and 5.3. In these water level graphs, it can be seen that inundations starting at certain dike breach locations will have similar, if not the same, water level graphs. For early warning systems, more and more data-driven models, such as neural networks, are used due to their low computational costs (in the order of minutes) which make them suitable in a more operational context. These models should be trained with simulations of hydrodynamic models. To accurately predict water depths and arrival times in the aforementioned urban areas, it is important to train these models with at least one simulation of a representative dike breach per dike section in Figure 45.

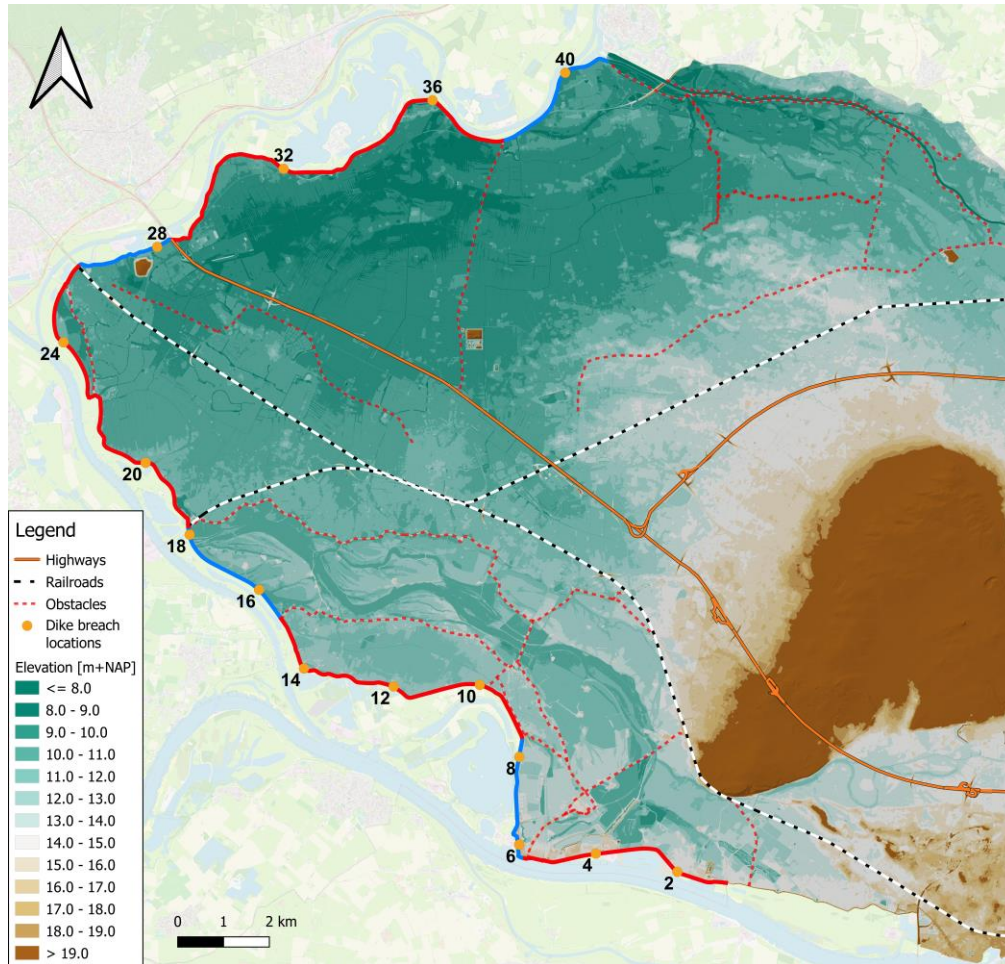


Figure 45 Dike sections (red and blue lines) where a dike breach will result in similar inundation extent, arrival times and maximum water depths.

## 6.2 LIMITATIONS IN THE METHODOLOGY

The limitations in the used methodology and their implications on the main findings will be discussed in the sections below.

### 6.2.1 Model set up

A limitation of this study is that the model cannot be validated with field measurements. The last inundation in the area happened in 1926 (Arends & Bisschop, 2014). No field measurements of this inundation are available. Due to the absence of these measurements, the sensitivity analysis lacks an objective reference. This means that the sensitivity analysis of computational grid relies heavily on the implicit assumption that reference model or the model with the finest grid produces more accurate results.

Moreover, the results of this study are only valid under the assumption that higher line elements in the study area do not fail. The strength of most regional dikes is highly uncertain especially under extreme load during flood events. A quickscan of some higher objects in the area by Van Berchum (2021) showed that roads will fail in case of overflow and that the dikes along the Rijnstrangen area are vulnerable to failure due to piping. If, for example, these dikes fail, the inundation pattern and extent of especially the inundations at the dike breach locations 2 to 18 will be completely different. It is not yet known to which

extent this will also change the findings about the sensitivity of the arrival times and the water depths to the dike breach location.

A limitation of the model schematisation is that the cross-sections of the major waterways except for the Oude IJssel are not added to the DEM or that these waterways are schematized as 1D branches. Floods propagate faster through waterways than over land due to less friction in waterways. This makes that areas along streams are more likely to experience flooding despite being far away from the dike breach location (Prinsen et al., 2020). Therefore, not adjusting the DEM at the location of the waterways results in later arrival times. Although the inundations at all dike breach locations experience this limitation, adjusting the DEM at the location of the waterways will change the sensitivity of the arrival times and thereby also of the water depth at some locations. For example, in the Rijnstrangen area, inundations at dike breaches 2 to 8, 16 and 18 will arrive earlier than in the current model while the inundations at dike breaches 10 to 14 will still arrive at the same time, because they are still blocked by the higher dike around the compartment where they are induced in. This means that the spread of arrival times will be larger in this area thus increasing the sensitivity of the arrival times to the dike breach location. Yet, it is expected that overall, this increase is only small in the largest part of the study area. Still, this could mean that at certain locations the sensitivity of the arrival times and water depths will become significant. However, as the complete study area and all simulations experience this limitation, the conclusions about the relative sensitivity of the different type of areas will not change. This means that arrival times and maximum water depths in lower-lying and centrally located areas will remain the least sensitive. Furthermore, the inundation pattern in more elevated, less centrally located areas will remain more sensitive than the inundation pattern in the lower-lying, centrally located areas.

#### 6.2.2 Used hydrograph

The results of this study are based a specific, similar hydrograph at all dike breach locations. Firstly, the computed sensitivities may be different for hydrograph of a different flood event as the inflow volume will be different. Furthermore, as mentioned in Section 3.4.3, this hydrograph was based on an outflow hydrograph of a simulated dike breach along the IJssel in the study of Bomers (2021). This hydrograph of Bomers (2021) was based on a dike breach at the highest point of the river discharge hydrograph. A dike breach at an earlier or later moment during the discharge event results in a larger or smaller inflow volume into the dike ring even for the same discharge event. Next to this, the hydrograph was adjusted for assumed breach width of 75 m. However, the breach width is very uncertain and a different breach width results in a different inflow volume. In all three cases (different flood event, different moment of dike breach and different breach width), the inflow volume at all dike breach locations will change. This will change the sensitivities at all locations in the hinterland. For example, in case of a lower inflow volume, there may be a larger spread in the arrival times and a later convergence of the water levels due to lower flow velocities and rise rates. This will lead to a higher sensitivity of the arrival times and maximum water depths at almost all locations. This means that at several locations, the sensitivity of the arrival times will become significant. Furthermore, the maximum water depths will be significantly sensitive at more locations and for a longer period. However, as this happens for almost the complete study area, it is expected that the relative sensitivity of the different type of areas will not change. This means that lower-lying and centrally located areas are still the least sensitive and higher-lying, less centrally located areas are still more sensitive.

As already mentioned, the hydrograph of Bomers (2021) was based on a dike breach along the IJssel. However, for the same extreme discharge event, discharges in the Rhine and the Pannerdensch Kanaal will be larger than the discharge in the IJssel (ten Brinke, 2013). This means that for the dike breaches along the Pannerdensch Kanaal and the Rhine, inflow discharges were underestimated. When different

hydrographs for the Pannerdensch Kanaal and the Rhine are used, the sensitivities of the arrival times and water depths will be impacted. For example, in Cluster North, the inflow volume at dike breach locations 20 and 24 will increase. This will lead to earlier arrival times in all compartments. Yet, the arrival times of inundations starting at dike breach locations 28 to 40 will not change. This means that the sensitivity of the arrival times will increase in compartments XII to XVI while it will decrease in compartment XVII. This also means that the relative sensitivity of the different type of areas will change. It is expected that locations which are further away from dike breach locations with a higher inflow volume and closer by dike breach locations with a lower inflow volume will become less sensitive. If these less-centrally located areas are also lower-lying, arrival times will be almost insensitive to the dike breach location. Arrival times in other less-centrally located and centrally located areas are expected to become more sensitive.

### 6.2.3 Significance of the sensitivity of the maximum water depths to the dike breach location

As mentioned in the methodology (Section 3.5.3), the maximum water depths are significantly sensitive when the MAD is higher than 20 centimetres. This may be significant when the maximum water depth is around 20 centimetres as emergency services cannot drive when the water depths are more than 20 centimetres. However, when water depths are larger (around 1 meter), an increase or decrease of 20 centimetres will be less significant for evacuation purposes. Furthermore, when water depths are higher than 2 metres, an increase or decrease of 20 centimetres will be even less significant for evacuation purposes. Therefore, care should be taken in labelling the maximum water depth at certain location as being significantly sensitive. Yet, this does not alter the conclusions about the relative sensitivity of the maximum water depths in the different parts of the study area. In areas where arrival times are most sensitive, maximum water depths are more sensitive and for a longer period than in areas where arrival times are less sensitive.

# 7. CONCLUSION AND RECOMMENDATIONS

---

## 7.1 CONCLUSIONS

The aim of this study was to assess the spatial and temporal sensitivity of inundation patterns to the location of a dike breach in dike ring 48 in the Netherlands. Four sub-questions were set up to guide the research and answer the main research questions. Each will be discussed below, and afterwards the main research question is answered.

1. *How can an accurate and computationally efficient hydrodynamic model be set up to compute inundation patterns?*

A subgrid based hydrodynamic model was set up which efficiently considers high resolution elevation data. The elevation of underpasses with an unrealistic bottom level were adjusted to enable flow of the water through the underpasses at the correct elevation. Furthermore, higher line elements were schematized as obstacles to prevent them from being overlooked by the modelling software. Due to the use of high resolution elevation data on the subgrid, larger computational grid sizes can be used which decreases computational time without significantly compromising the accuracy of the simulated inundation water depth and arrival times. The sensitivity analysis of the computational grid also showed that an incorrect schematization of underpasses in the computational grid can have a large influence on the accuracy of the simulated water depths and arrival times. Therefore, the computational grid was locally refined around the underpasses which increased the accuracy of the water depths and arrival times. Refining all obstacles instead of all openings did not further increase this accuracy while the computational time increased.

2. *Which dike breaches result in qualitatively similar maximum inundation extents?*

The dike breaches at the different dike breach locations result in two distinct types of maximum inundation extents after three days. Dike breaches south of the high regional dike along the Rijnstrangen area result in a qualitatively similar maximum inundation extent while dike breaches north of this dike also result in a qualitatively similar maximum inundation extent. Although some areas are only inundated in some simulations, these areas are small compared to the area of the maximum inundation extent which is qualitatively similar. The distinction in the maximum inundation extent between the dike breaches north and south of the high regional dike along the Rijnstrangen area shows the importance of this dike for defining the inundation patterns in the study area.

3. *What is the spatial sensitivity of the arrival times to dike breach location?*

Three characteristics of study area determine the spatial sensitivity of the arrival times to the dike breach location in a certain cluster, namely the elevation, the presence of higher line elements and the distance to the dike breach locations. Arrival times in areas which are lower lying and centrally located are slightly sensitive to the dike breach location while arrival times in areas with similar elevation and a less central location are slightly more sensitive to the dike breach location. In more elevated areas which are less centrally located, arrival times are significantly sensitive to the dike breach location. Contrary to this, if these elevated areas are located at the edges of the lower areas and further away from all dike breach locations, arrival times in these areas will be almost insensitive to the dike breach location. Moreover, arrival times in small compartments which are completely enclosed by obstacles without large openings and underpasses are significantly sensitive to the dike breach location.

4. *What is the spatial and temporal sensitivity of the maximum inundation water depths to dike breach locations?*

The sensitivity of maximum water depths to dike breach location changes over time. In the period directly after the arrival of the first inundation, maximum water depths are most sensitive to the dike breach location. After the inundations in all simulations arrived, water depths tend to get less sensitive over time especially if the rise rate of water level for the later arriving inundations is high. This means that in areas where arrival times are sensitive to the dike breach location, the maximum inundation water depths are most sensitive to dike breach location. Furthermore, in these areas, maximum inundation water depths tend to be sensitive for a longer period. In general, it can be concluded that the sensitivity of the maximum water depth mostly decreases over time.

*To which extent is the progress of the inundation pattern sensitive to the location of a dike breach in the primary flood defences of dike ring 48?*

Although there are several limitations to the used methodology, it can still be concluded that the sensitivity of the inundation pattern to the dike breach location is determined to a large extent by three characteristics. These characteristics are the elevation, the presence of higher line elements and the distance to the dike breach locations. In lower-lying and centrally located areas, the inundation pattern is only slightly sensitive to the dike breach location and for a short period. In areas with similar elevation and at a less central location, the inundation pattern is slightly more sensitive to the dike breach location. In more elevated areas which are less centrally located, the inundation pattern is significantly sensitive to the dike breach location and for a longer period. Contrary to this, if these elevated areas are located at the edges of the lower areas and further away from all dike breach locations, the inundation pattern in these areas will be almost insensitive to the dike breach location. Moreover, the inundation pattern in small compartments which are completely enclosed by obstacles without large openings and underpasses is significantly sensitive to the dike breach location and for a long period. Furthermore, in general, it can be concluded that the sensitivity of inundation pattern mostly decreases over time. However, in certain specific cases, the inundation pattern tends to become temporarily more sensitive. This is the case when the rise rate of the later arriving inundations decreases.

## 7.2 RECOMMENDATIONS FOR FUTURE RESEARCH

In new research, several limitations in the methodology can be addressed. Firstly, it is recommended to verify the conclusions of this research in a different area. This study was site-specific and future research in a completely different area (i.e., less flat) could show to what extent the results of this study translate to other areas. Moreover, it can be studied what the influence of the failure of obstacles in the current study area, such as regional dikes and roads, is on the sensitivity of the inundation pattern to the dike breach location. Furthermore, this study was limited to the use of the same hydrograph for all dike breach locations. This hydrograph was based on a dike breach along the IJssel. However, for the same extreme discharge event, discharges in the Rhine and the Pannerdensch Kanaal will be larger than the discharge in the IJssel. In future research, this limitation can be addressed by using a different hydrograph for dike breach locations along the Pannerdensch Kanaal and another hydrograph for dike breach locations along the Rhine. Lastly, in future research, it is recommended to study the relative magnitude of the sensitivity of the inundation pattern to dike breach location compared to other model parameters. This will give an indication to which model parameters should be prioritized for reducing uncertainty in the parameter itself and thereby also in the model results.

# REFERENCES

---

- Alipour, A., Jafarzadegan, K., & Moradkhani, H. (2022). Global sensitivity analysis in hydrodynamic modeling and flood inundation mapping. *Environmental Modelling and Software*, 152. <https://doi.org/10.1016/j.envsoft.2022.105398>
- Alonso Vicario, S., Mazzoleni, M., Bhamidipati, S., Gharesifard, M., Ridolfi, E., Pandolfo, C., & Alfonso, L. (2020). Unravelling the influence of human behaviour on reducing casualties during flood evacuation. *Hydrological Sciences Journal*, 65(14), 2359–2375. <https://doi.org/10.1080/02626667.2020.1810254>
- Apel, H., Merz, B., & Thielen, A. H. (2009). Influence of dike breaches on flood frequency estimation. *Computers and Geosciences*, 35(5), 907–923. <https://doi.org/10.1016/j.cageo.2007.11.003>
- Apel, H., Thielen, A. H., Merz, B., & Blöschl, G. (2006). A probabilistic modelling system for assessing flood risks. *Natural Hazards*, 38(1–2), 79–100. <https://doi.org/10.1007/s11069-005-8603-7>
- Arends, M., & Bisschop, C. (2014). *Overstromingsrisico Dijkkring 48 Rijn en IJssel*.
- Bates, P. D. (2022). Flood Inundation Prediction. *Annual Review of Fluid Mechanics*, 54(1), 287–315. <https://doi.org/10.1146/annurev-fluid-030121>
- Beven, K., Leedal, D., McCarthy, S., Lamb, R., Hunter, N., Bates, P., Neal, J., & Wicks, J. (2014). *Framework for assessing uncertainty in fluvial flood risk mapping*. [www.ciria.org](http://www.ciria.org)
- Bomers, A. (2021). Predicting outflow hydrographs of potential dike breaches in a bifurcating river system using narx neural networks. *Hydrology*, 8(2). <https://doi.org/10.3390/HYDROLOGY8020087>
- Bomers, A., Schielen, R. M. J., & Hulscher, S. J. M. H. (2019). Consequences of dike breaches and dike overflow in a bifurcating river system. *Natural Hazards*, 97(1), 309–334. <https://doi.org/10.1007/s11069-019-03643-y>
- Casulli, V. (2009). A high-resolution wetting and drying algorithm for free-surface hydrodynamics. *International Journal for Numerical Methods in Fluids*, 60, 391–408. <https://doi.org/10.1002/flid.1896>
- Caviedes-Voullième, D., García-Navarro, P., & Murillo, J. (2012). Influence of mesh structure on 2D full shallow water equations and SCS Curve Number simulation of rainfall/runoff events. <https://doi.org/10.1016/j.jhydrol.2012.04.006>
- Chevron, B., & Moussa, R. (2016). Determinants of modelling choices for 1-D free-surface flow and morphodynamics in hydrology and hydraulics: A review. In *Hydrology and Earth System Sciences* (Vol. 20, Issue 9, pp. 3799–3830). Copernicus GmbH. <https://doi.org/10.5194/hess-20-3799-2016>
- Courage, W., Vrouwenvelder, T., van Mierlo, T., & Schweckendiek, T. (2013). System behaviour in flood risk calculations. *Georisk*, 7(2), 62–76. <https://doi.org/10.1080/17499518.2013.790732>
- CRED. (2022). *2021 Disasters in numbers*. <https://doi.org/10.1787/eee82e6e-en>
- Curran, A., de Bruijn, K., Domeneghetti, A., Bianchi, F., Kok, M., Vorogushyn, S., & Castellarin, A. (2020). Large-scale stochastic flood hazard analysis applied to the Po River. *Natural Hazards*, 104(3), 2027–2049. <https://doi.org/10.1007/s11069-020-04260-w>

- Curran, A., de Bruijn, K. M., Klerk, W. J., & Kok, M. (2019). Large scale flood hazard analysis by including defence failures on the Dutch river system. *Water (Switzerland)*, 11(8). <https://doi.org/10.3390/w11081732>
- De Bruijn, K. M., Diermanse, F. L. M., & Beckers, J. V. L. (2014). An advanced method for flood risk analysis in river deltas, applied to societal flood fatality risk in the Netherlands. *Natural Hazards and Earth System Sciences*, 14(10), 2767–2781. <https://doi.org/10.5194/nhess-14-2767-2014>
- De Bruijn, K. M., Slager, K., Piek, I. S. M. R., Riedstra, D., & Slomp, R. (2018). *Leidraad voor het maken van overstromingssimulaties*.
- Di Baldassarre, G., Castellarin, A., Montanari, A., & Brath, A. (2009). Probability-weighted hazard maps for comparing different flood risk management strategies: A case study. *Natural Hazards*, 50(3), 479–496. <https://doi.org/10.1007/s11069-009-9355-6>
- D’Oria, M., Maranzoni, A., & Mazzoleni, M. (2019). Probabilistic Assessment of Flood Hazard due to Levee Breaches Using Fragility Functions. *Water Resources Research*, 55(11), 8740–8764. <https://doi.org/10.1029/2019WR025369>
- ESA. (2020, March 20). *Europe land-cover mapped in 10 m resolution*. [https://www.esa.int/ESA\\_Multimedia/Images/2020/03/Europe\\_land-cover\\_mapped\\_in\\_10\\_m\\_resolution](https://www.esa.int/ESA_Multimedia/Images/2020/03/Europe_land-cover_mapped_in_10_m_resolution)
- Ferrari, A., Dazzi, S., Vacondio, R., & Mignosa, P. (2020). Enhancing the resilience to flooding induced by levee breaches in lowland areas: A methodology based on numerical modelling. *Natural Hazards and Earth System Sciences*, 20(1), 59–72. <https://doi.org/10.5194/nhess-20-59-2020>
- Geodateninfrastruktur NRW. (n.d.). *GEOportal.NRW*. Retrieved March 22, 2023, from <https://www.geoportal.nrw/?activetab=map>
- Ghostine, R., Hoteit, I., Vazquez, J., Terfous, A., Ghenaim, A., & Mose, R. (2015). Comparison between a coupled 1D-2D model and a fully 2D model for supercritical flow simulation in crossroads. *Journal of Hydraulic Research*, 53(2), 274–281. <https://doi.org/10.1080/00221686.2014.974081>
- Goeury, C., Bacchi, V., Zaoui, F., Bacchi, S., Pavan, S., & el kadi Abderrezzak, K. (2022). Uncertainty Assessment of Flood Hazard Due to Levee Breaching. *Water (Switzerland)*, 14(23). <https://doi.org/10.3390/w14233815>
- Hall, J. W., Boyce, S. A., Wang, Y., Dawson, R. J., Tarantola, S., & Saltelli, A. (2019). Sensitivity Analysis for Hydraulic Models. *Journal of Hydraulic Engineering*, 135(11), 959–969. <https://doi.org/10.1061/ASCEHY.1943-7900.0000098>
- Hesselink, A. W., Stelling, G. S., Kwadijk, J. C. J., & Middelkoop, H. (2003). Inundation of a Dutch river polder, sensitivity analysis of a physically based inundation model using historic data. *Water Resources Research*, 39(9). <https://doi.org/10.1029/2002WR001334>
- Hoorweg, M. K. (2014). *Visserijkundig Onderzoek De Oude IJssel van Doesburg tot en met Ulft*. [www.sportvisserijnederland.nl](http://www.sportvisserijnederland.nl)

- Hoss, F., Jonkman, S. N., & Maaskant, B. (2013). *A comprehensive assessment of multilayered safety in flood risk management-The Dordrecht case study*. 27–29. <https://www.researchgate.net/publication/265919359>
- Hunter, N. M., Bates, P. D., Horritt, M. S., & Wilson, M. D. (2007). Simple spatially-distributed models for predicting flood inundation: A review. In *Geomorphology* (Vol. 90, Issues 3–4, pp. 208–225). <https://doi.org/10.1016/j.geomorph.2006.10.021>
- Huthoff, F., Remo, J. W. F., & Pinter, N. (2015). Improving flood preparedness using hydrodynamic levee-breach and inundation modelling: Middle Mississippi River, USA. *Journal of Flood Risk Management*, 8(1), 2–18. <https://doi.org/10.1111/jfr3.12066>
- Jodhani, K. H., Patel, D., & Madhavan, N. (2022). A review on analysis of flood modelling using different numerical models. *Materials Today: Proceedings*. <https://doi.org/10.1016/j.matpr.2021.07.405>
- Jongman, B. (2021). Fraction of population at risk of floods is growing. *Nature*, 596(7870). <https://doi.org/10.1038/s41893-021-00732-4>
- Jongman, B., Ward, P. J., & Aerts, J. C. J. H. (2012). Global exposure to river and coastal flooding: Long term trends and changes. *Global Environmental Change*, 22(4), 823–835. <https://doi.org/10.1016/j.gloenvcha.2012.07.004>
- Jonkman, S. N., & Vrijling, J. K. (2008). Loss of life due to floods. *Journal of Flood Risk Management*, 1(1), 43–56. <https://doi.org/10.1111/j.1753-318x.2008.00006.x>
- Kadir, M. A. A., Abustan, I., & Razak, M. F. A. (2019). 2D Flood Inundation Simulation Based on a Large Scale Physical Model Using Course Numerical Grid Method. *International Journal of GEOMATE*, 17(59), 230–236. <https://doi.org/10.21660/2019.59.ICEE17>
- Kakinuma, T., & Shimizu, Y. (2014). Large-Scale Experiment and Numerical Modeling of a Riverine Levee Breach. *Journal of Hydraulic Engineering*, 140(9). [https://doi.org/10.1061/\(asce\)hy.1943-7900.0000902](https://doi.org/10.1061/(asce)hy.1943-7900.0000902)
- Kok, M., Jongejan, R., Nieuwjaar, M., & Tónczos, I. (2017). *Fundamentals of Flood Protection*.
- Liu, Z., Merwade, V., & Jafarzadegan, K. (2019). Investigating the role of model structure and surface roughness in generating flood inundation extents using one- and two-dimensional hydraulic models. *Journal of Flood Risk Management*, 12(1). <https://doi.org/10.1111/jfr3.12347>
- Maranzoni, A., D’Oria, M., & Mazzoleni, M. (2022). Probabilistic Flood Hazard Mapping Considering Multiple Levee Breaches. *Water Resources Research*, 58(4). <https://doi.org/10.1029/2021WR030874>
- Mazzoleni, M., Bacchi, B., Barontini, S., di Baldassarre, G., Pilotti, M., & Ranzi, R. (2014). Flooding Hazard Mapping in Floodplain Areas Affected by Piping Breaches in the Po River, Italy. *Journal of Hydrologic Engineering*, 19(4), 717–731. [https://doi.org/10.1061/\(asce\)he.1943-5584.0000840](https://doi.org/10.1061/(asce)he.1943-5584.0000840)
- Mazzoleni, M., Dottori, F., Brandimarte, L., Tekle, S., & Martina, M. L. V. (2017). Effects of levee cover strength on flood mapping in the case of levee breach due to overtopping. *Hydrological Sciences Journal*, 62(6), 892–910. <https://doi.org/10.1080/02626667.2016.1246800>

- Meunier, B., & Merwade, V. (2014). Prioritizing levee repairs: A case study for the city of Indianapolis, Indiana. *Natural Hazards*, 72(2), 997–1019. <https://doi.org/10.1007/s11069-014-1057-z>
- Mooijaart, J. B. (2023). *Assessment of 1D and 2D model choices on model accuracy and computation time in D-Hydro*.
- Mudashiru, R. B., Sabtu, N., Abustan, I., & Balogun, W. (2021). Flood hazard mapping methods: A review. In *Journal of Hydrology* (Vol. 603). Elsevier B.V. <https://doi.org/10.1016/j.jhydrol.2021.126846>
- Nelen & Schuurmans. (2022). *3Di Documentation*. <https://docs.3di.live/>
- Oubennaceur, K., Chokmani, K., Nastev, M., Gauthier, Y., Poulin, J., Tanguy, M., Raymond, S., & Lhissou, R. (2019). New sensitivity indices of a 2D flood inundation model using gauss quadrature sampling. *Geosciences (Switzerland)*, 9(5). <https://doi.org/10.3390/geosciences9050220>
- Papanicolaou, A. N., Elhakeem, M., & Wardman, B. (2010). Calibration and Verification of a 2D Hydrodynamic Model for Simulating Flow around Emergent Bendway Weir Structures. *Journal of Hydraulic Engineering*, 137(1), 75–89. [https://doi.org/10.1061/\(ASCE\)HY.1943-7900.0000280](https://doi.org/10.1061/(ASCE)HY.1943-7900.0000280)
- Pasquale, N., Perona, P., Wombacher, A., & Burlando, P. (2014). Hydrodynamic model calibration from pattern recognition of non-orthorectified terrestrial photographs. *Computers and Geosciences*, 62, 160–167. <https://doi.org/10.1016/j.cageo.2013.06.014>
- PDOK. (n.d.-a). *Dataset: Actueel Hoogtebestand Nederland (AHN)*. Retrieved March 23, 2023, from <https://www.pdok.nl/downloads/-/article/actueel-hoogtebestand-nederland-ahn>
- PDOK. (n.d.-b). *Dataset: Basisregistratie Grootchalige Topografie (BGT)*.
- Pinos, J., & Timbe, L. (2019). Performance assessment of two-dimensional hydraulic models for generation of flood inundation maps in mountain river basins. *Water Science and Engineering*, 12(1), 11–18. <https://doi.org/10.1016/J.WSE.2019.03.001>
- Prinsen, G., Hutten, R., & Verhoeven, G. (2020). *Modelling dijkring 48 met D-HYDRO*.
- Rifai, I., El Kadi Abderrezzak, K., Ercicum, S., Archambeau, P., Violeau, D., Piroton, M., & Dewals, B. (2018). Floodplain Backwater Effect on Overtopping Induced Fluvial Dike Failure. *Water Resources Research*, 54(11), 9060–9073. <https://doi.org/10.1029/2017WR022492>
- Savage, J. T. S., Pianosi, F., Bates, P., Freer, J., & Wagener, T. (2016). Quantifying the importance of spatial resolution and other factors through global sensitivity analysis of a flood inundation model. *Water Resources Research*, 52(11), 9146–9163. <https://doi.org/10.1002/2015WR018198>
- Schmitz, V., Ercicum, S., El kadi Abderrezzak, K., Rifai, I., Archambeau, P., Piroton, M., & Dewals, B. (2021). Overtopping-Induced Failure of Non-Cohesive Homogeneous Fluvial Dikes: Effect of Dike Geometry on Breach Discharge and Widening. *Water Resources Research*, 57(7). <https://doi.org/10.1029/2021WR029660>
- Tadesse, Y. B., & Fröhle, P. (2020). Modelling of flood inundation due to levee breaches: Sensitivity of flood inundation against breach process parameters. *Water (Switzerland)*, 12(12). <https://doi.org/10.3390/w12123566>

- TAW. (1998). *Fundamentals on Water Defences*.
- TAW. (1999). *Technical Report on Sand Boils (Piping)*.
- TAW. (2001). *Technical Report Water Retaining Soil Structures*.
- Tellman, B., Sullivan, J. A., Kuhn, C., Kettner, A. J., Doyle, C. S., Brakenridge, G. R., Erickson, T., & Slayback, D. A. (2021). Satellite observations indicate increasing proportion of population exposed to floods. *Nature*, 596(7870), 80–86.
- ten Brinke, W. (2013). *Fact finding afvoerverdeling Rijntakken*.
- Teng, J., Jakeman, A. J., Vaze, J., Croke, B. F. W., Dutta, D., & Kim, S. (2017). Flood inundation modelling: A review of methods, recent advances and uncertainty analysis. In *Environmental Modelling and Software* (Vol. 90, pp. 201–216). Elsevier Ltd. <https://doi.org/10.1016/j.envsoft.2017.01.006>
- Van Berchum, E. (2021). *Quickscan Lijnvormige Kerende Elementen*.
- Van Bergeijk, V. M., Verdonk, V. A., Warmink, J. J., & Hulscher, S. J. M. H. (2021). The cross-dike failure probability by wave overtopping over grass-covered and damaged dikes. *Water (Switzerland)*, 13(5), 1–22. <https://doi.org/10.3390/w13050690>
- Van Mierlo, M. C. L. M., Vrouwenvelder, A. C. W. M., Calle, E. O. F., Vrijling, J. K., Jonkman, S. N., de Bruijn, K. M., & Weerts, A. H. (2007). Assessment of flood risk accounting for river system behaviour. *International Journal of River Basin Management*, 5(2), 93–104. <https://doi.org/10.1080/15715124.2007.9635309>
- Verwey, A., Kerblat, Y., & Chia, B. (2017). *Flood Risk Management at River Basin Scale: The Need to Adopt a Proactive Approach*. <https://doi.org/10.1596/27472>
- VNK2 Project Office. (2012). *The National Flood Risk Analysis for the Netherlands*.
- Volp, N. D., Van Prooijen, B. C., & Stelling, G. S. (2013). A finite volume approach for shallow water flow accounting for high-resolution bathymetry and roughness data. *Water Resources Research*, 49(7), 4126–4135. <https://doi.org/10.1002/wrcr.20324>
- Vorogushyn, S., Lindenschmidt, K. E., Kreibich, H., Apel, H., & Merz, B. (2012). Analysis of a detention basin impact on dike failure probabilities and flood risk for a channel-dike-floodplain system along the river Elbe, Germany. *Journal of Hydrology*, 436–437, 120–131. <https://doi.org/10.1016/j.jhydrol.2012.03.006>
- Vorogushyn, S., Merz, B., & Apel, H. (2009). Development of dike fragility curves for piping and micro-instability breach mechanisms. *Natural Hazards and Earth System Sciences*, 9, 1383–1401. [www.nat-hazards-earth-syst-sci.net/9/1383/2009/](http://www.nat-hazards-earth-syst-sci.net/9/1383/2009/)
- Vorogushyn, S., Merz, B., Lindenschmidt, K. E., & Apel, H. (2010). A new methodology for flood hazard assessment considering dike breaches. *Water Resources Research*, 46(8). <https://doi.org/10.1029/2009WR008475>
- Wageningen Environmental Research. (n.d.). *LGN: Bestanden*. <https://doi.org/10.4121/e2971c99-f4f2-4786-b7ba-2d16a24bcd83.v1>

- Waterschap Rijn en IJssel. (2023). *Waterstanden Oude IJssel*. <https://waterdata.wrij.nl/grafiek-kiwis-multi.php?graphid=306600>
- Winsemius, H. C., Aerts, J. C. J. H., Van Beek, L. P. H., Bierkens, M. F. P., Bouwman, A., Jongman, B., Kwadijk, J. C. J., Ligtoet, W., Lucas, P. L., Van Vuuren, D. P., & Ward, P. J. (2016). Global drivers of future river flood risk. *Nature Climate Change*, 6(4), 381–385. <https://doi.org/10.1038/nclimate2893>
- Xu, L., Yang, X., Cui, S., Tang, J., Ding, S., & Zhang, X. (2023). *Co-occurrence of pluvial and fluvial floods exacerbates inundation and economic losses: evidence from a scenario-based analysis in Longyan, China*. <https://doi.org/10.1080/19475705.2023.2218012>
- Yu, D., & Lane, S. N. (2006a). Urban fluvial flood modelling using a two-dimensional diffusion-wave treatment, part 1: Mesh resolution effects. *Hydrological Processes*, 20(7), 1541–1565. <https://doi.org/10.1002/hyp.5935>
- Yu, D., & Lane, S. N. (2006b). Urban fluvial flood modelling using a two-dimensional diffusion-wave treatment, part 2: Development of a sub-grid-scale treatment. *Hydrological Processes*, 20(7), 1567–1583. <https://doi.org/10.1002/HYP.5936>
- Zhao, G., Visser, P. J., Ren, Y., & Uijtewaal, W. S. J. (2015). Flow hydrodynamics in embankment breach. *Journal of Hydrodynamics*, 27(6), 835–844. [https://doi.org/10.1016/S1001-6058\(15\)60546-7](https://doi.org/10.1016/S1001-6058(15)60546-7)

# APPENDIX A: ROUGHNESS

*Table 3 Conversion table land use to Manning's roughness coefficient used in 3Di*

<b>Land use</b>	<b>Manning's roughness coefficient [s m<sup>-1/3</sup>]</b>
Roof	0.058
Sand	0.03
Semi-paved	0.03
Yard	0.03
Closed pavement	0.013
Unpaved	0.03
Open pavement	0.016
Green space	0.03
Coniferous forest	0.058
Grassland	0.03
Shrubbery	0.058
Nature area	0.058
Arboriculture	0.058
Heathland	0.058
Cropland	0.034
Decideous forest	0.058
Orchard	0.058
Mixed forest	0.058
Wasteland	0.058
Swamps	0.058
Water berm	0.03
Water	0.026
Other	0.03

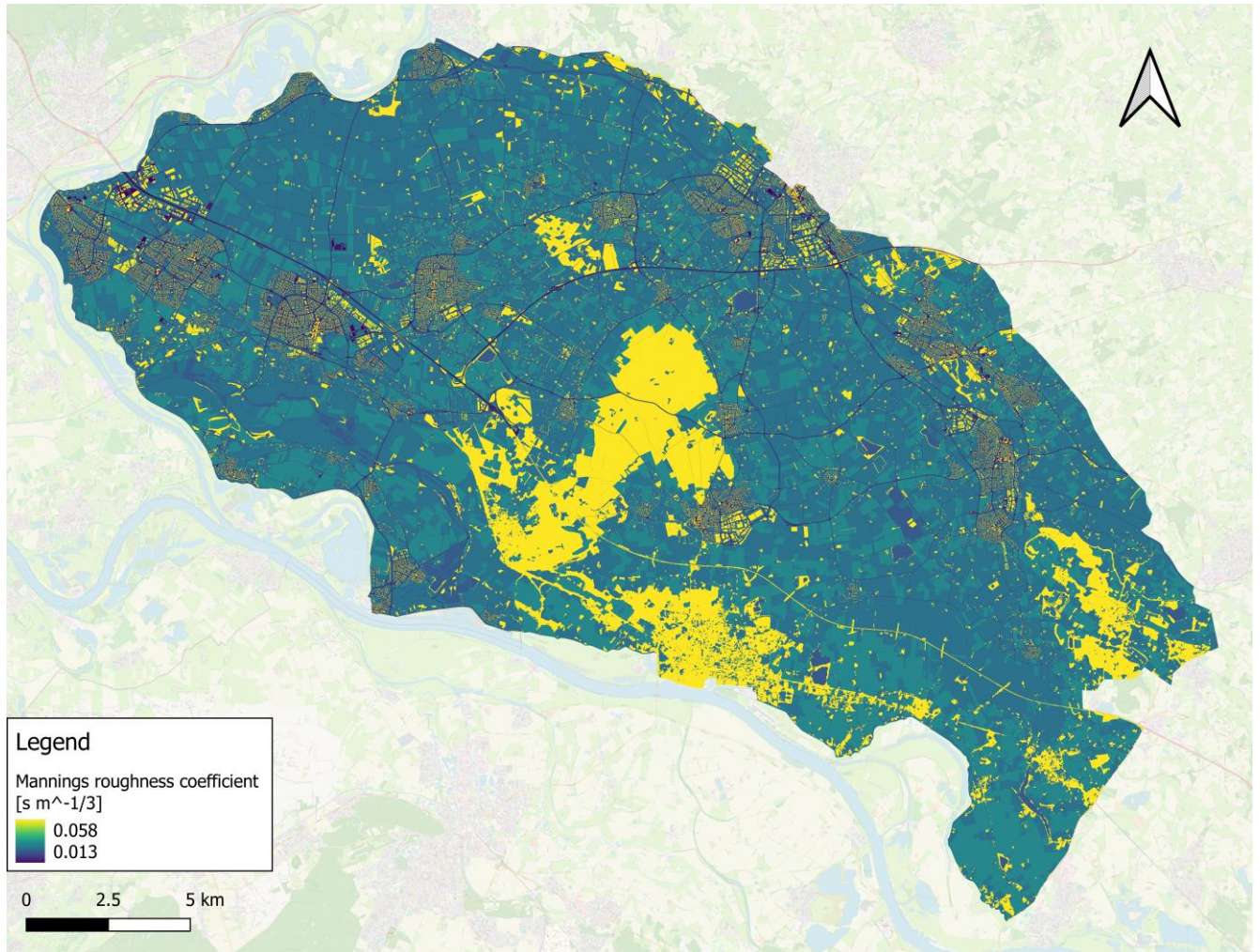


Figure 46 Implemented Mannings roughness coefficients

# APPENDIX B: OBSTACLES

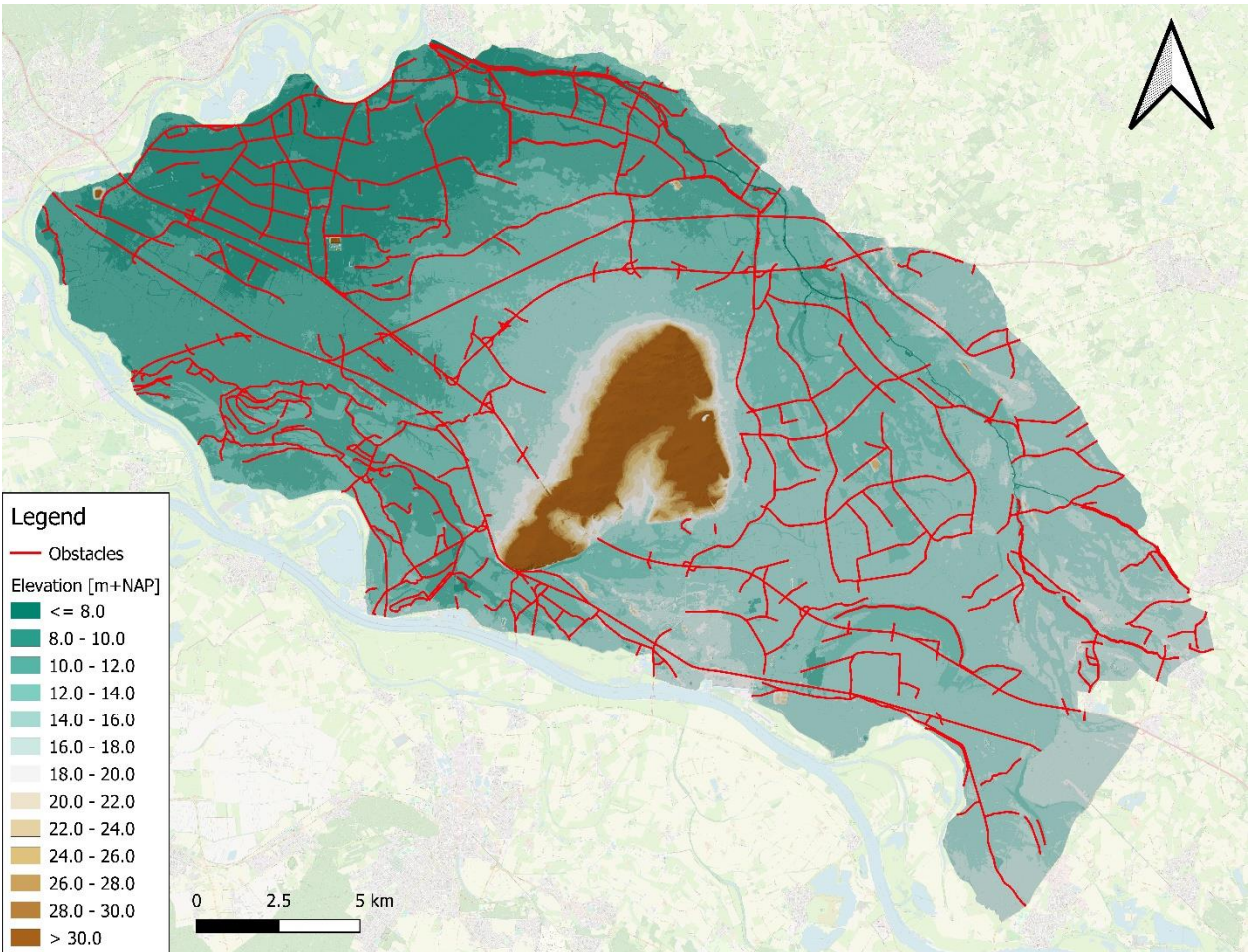


Figure 47 Map with all defined obstacles in the model schematisation of 3Di

# APPENDIX C: GRID REFINEMENTS

---

Table 4 Grid refinements around openings/underpasses in obstacles

Width of openings/underpasses [m]	Grid refinement [m <sup>2</sup> ]
0-15	8×8
15-30	16×16
30-60	32×32

Table 5 Grid refinements around waterways which have embankments around both banks

Waterway	Grid refinement [m <sup>2</sup> ]
Oude IJssel	32×32
Issel (German part of Oude IJssel)	16×16
De Keel (connection between Rijnstrangen area and the Rhine)	16×16
Hoge Leiding	8×8
Wehlsche Beek	8×8

## APPENDIX D: INITIAL WATER LEVELS OUDE IJSSEL

---

*Table 6 Initial water levels in the different trajectories of the Oude IJssel*

<b>Trajectory</b>	<b>Water level [m+NAP]</b>
Weir at Doesburg – weir de Pol	10.03
Weir de Pol – weir at Uft	12.40
Weir at Uft – weir at Voorst	13.50

# APPENDIX E: RESULTS OF THE SENSITIVITY ANALYSIS OF THE COMPUTATIONAL GRID

## E.1 RESULTS PHASE 1: DIKE BREACH AT LOO

### E.1.1 Arrival times

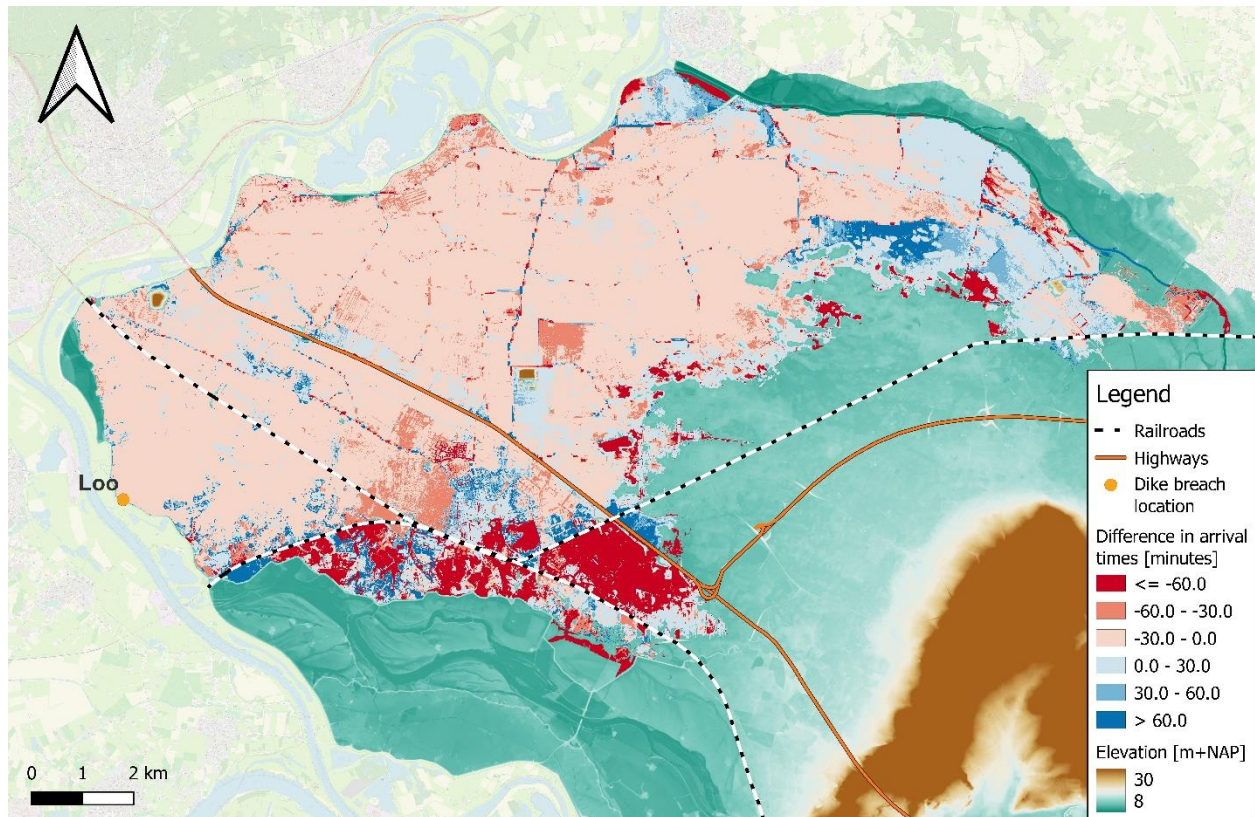


Figure 48 Differences in arrival time between a grid with resolution of  $80 \times 80 \text{ m}^2$  and  $40 \times 40 \text{ m}^2$  (reference grid) for a dike breach at Loo. Positive differences (blue) indicate that the water arrives later in the grid with a resolution of  $80 \times 80 \text{ m}^2$  than in the reference grid.

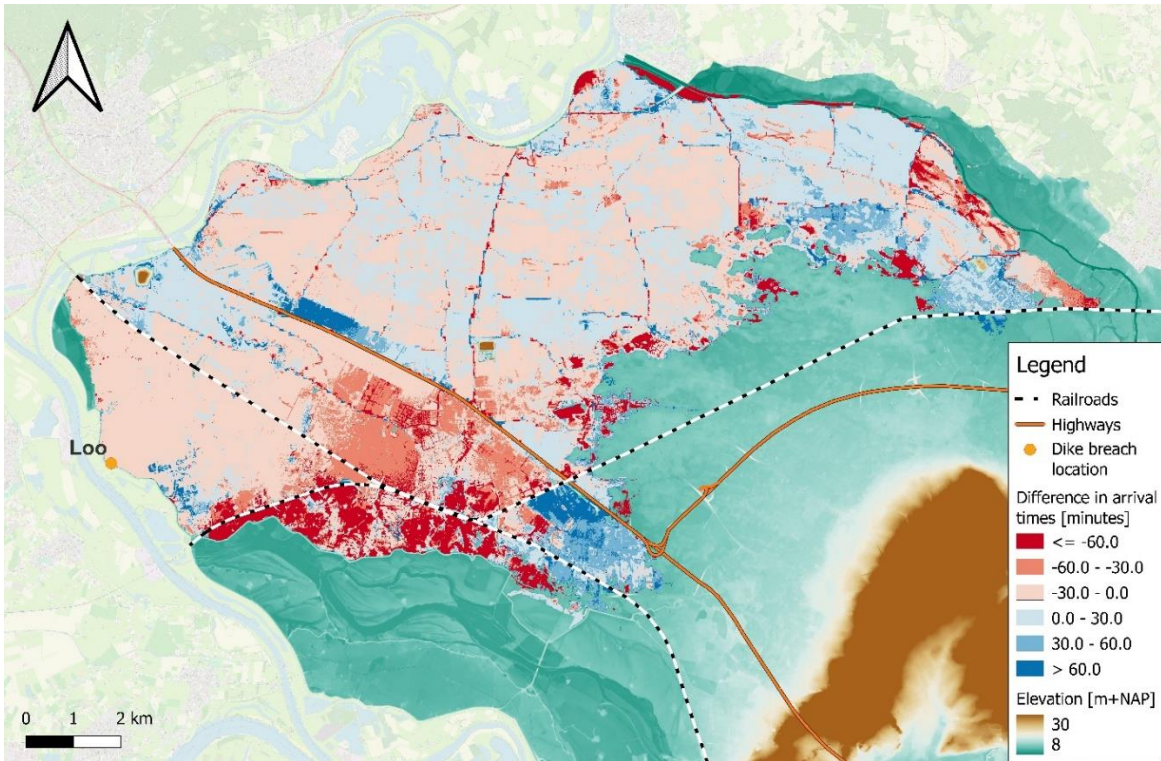


Figure 49 Differences in arrival time between a grid with resolution of  $100 \times 100 \text{ m}^2$  and  $40 \times 40 \text{ m}^2$  (reference grid) for a dike breach at Loo. Positive differences (blue) indicate that the water arrives later in the grid with a resolution of  $100 \times 100 \text{ m}^2$  than in the reference grid.

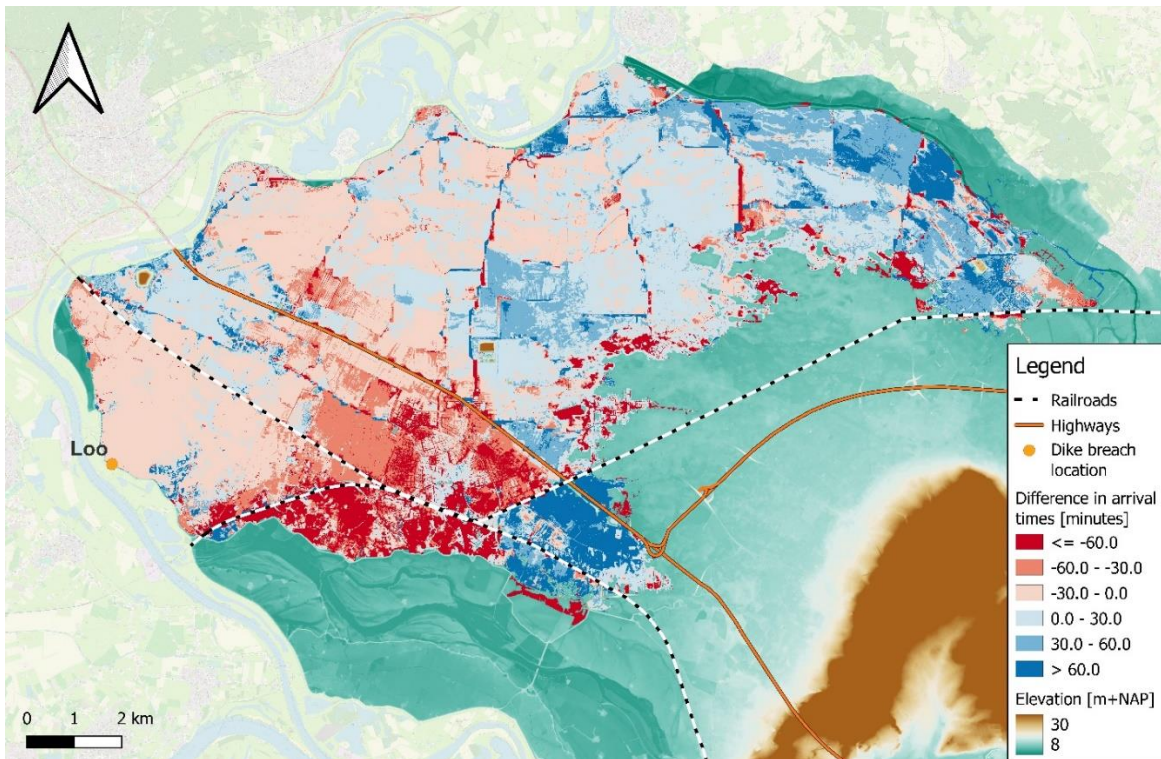


Figure 50 Differences in arrival time between a grid with resolution of  $160 \times 160 \text{ m}^2$  and  $40 \times 40 \text{ m}^2$  (reference grid) for a dike breach at Loo. Positive differences (blue) indicate that the water arrives later in the grid with a resolution of  $160 \times 160 \text{ m}^2$  than in the reference grid.

### E.1.2 Water depths after 12 hours

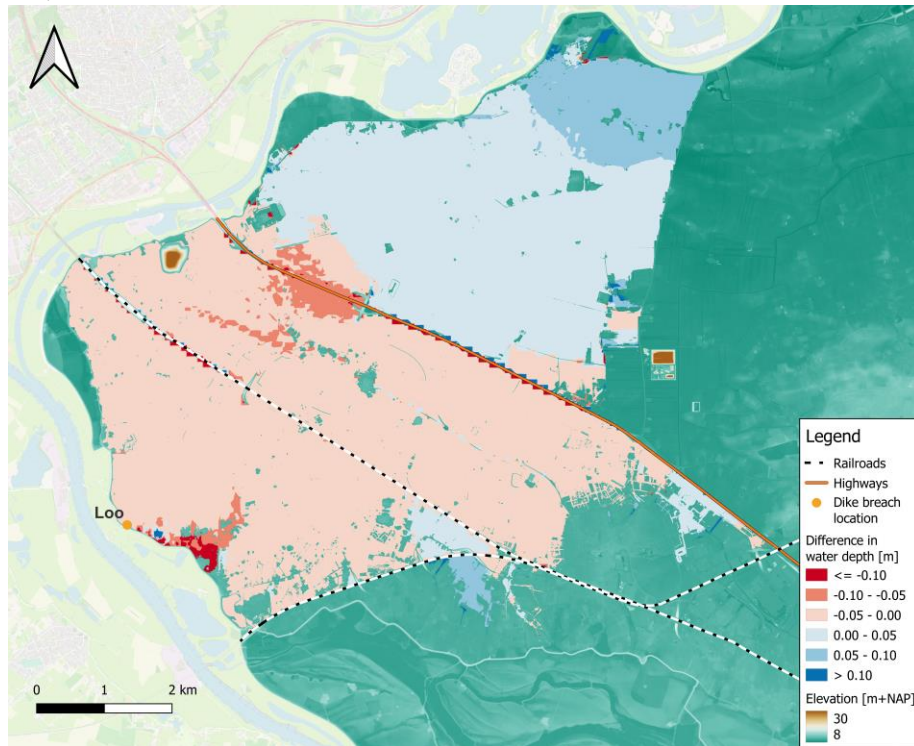


Figure 51 Differences in water depth between a grid with resolution of 80x80 m<sup>2</sup> and 40x40 m<sup>2</sup> (reference grid) after 12 hours for a dike breach at Loo. Positive differences (blue) indicate that the water depth in the grid with a resolution of 80x80 m<sup>2</sup> is larger than in the reference grid.

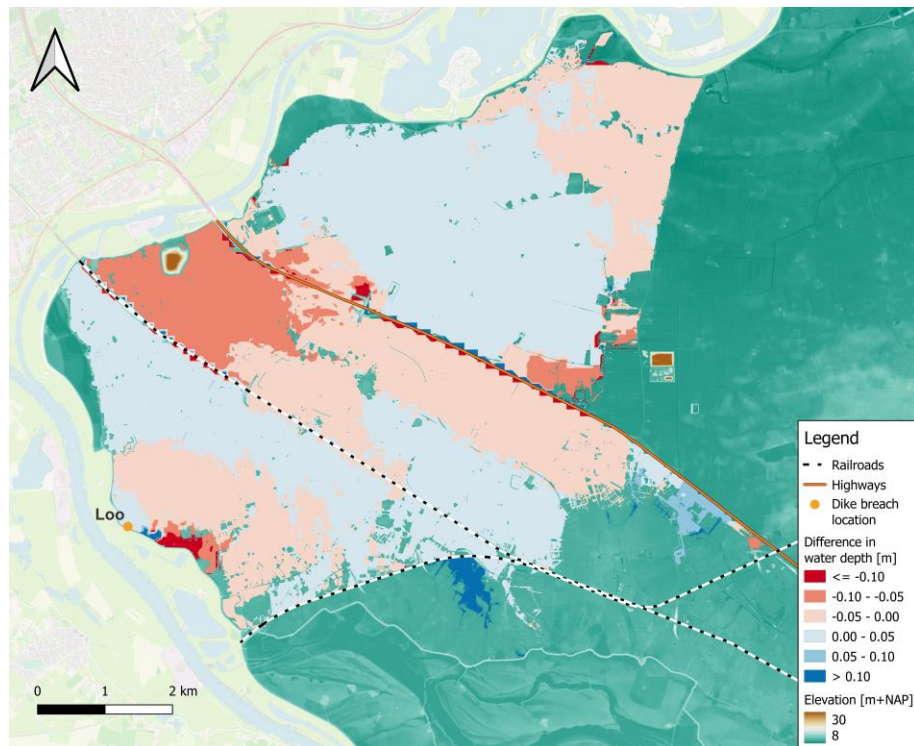


Figure 52 Differences in water depth between a grid with resolution of 100x100 m<sup>2</sup> and 40x40 m<sup>2</sup> (reference grid) after 12 hours for a dike breach at Loo. Positive differences (blue) indicate that the water depth in the grid with a resolution of 100x100 m<sup>2</sup> is larger than in the reference grid.

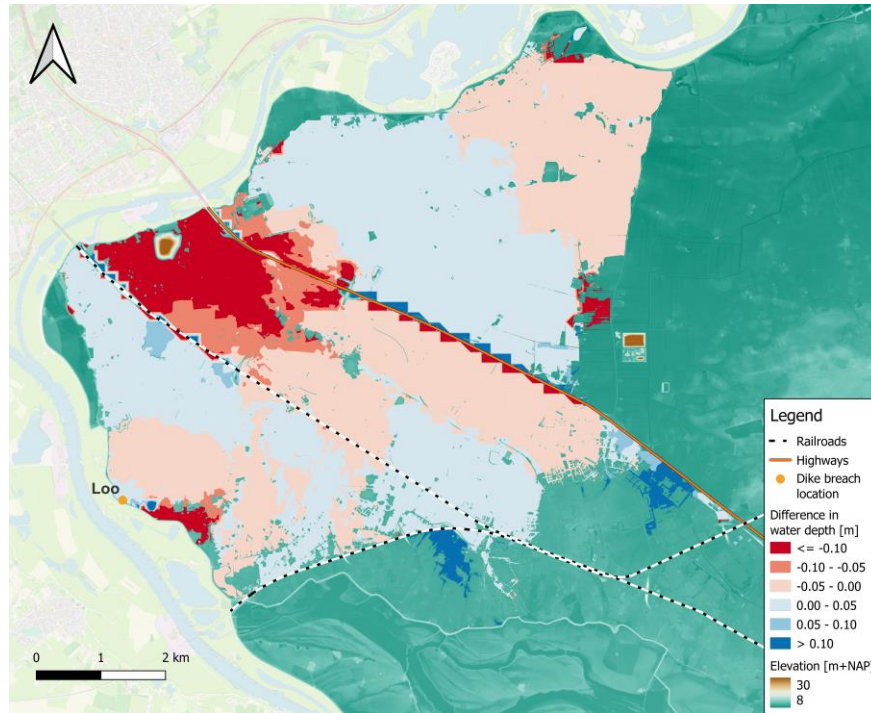


Figure 53 Differences in water depth between a grid with resolution of 160x160 m<sup>2</sup> and 40x40 m<sup>2</sup> (reference grid) after 12 hours for a dike breach at Loo. Positive differences (blue) indicate that the water depth in the grid with a resolution of 160x160 m<sup>2</sup> is larger than in the reference grid.

### E.1.3 Water depths after 1 day

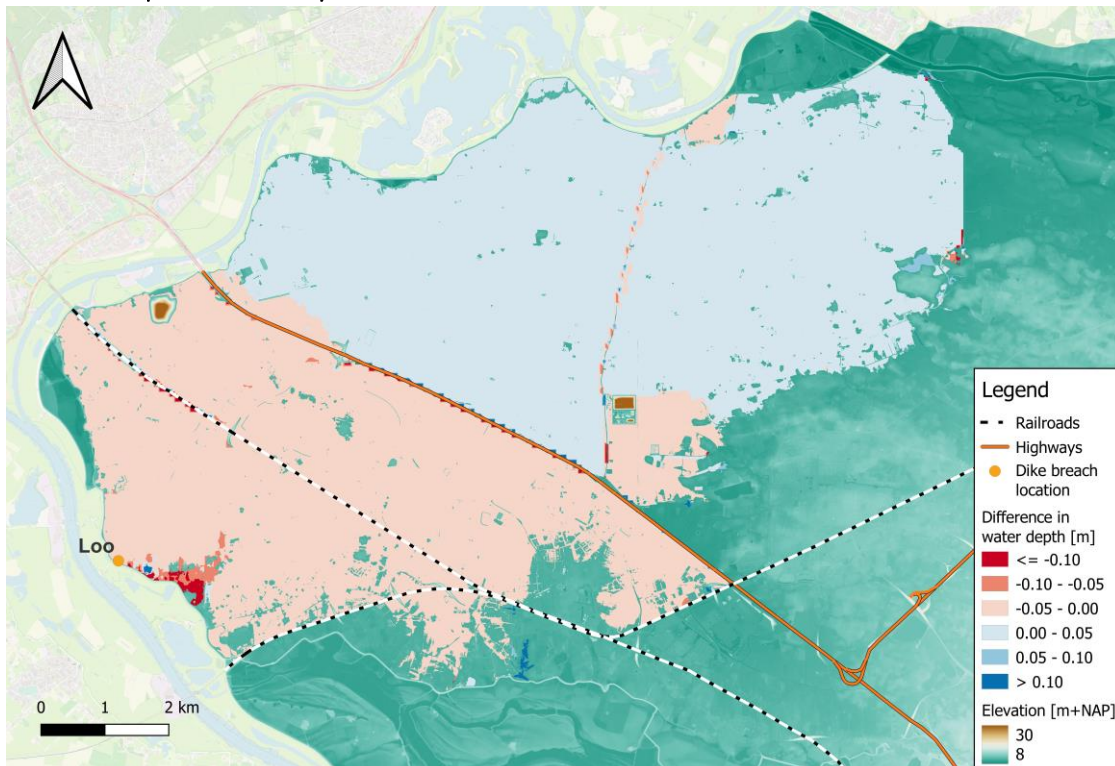


Figure 54 Differences in water depth between a grid with resolution of 80x80 m<sup>2</sup> and 40x40 m<sup>2</sup> (reference grid) after 1 day for a dike breach at Loo. Positive differences (blue) indicate that the water depth in the grid with a resolution of 160x160 m<sup>2</sup> is larger than in the reference grid.

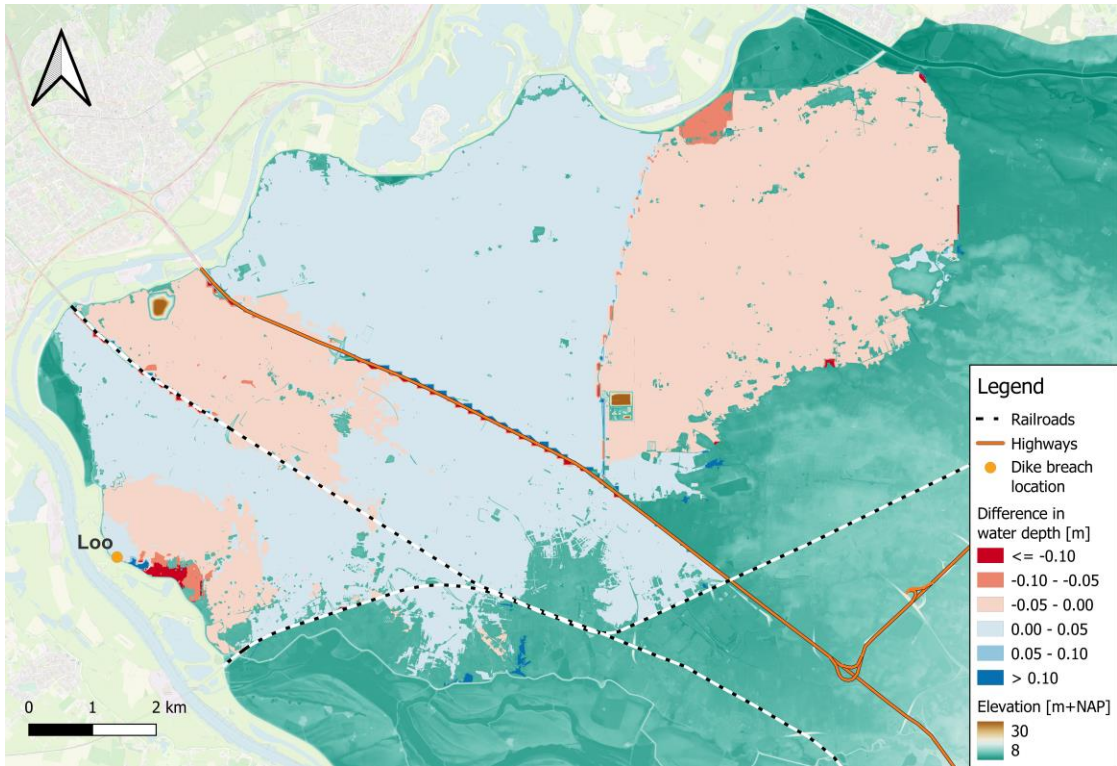


Figure 55 Differences in water depth between a grid with resolution of  $100 \times 100 \text{ m}^2$  and  $40 \times 40 \text{ m}^2$  (reference grid) after 1 day for a dike breach at Loo. Positive differences (blue) indicate that the water depth in the grid with a resolution of  $100 \times 100 \text{ m}^2$  is larger than in the reference grid.

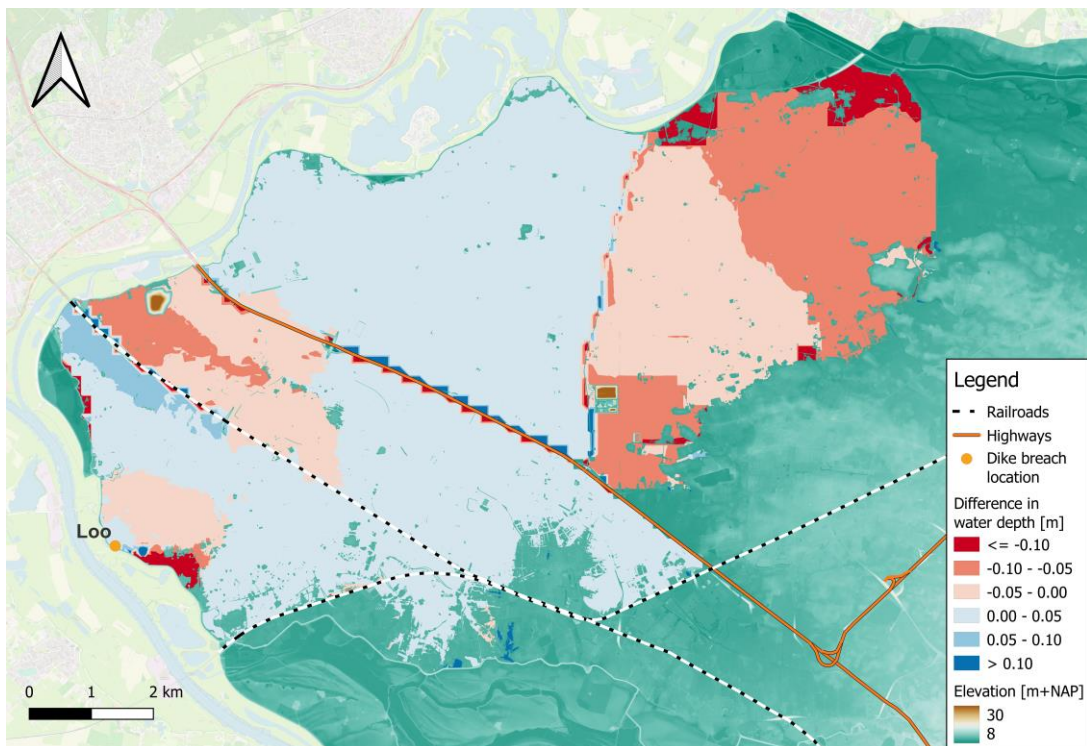


Figure 56 Differences in water depth between a grid with resolution of  $160 \times 160 \text{ m}^2$  and  $40 \times 40 \text{ m}^2$  (reference grid) after 1 day for a dike breach at Loo. Positive differences (blue) indicate that the water depth in the grid with a resolution of  $160 \times 160 \text{ m}^2$  is larger than in the reference grid.

## E.2 RESULTS PHASE 2: DIKE BREACH AT DOESBURG

Table 7 Computational time of five-day simulation with the reference model and model 80. Computational times are based on computations of 3Di in the cloud

Breach location	Name	Grid size major part study area [m <sup>2</sup> ]	Computational time [h]
Doesburg	Reference model	40×40	25.88
	Model 80	80×80	7.02
Spijk	Reference model	40×40	27.17
	Model 80	80×80	7.35

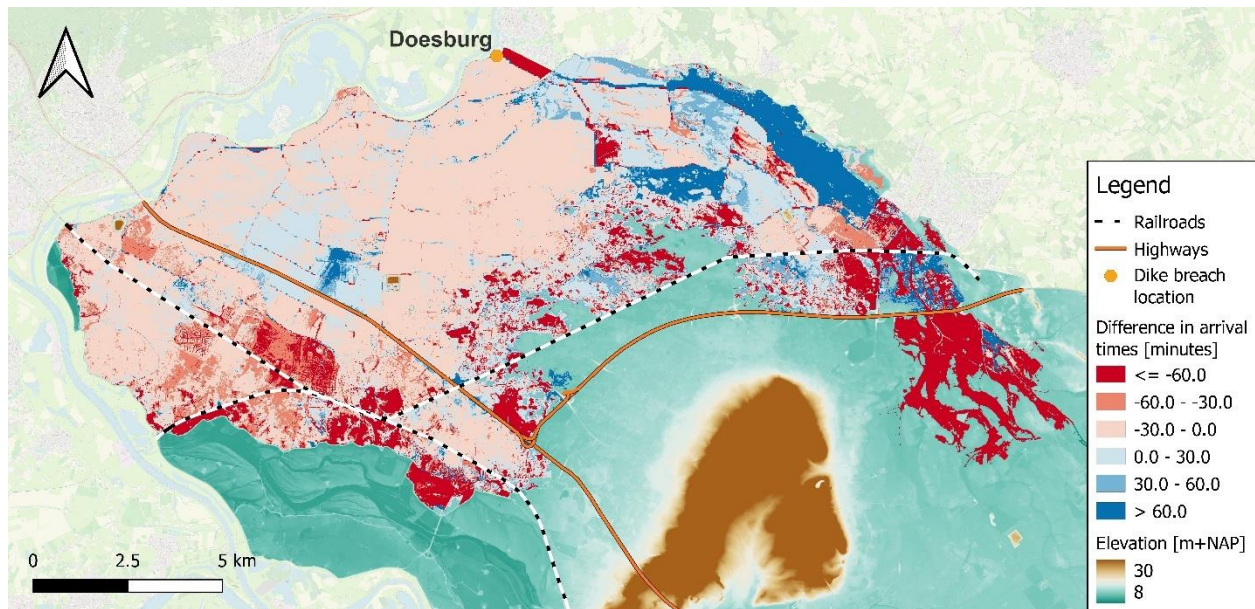


Figure 57 Differences in arrival time between a grid with resolution of 80×80 m<sup>2</sup> and 40×40 m<sup>2</sup> (reference grid) for a dike breach at Doesburg. Positive differences (blue) indicate that the water arrives later in the grid with a resolution of 80×80 m<sup>2</sup> than in the reference grid.

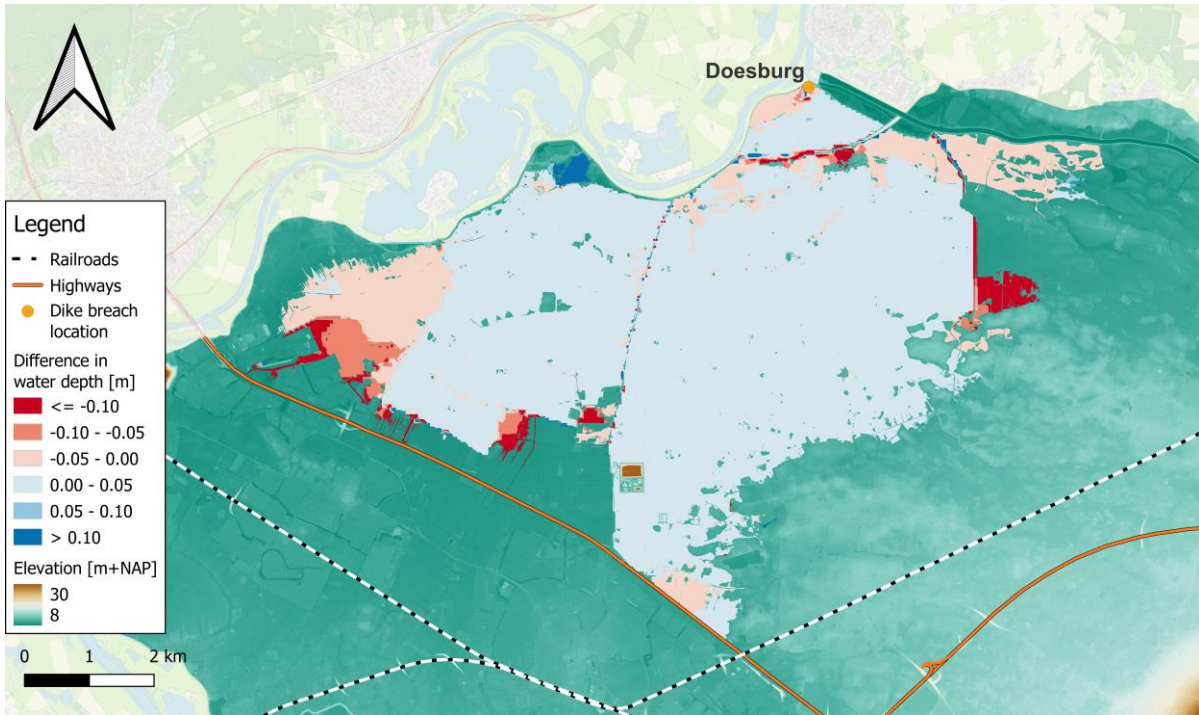


Figure 58 Differences in water depth between a grid with resolution of  $80 \times 80 \text{ m}^2$  and  $40 \times 40 \text{ m}^2$  (reference grid) after 12 hours for a dike breach at Doesburg. Positive differences (blue) indicate that the water depth in the grid with a resolution of  $80 \times 80 \text{ m}^2$  is larger than in the reference grid.

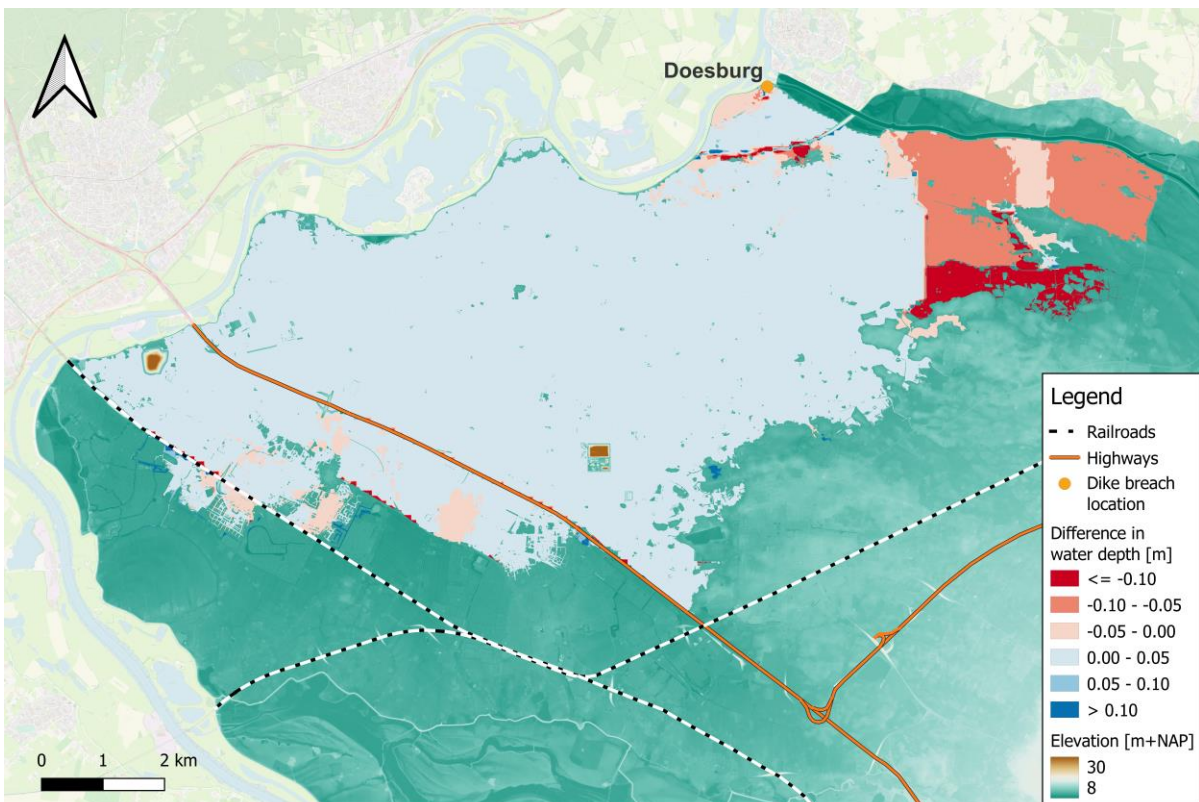


Figure 59 Differences in water depth between a grid with resolution of  $80 \times 80 \text{ m}^2$  and  $40 \times 40 \text{ m}^2$  (reference grid) after 1 day for a dike breach at Doesburg. Positive differences (blue) indicate that the water depth in the grid with a resolution of  $80 \times 80 \text{ m}^2$  is larger than in the reference grid.

## E.3 RESULTS PHASE 2: DIKE BREACH AT SPIJK

### E.3.1 Arrival times

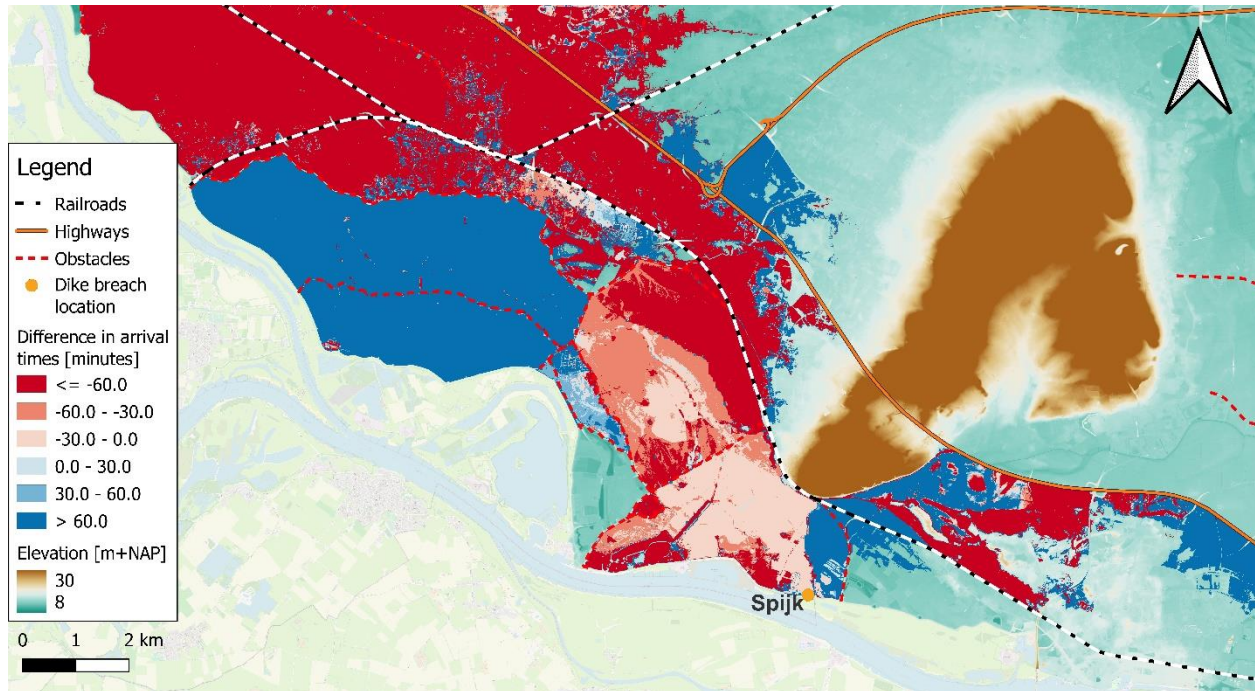


Figure 60 Differences in arrival time between a grid with resolution of  $80 \times 80 \text{ m}^2$  and the reference grid for a dike breach at Spijk. Positive differences (blue) indicate that the water arrives later in the grid with a resolution of  $80 \times 80 \text{ m}^2$  than in the reference grid.

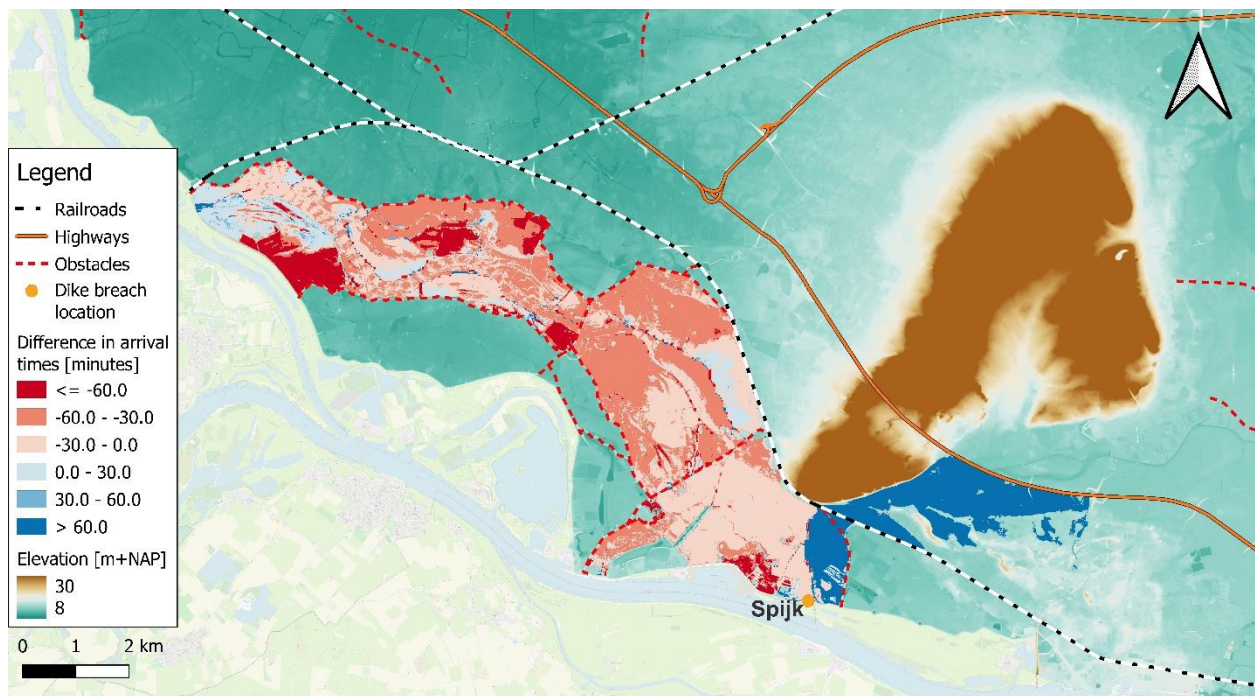


Figure 61 Differences in arrival time between adjusted grid 1 and reference grid for a dike breach at Spijk. Positive differences (blue) indicate that the water arrives later in adjusted grid 1 than in the reference grid. For the resolution of both grids, see Table 2.

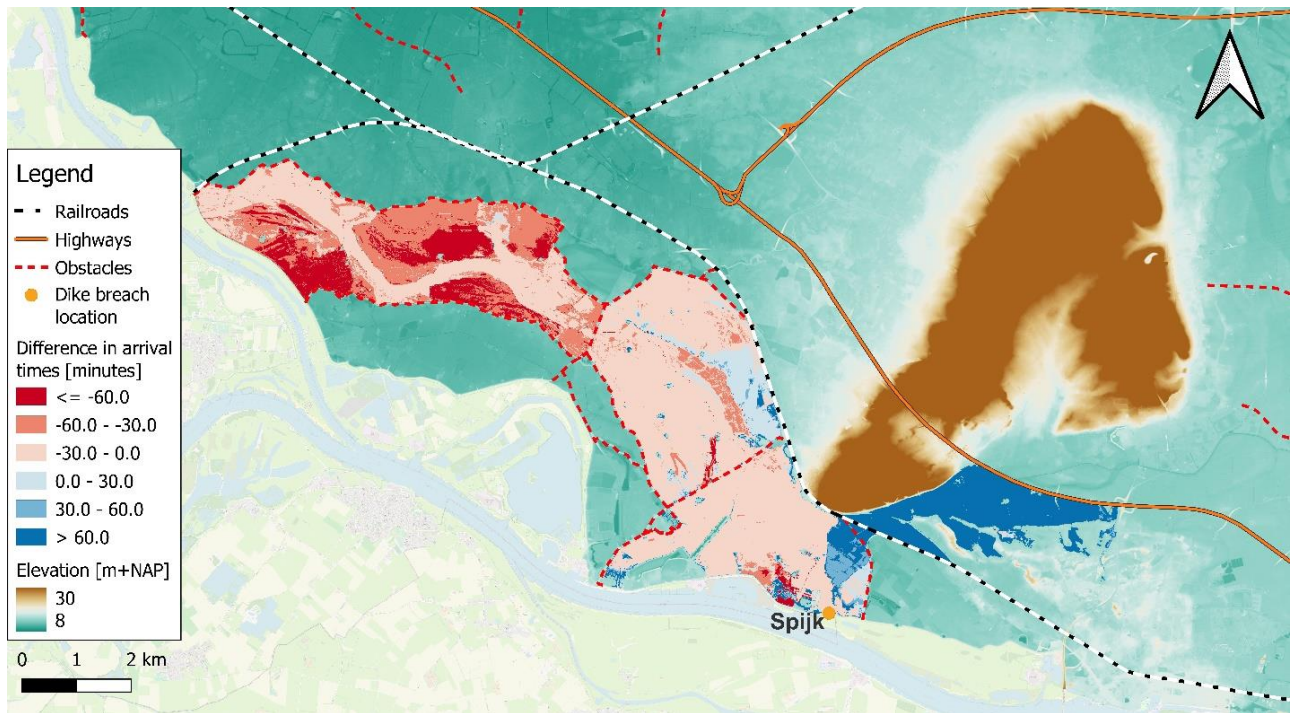


Figure 62 Differences in arrival time between adjusted grid 2 and reference grid for a dike breach at Spijk. Positive differences (blue) indicate that the water arrives later in adjusted grid 2 than in the reference grid. For the resolution of both grids, see Table 2.

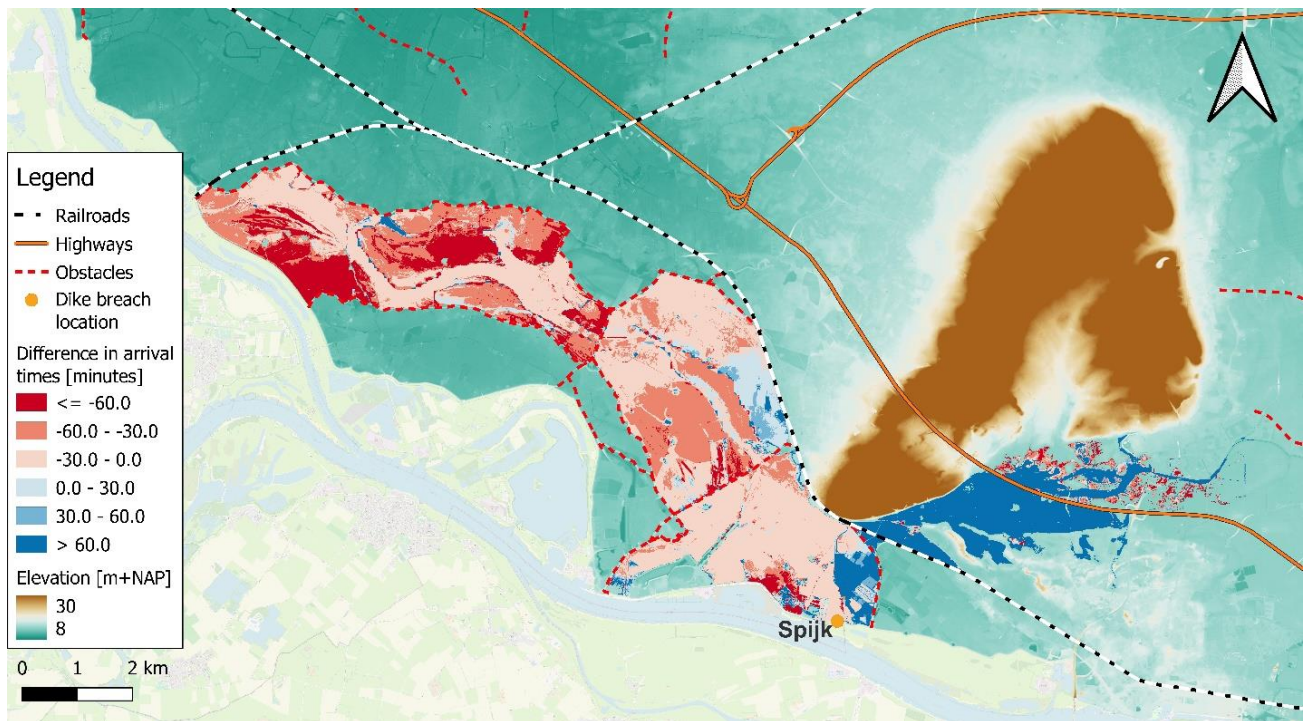


Figure 63 Differences in arrival time between adjusted grid 3 and reference grid for a dike breach at Spijk. Positive differences (blue) indicate that the water arrives later in adjusted grid 3 than in the reference grid. For the resolution of both grids, see Table 2.

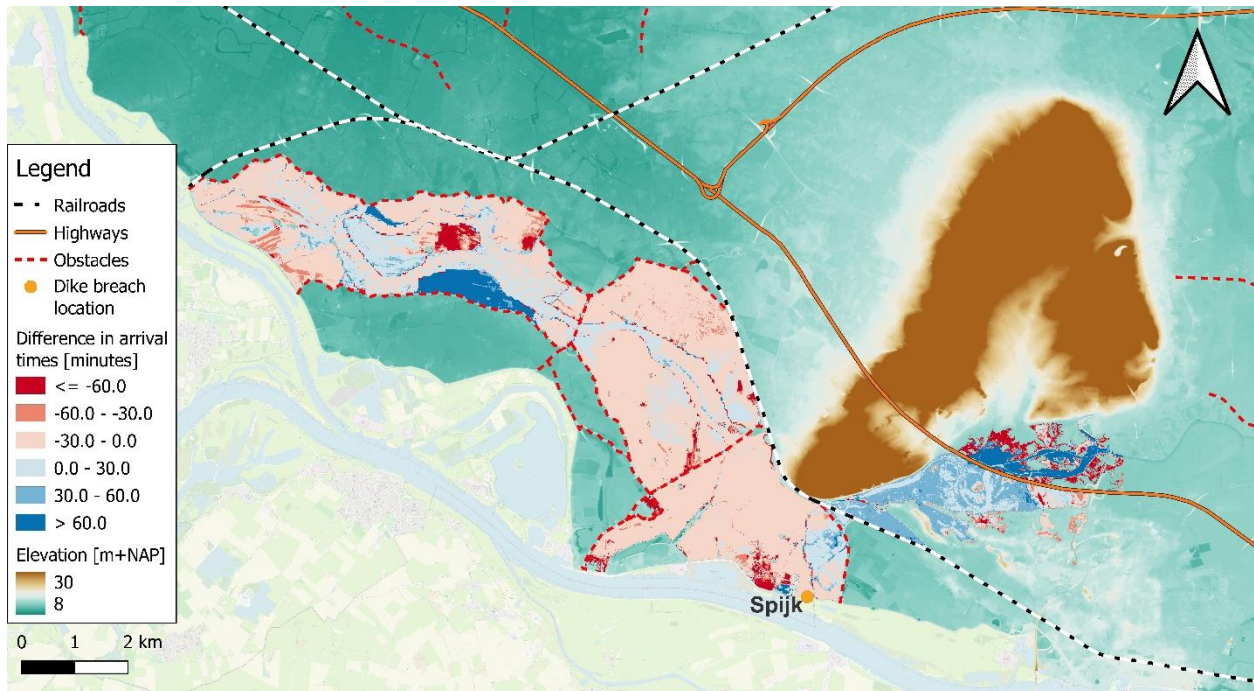


Figure 64 Differences in arrival times between adjusted grid 4 and reference grid for a dike breach at Spijk. Positive differences (blue) indicate that the water arrives later in adjusted grid 4 than in the reference grid. For the resolution of both grids, see Table 2

### E.3.2 Water depths after 12 hours

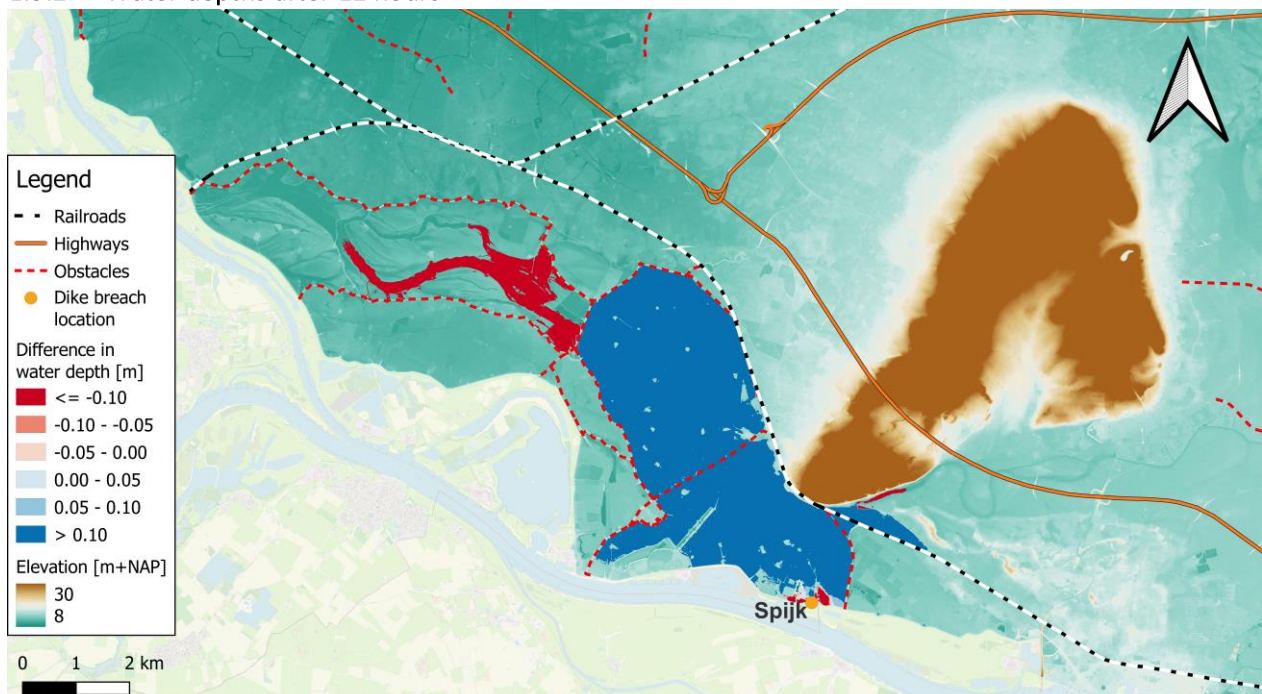


Figure 65 Differences in water depth between a grid with resolution of  $80 \times 80 \text{ m}^2$  and  $40 \times 40 \text{ m}^2$  (reference grid) after 12 hours for a dike breach at Spijk. Positive differences (blue) indicate that the water depth in the grid with a resolution of  $80 \times 80 \text{ m}^2$  is larger than in the reference grid.

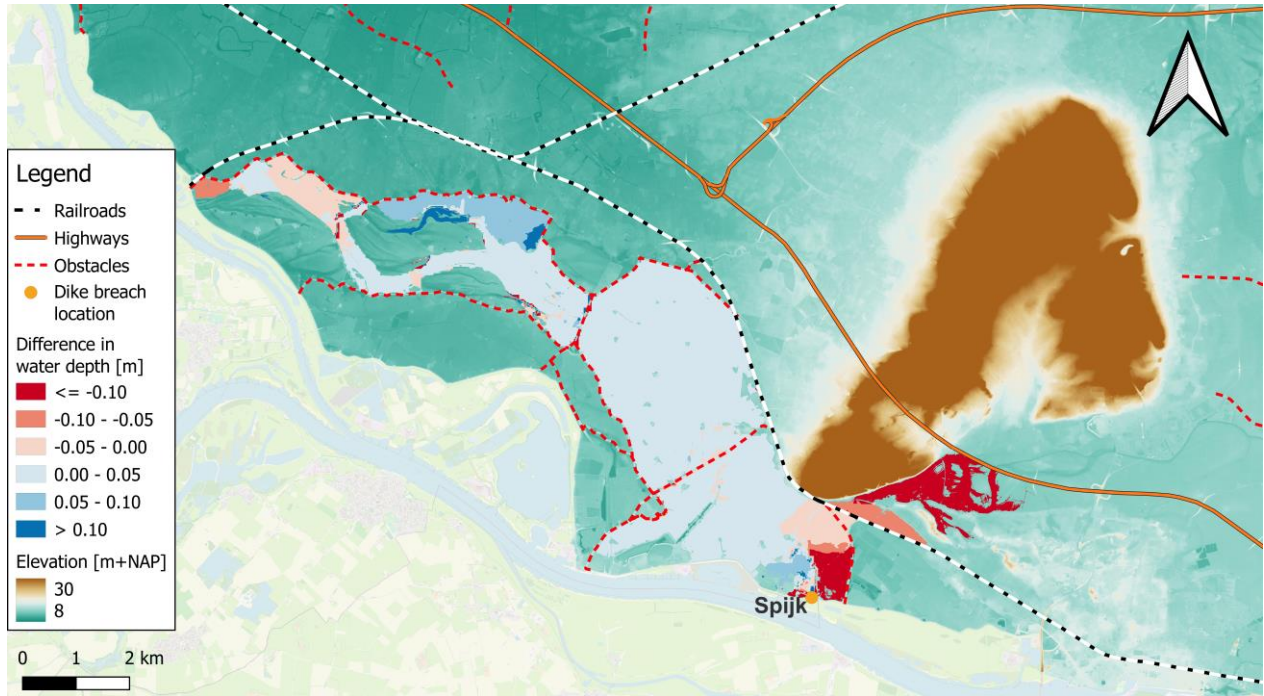


Figure 66 Differences in water depth after 12 hours between adjusted grid 1 and reference grid for a dike breach at Spijk. Positive differences (blue) indicate that the water depth in adjusted grid 1 is larger than in the reference grid. For the resolution of both grids, see Table 2.

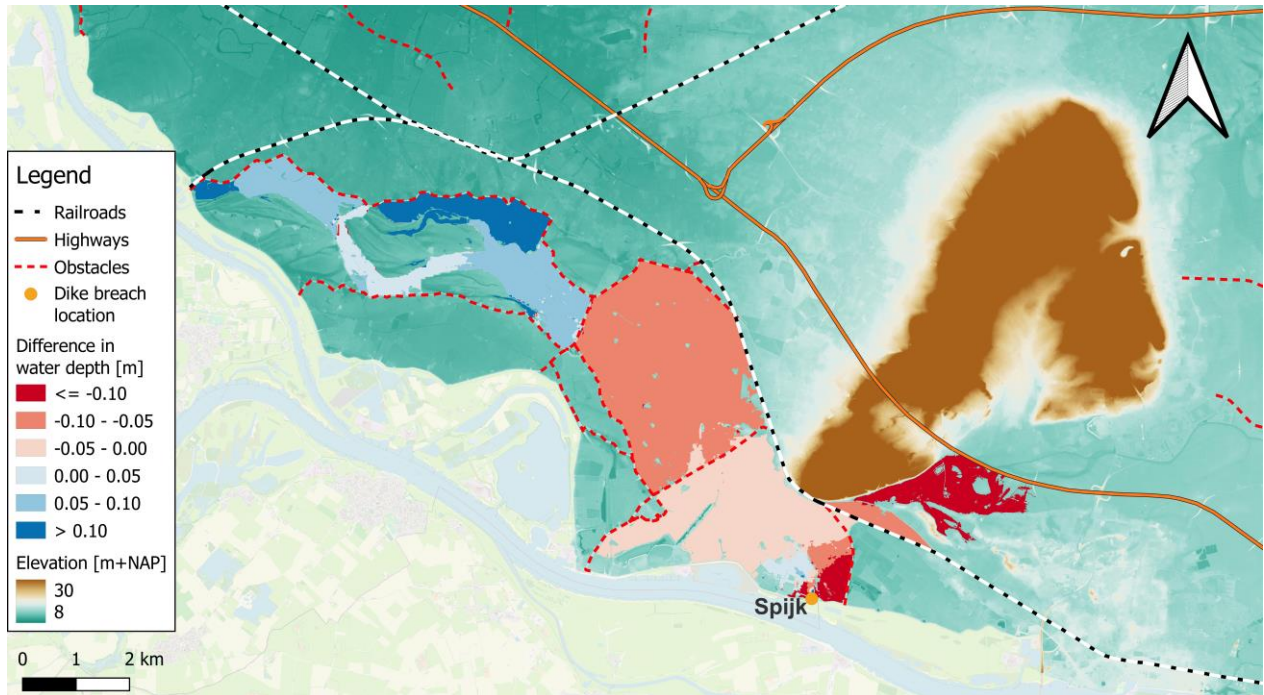


Figure 67 Differences in water depth after 12 hours between adjusted grid 2 and reference grid for a dike breach at Spijk. Positive differences (blue) indicate that the water depth in adjusted grid 2 is larger than in the reference grid. For the resolution of both grids, see Table 2.

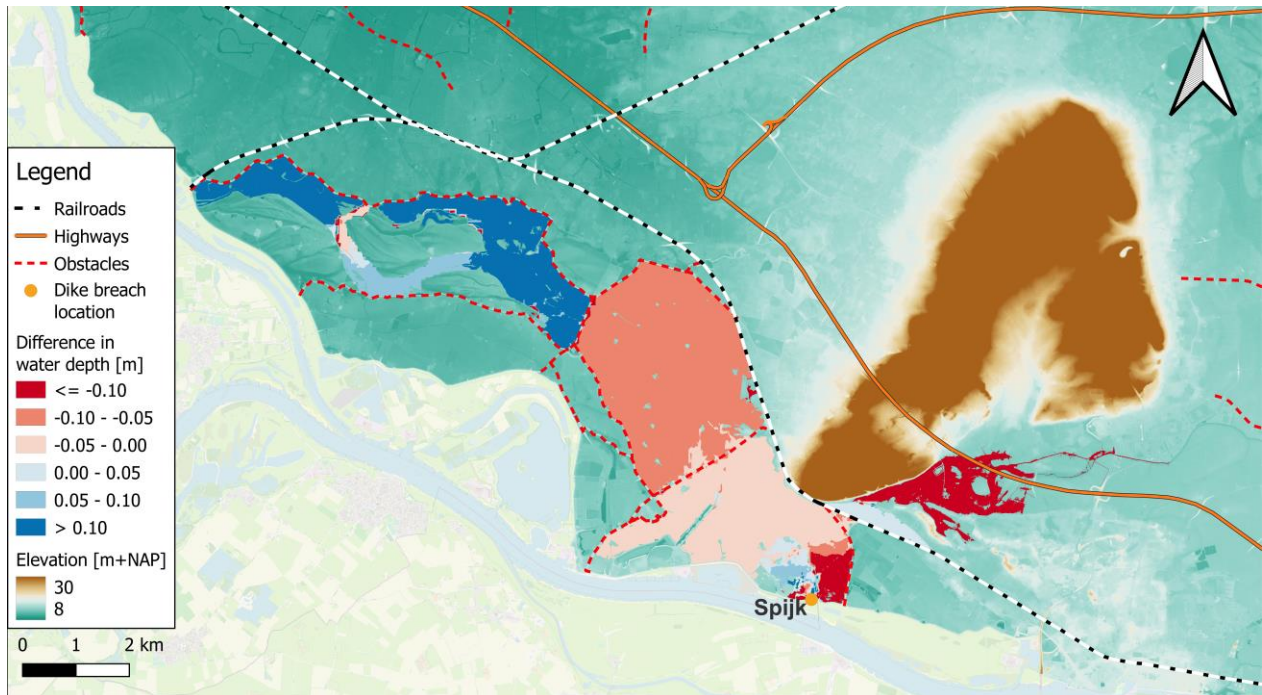


Figure 68 Differences in water depth after 12 hours between adjusted grid 3 and reference grid for a dike breach at Spijk. Positive differences (blue) indicate that the water depth in adjusted grid 3 is larger than in the reference grid. For the resolution of both grids, see Table 2.

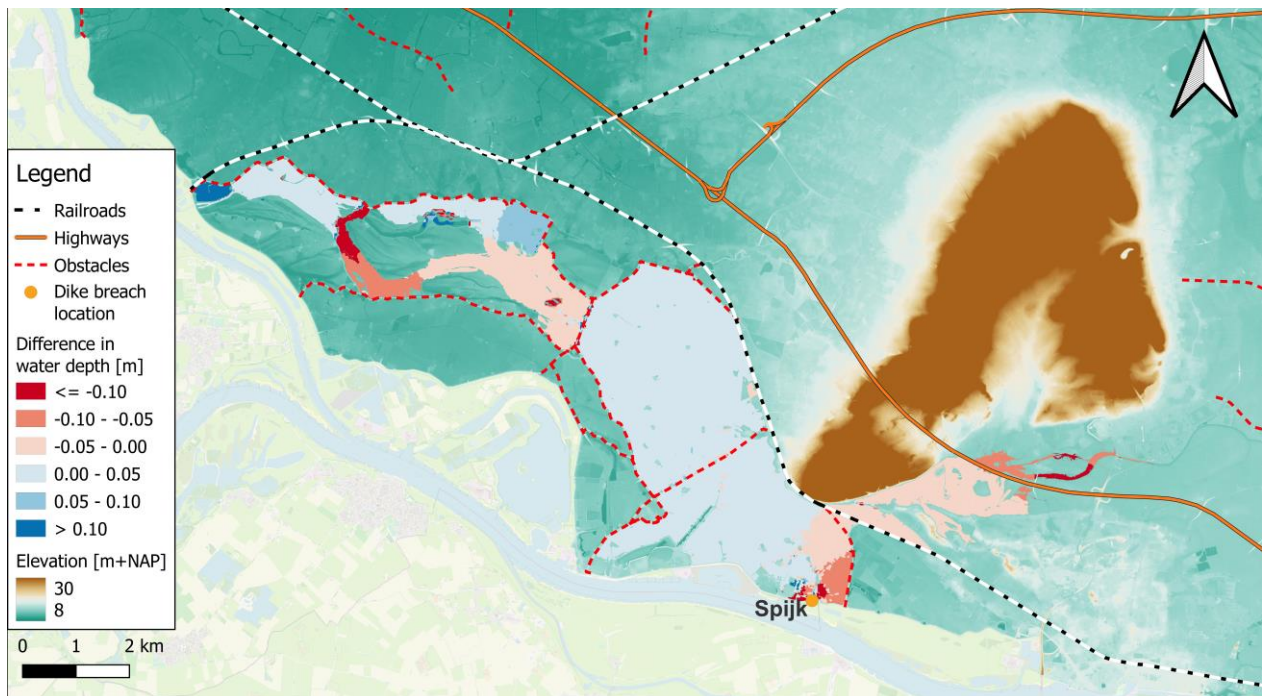


Figure 69 Differences in water depth after 12 hours between adjusted grid 4 and reference grid for a dike breach at Spijk. Positive differences (blue) indicate that the water depth in adjusted grid 4 is larger than in the reference grid. For the resolution of both grids, see Table 2.

### E.3.3 Water depths after 1 day

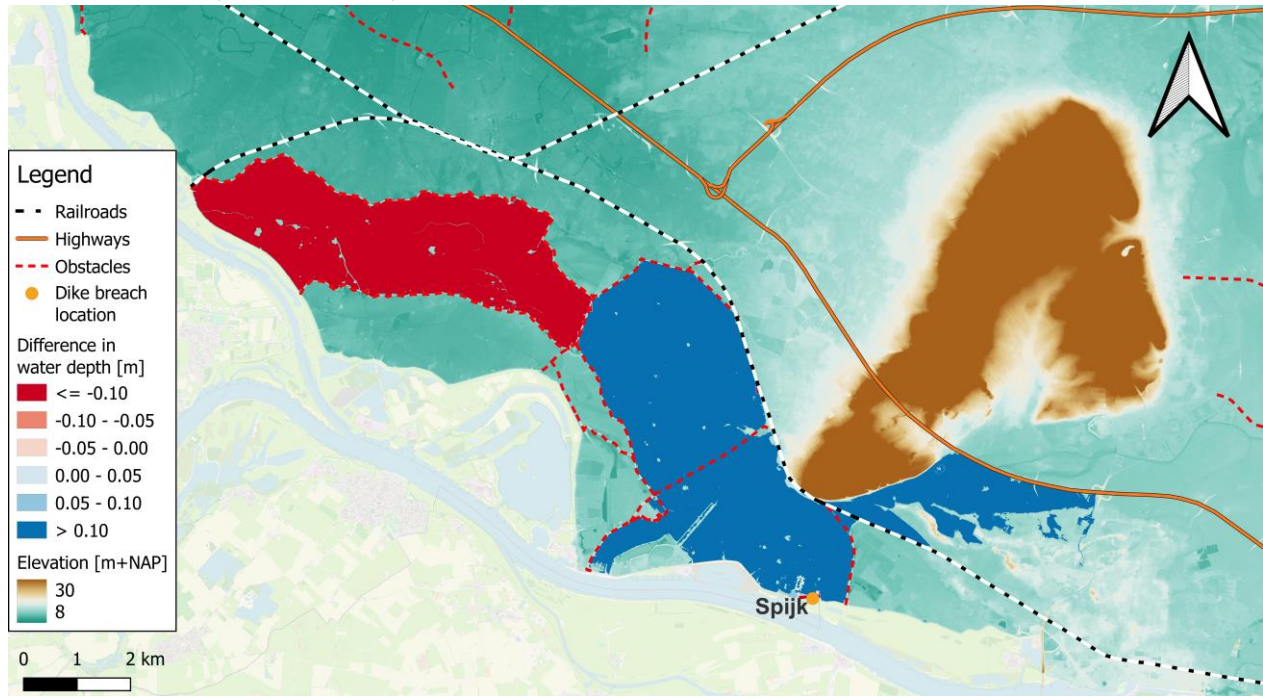


Figure 70 Differences in water depth after 1 day between a grid with resolution of  $80 \times 80 \text{ m}^2$  and  $40 \times 40 \text{ m}^2$  (reference grid) for a dike breach at Spijk. Positive differences (blue) indicate that the water depth in the grid with a resolution of  $80 \times 80 \text{ m}^2$  is larger than in the reference grid.

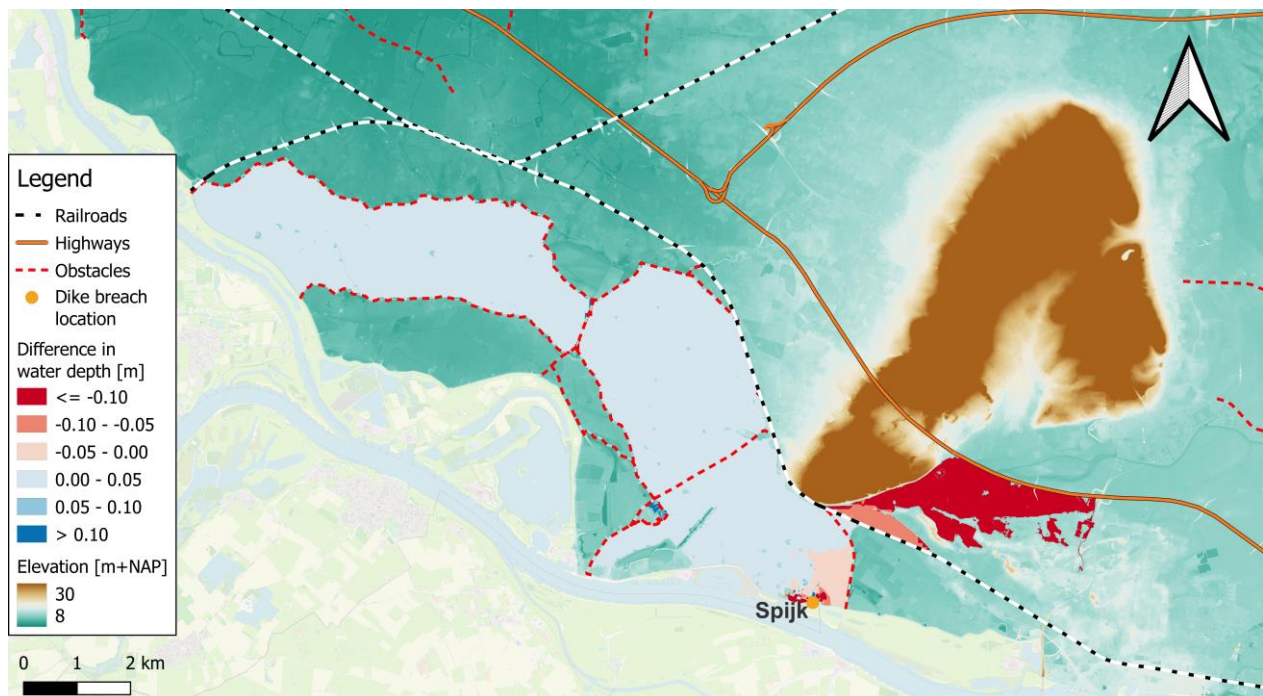


Figure 71 Differences in water depth after 1 day between adjusted grid 1 and reference grid for a dike breach at Spijk. Positive differences (blue) indicate that the water depth in adjusted grid 1 is larger than in the reference grid. For the resolution of both grids, see Table 2.

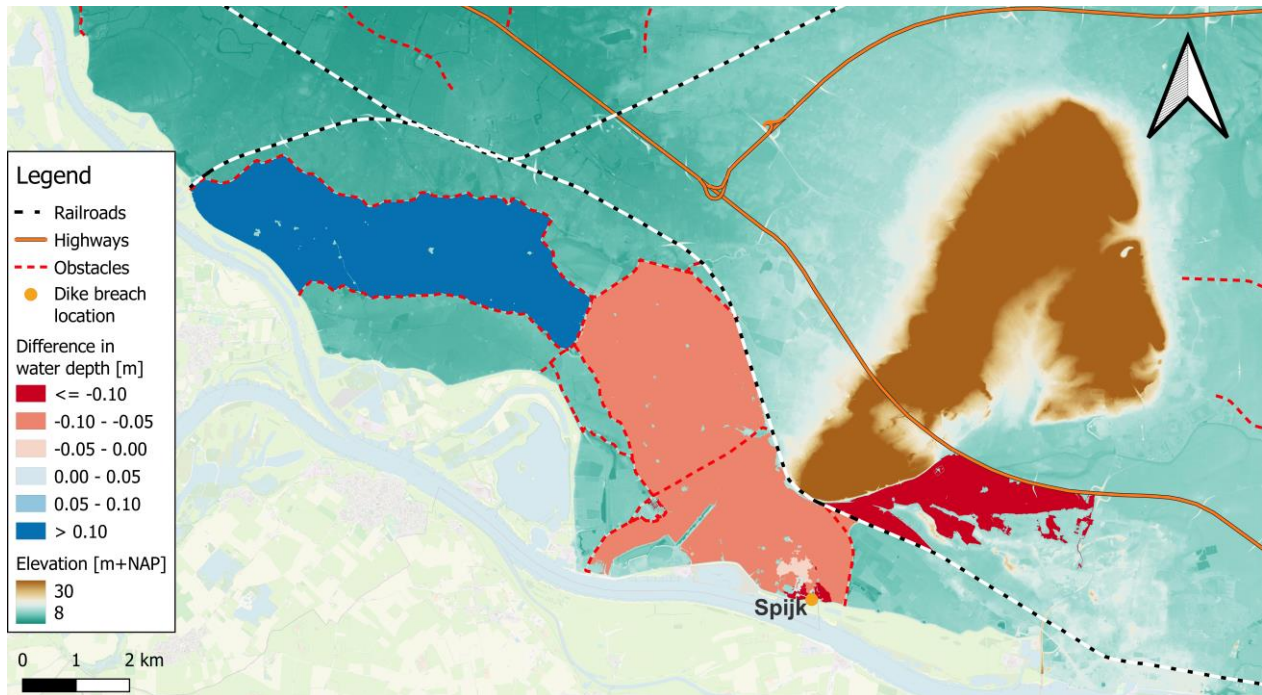


Figure 72 Differences in water depth after 1 day between adjusted grid 2 and reference grid for a dike breach at Spijk. Positive differences (blue) indicate that the water depth in adjusted grid 2 is larger than in the reference grid. For the resolution of both grids, see Table 2.

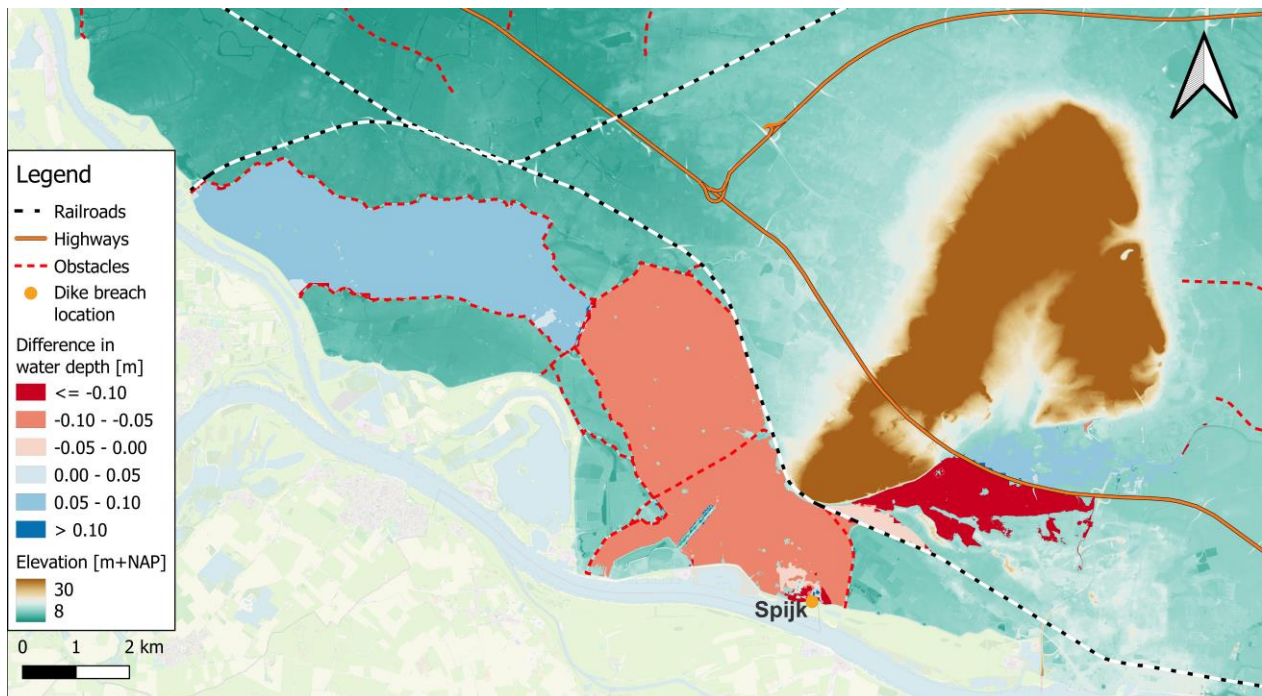


Figure 73 Differences in water depth after 1 day between adjusted grid 3 and reference grid for a dike breach at Spijk. Positive differences (blue) indicate that the water depth in adjusted grid 3 is larger than in the reference grid. For the resolution of both grids, see Table 2.

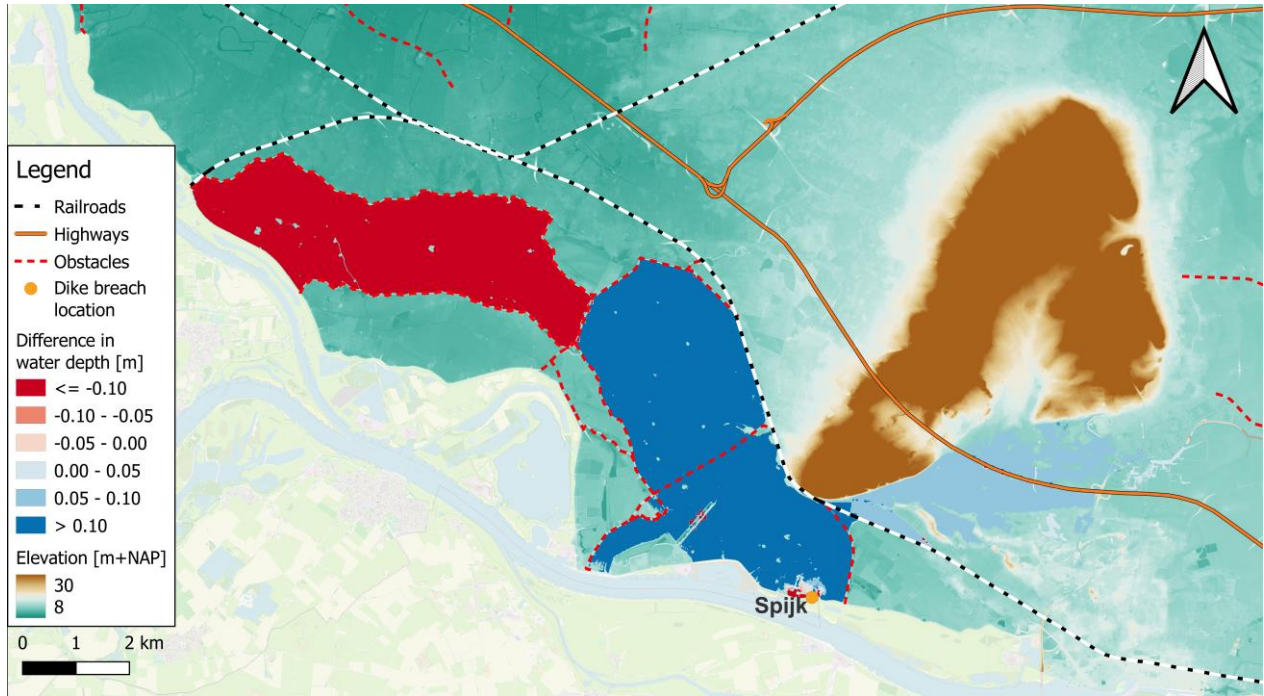


Figure 74 Differences in water depth after 1 day between adjusted grid 1 and reference grid for a dike breach at Spijk. Positive differences (blue) indicate that the water depth in adjusted grid 1 is larger than in the reference grid. For the resolution of both grids, see Table 2.